

***New Luminescent Europium Complexes as Indicators and in
Sensors for pH in Biosamples and Water Samples***

Dissertation zur Erlangung des Doktorgrades der Naturwissenschaften

(Dr. rer. nat.)

der Fakultät Chemie und Pharmazie

der Universität Regensburg

Deutschland



vorgelegt von

Wafaa Waleed Nafea Al-Qaysi

aus Iraq (Baghdad city)

im Jahr 2018

Die vorgelegte Dissertation entstand in der Zeit von November 2014 bis November 2018 am Institut für Analytische Chemie, Chemo- und Biosensorik der Universität Regensburg.

Die Arbeit wurde angeleitet von PD Dr. Axel Dürkop.

Promotionsgesuch eingereicht am: 03.10.2018
Kolloquiumstermin: 15.11.2018

Prüfungsausschuss

Vorsitzender: Prof. Dr. Oliver Tepner
Erstgutachterin: PD. Dr. Axel Dürkop
Zweitgutachter: Prof. Dr. Antje J. Bäumner
Drittprüfer: Prof. Dr. Rainer Müller

“To raise new questions, new possibilities, to regard old problems from a new angle, requires creative imagination and marks real advance in science.”

Albert Einstein

Acknowledgements

All praises and thanks are to Allah, the Lord of all the worlds, the most Beneficent, the most Merciful for giving me the opportunity to start and successfully complete this work.

I am indebted to a number of individuals and organizations who made the completion of this work possible. First of all, I'd like to thank my supervisor PD Dr. Axel Düerkop a lot for providing me with this interesting topic, for his readiness at all times to help and his critical suggestions, good advices, scientific discussions, as well as for his tireless support, encouragement during this thesis, and guidance were invaluable to the logical conclusion of this work. Moreover, I thank Prof. Dr. Joachim Wegener for continuous encouragement, for his valuable guidance and support. Furthermore, I thank Dr. Judith Stolwijk for continuous encouragement and for reading my thesis. And, I thank Prof. Dr. Antje J. Bäumner as a co-supervisor for providing me for the opportunity to work independently, develop my scientific background, valuable discussions and her continuous support and for her acceptance to take part in my defense in a short time.

I also thank my group members, especially, Dr. Nongnoot Wongkaew for continuous encouragement and for frequent help at any time, Arne Behrent, a Ph.D student, for helping me in all kinds of situations, especially in the flow cell measurements, and kind thanks to Marcel Simesk, who helped whenever I was in need for anything.

A great thank you to Frau Angelika Stoiber, who helped me and left me her key for spectrometer instrument.

Kind thanks to Barbara Goricnik, who helped me whenever I was in need for finding chemicals, or anything else.

Furthermore, I would like to thank all my colleagues at the Institute of Analytical Chemistry, Chemo- and Biosensors at the University of Regensburg, for the excellent atmosphere and their help.

Great thanks to acknowledge the financial support of German Academic Exchange Service (DAAD) and the Iraqi Ministry of Higher Education for giving me the opportunity to pursue my doctoral degree in Germany with grant no. 57076438 within the BaghDAAD program.

Finally, very special thank to my whole family and especially my father and my mother for their invaluable support and their love.

Dedication to the spirit of my father

Contents

1.	Introduction and aim of work.....	1
1.1	Lanthanides.....	1
1.1.1	The lanthanide series.....	2
1.1.2	Photophysics of lanthanide ions.....	5
1.1.3	Coordination chemistry.....	11
1.1.4	Luminescence quenching.....	11
1.1.5	Quantum yields (Φ).....	12
1.2	Optical wide-range pH sensors.....	12
1.2.1	Theoretical Definition of pH that Uses the Hydrogen Ion Activity.....	13
1.2.2	The Experimental Definition.....	13
1.2.3	The glass electrode for wide range pH sensing.....	14
1.3	Optical sensors for wide range pH sensing.....	19
1.3.1	Absorbance and reflectance-based pH sensors.....	22
1.3.2	Luminescence-based pH sensors.....	30
1.4	pH sensors in real samples.....	41
1.5	Response time & lifetime.....	43
1.6	Precision of pH measurements.....	44
1.7	Repeatability& reproducibility of pH measurements.....	44
1.8	Effect of ionic strength.....	45
1.9	Aim of work.....	46
1.10	References.....	47
2.	A luminescent europium complex for wide-range pH sensors and sensor microtiterplates.....	59
2.1	Introduction.....	59
2.2	Results and discussion.....	62
2.2.1	Tested Eu/Tb - complexes with different ligands as a potential wide-range pH indicator.....	62
2.2.2	Choice of ligands and conceptual remarks.....	67
2.2.3	Absorption spectra.....	68
2.2.4	Excitation spectra.....	71
2.2.5	Emission spectra.....	73
2.2.6	Excitation spectra of pH-sensor membrane.....	78
2.2.7	Emission spectra of pH-sensor membrane.....	80
2.2.8	Response time and reversibility of pH-sensor membrane.....	81
2.2.9	pH sensor microtiterplate.....	83
2.3	Conclusion.....	85
2.4	Experimental section.....	85
2.5	References.....	87
3.	Sensor and sensor microtiterplate with expanded pH detection range and their use in real samples.....	91
3.1	Introduction.....	91
3.2	Results and discussion.....	94
3.2.1	Choice of ligands and conceptual remarks.....	94
3.2.2	Absorption spectra of the indicator.....	95
3.2.3	Excitation spectra of the indicator.....	97
3.2.4	Emission spectra of the indicator.....	98

3.2.5	Excitation spectra of pH-sensor membrane	100
3.2.6	Emission spectra of pH-sensor membrane	101
3.2.7	Response time and reversibility of pH-sensor membrane.....	102
3.2.8	pH sensor microtiterplate	104
3.2.9	Application of the pH sensor microtiterplate to real samples	105
3.3	Conclusion	106
3.4	Materials and methods	107
3.5	References.....	109
4.	Abbreviations.....	112
5.	Summary.....	114
5.1	In English.....	114
5.2	Zusammenfassung auf Deutsch	117
5.3	الخلاصة بال عربي.....	121
6.	Curriculum Vitae	127
7.	Eidesstattliche Erklärung.....	130

1. Introduction and aim of work

1.1 Lanthanides

The word lanthanide originates from the Greek word *lanthaneien* translating into “lying hidden” [1]. The lanthanides represent the chemical elements from lanthanum to lutetium. The 18th century was the era of lanthanides. In 1752, a Swedish mineralogist discovered a heavy mineral from a mine. In 1789, Klaproth discovered the element uranium in *pitchblende* and uranium was isolated as a metal in 1841, by Peligot. In 1794, a Finnish mineralogist in Sweden discovered a heavy mineral then isolated an oxide named “ytterbia” (from the village, Ytterby). Later this oxide was separated into several fractions “yttria”, “erbia”, and “terbia”, these were found to be complex mixtures. The isolation of lanthanum, yttrium, and scandium was not completed until 1908-1909 owing to the difficulties in separating them by fractional crystallization: C. James obtained “pure” $\text{Tm}(\text{BrO}_3)_3$ by 15000 recrystallizations. These difficulties arose because lanthanides have very similar chemical properties, with their dominant valence state being plus three (3+), while showing only small differences in formation and solubility of complexes. These small differences decrease in size with increasing atomic number. In 1913 it was conclusively shown that there exist only 14 elements between La and Hf by X-ray spectroscopy. Until World War II, the only major advance in separating lanthanide ions was made by McCoy, who purified considerable quantities of Eu by reducing Eu^{3+} to Eu^{2+} , followed by precipitation as EuSO_4 . During the 1930s & 1940s the first spectroscopic studies on aqueous lanthanide solutions were carried out [2]. It was found that some organic ligands (such as salicylaldehyde or benzoylacetate) when excited in the ultraviolet (UV) region, can photosensitize the luminescence of europium ions, where Eu does not absorb light. Eu is found only at about 0.1% in the earth's crust. In 1945, the first radioactive promethium Pm was prepared. In 1962, cells were first stained with Eu and in the 1970s, a Finnish company, Wallac Oy (currently part of Perkin Elmer), began the studies with lanthanides as luminescent reporters for

time resolved immunoassays [3]. The technology developed by Wallac Oy spurred a rapid increase in the number of studies and applications in the field.

1.1.1 The lanthanide series

The lanthanide series consist of 15 elements from lanthanum La^{3+} (atomic number 57) to lutetium Lu^{3+} (atomic number 71) where the 4f-shell is filled from 0 to 14 electrons. These are called f-block elements because of the gradual filling of the last electrons in f-orbitals of the antepenultimate shell. Lanthanides can be extended with the elements scandium ($Z = 21$) and yttrium ($Z = 39$), having similar chemical and physical properties. Lanthanides are sometimes called rare earth elements [4]. Despite their name, rare earths are not less abundant in nature than tin, silver, gold, or platinum. In 1906, Becquerel, the first time observed the unusually sharp absorption lines of rare earth compounds, when he measured the spectrum of the mineral xenotime (YPO_4 with traces of Er, Ce and Th). Around 1930, the sharpness of these lines could not be understood till Bethe [6], Kramers [7], and Becquerel [8] suggested that the lines may be due to electronic transitions within the 4f configuration, referred to as f-f transitions. In 1937, Van Vleck [9], showed using a very highly and simple instructive model of f-f transitions and that they become partially allowed as electronic dipole transitions. When we progress from cerium to lutetium, the 4f orbitals are gradually filled. These f orbitals have low radial expansion, and they are shielded from the chemical environment by the filled, energetically lower 5s and 5p sub-shells. Although lower in energy, these sub-shells are spatially located outside the 4f orbitals, causing the 4f electrons to have very little interaction with the chemical environment, and leading to the difficult separation of the lanthanides [10],[2]. Freed *et al.*[11], found that the relative intensities of the absorption lines of Eu^{3+} were different in different solvents and Weissman [12] discovered that complexes of Eu^{3+} with certain ultraviolet absorbing ligands were highly luminescent when excited by ultraviolet light. Since Eu^{3+} it self has only a few, very weak absorption bands, solutions of this ion are not very brightly photoluminescent. Obviously, certain organic ligands can serve to photosensitise the luminescence of lanthanide ions. It was also found that lanthanide ions quench the fluorescence of

organic ligands. At that time, the optical spectra of lanthanide ions and the electronic energy level structure were only qualitatively understood. In the 1960s, Dieke [13] gave the $4f^n$ energy levels of all trivalent lanthanides in the IR, visible and the UV spectral region. At the beginning of the 1960s, systematic studies of luminescent lanthanide complexes and their photophysics took place and these studies were mainly related to the β -diketonate complexes of Eu and Tb. In 1962, during the theoretical work of Judd [14], and Ofelt [15], calculation of the intensities of the electric dipole transitions between energy levels of the lanthanide ions. Today, the Judd-Ofelt theory is used to describe and find the electronic spectra of lanthanide ions present in glasses and crystals. All lanthanides, except lanthanum, are f-block elements (have valence electrons in f orbitals). In general, electronic configuration of lanthanide atoms is usually represented as $[\text{Xe}] 4f^n 5d^1 6s^2$, where $[\text{Xe}]$ represents the electronic configuration of the noble gas xenon, and n represents the number of electrons from 0 to 14 (0 with La to 14 with Lu). Depending on the relative energy levels, there are two types of electronic configurations for the lanthanide atoms: $[\text{Xe}] 4f^n 6s^2$ and $[\text{Xe}] 4f^{n-1} 5d^1 6s^2$ ($n = 1-14$). Lanthanum, cerium, gadolinium, and lutetium belong to the latter type, while in terbium both types of electronic configurations similar can be used any one. Ln^{3+} (with Ln referring to any lanthanide) is the most common oxidation state of lanthanide ions in aqueous solvents. Most lanthanide ions are stable. The electronic configuration of all the trivalent lanthanide ions is $[\text{Xe}] 4f^n$, represented by the two 6s electrons, and the lost 5d electron [16].

A summary of the electronic configurations of lanthanide atoms and trivalent lanthanide ions is presented in Table 1. Some lanthanides are found as Ln^{2+} ions, because the 4f shell of the divalent ion is half filled [17]. While the other of lanthanides are found as Ln^{4+} ions, such as Ce^{4+} . The highest oxidation state of lanthanides is the tetravalent state [18].

Table 1 The electronic configurations of rare earth elements [17]. The lanthanides (from La to Lu) have filled inner orbitals with 46 electrons. Scandium and yttrium have 18 electrons in the inner orbitals.

Z	Element	Configurations of neutral atoms					Configurations of trivalent ions	Atomic weight
		4f	5s	5p	5d	6s		
57	La	0	2	6	1	2	[Xe]4f ⁰	138.9
58	Ce	1	2	6	1	2	[Xe]4f ¹	140.12
59	Pr	3	2	6		2	[Xe]4f ²	140.91
60	Nd	4	2	6		2	[Xe]4f ³	144.24
61	Pm	5	2	6		2	[Xe]4f ⁴	(147)
62	Sm	6	2	6		2	[Xe]4f ⁵	150.36
63	Eu	7	2	6		2	[Xe]4f ⁶	151.96
64	Gd	7	2	6	1	2	[Xe]4f ⁷	157.25
65	Tb	9	2	6		2	[Xe]4f ⁸	158.93
66	Dy	10	2	6		2	[Xe]4f ⁹	162.50
67	Ho	11	2	6		2	[Xe]4f ¹⁰	164.93
68	Er	12	2	6		2	[Xe]4f ¹¹	167.26
69	Tm	13	2	6		2	[Xe]4f ¹²	168.93
70	Yb	14	2	6		2	[Xe]4f ¹³	173.04
71	Lu	14	2	6	1	2	[Xe]4f ¹⁴	174.97
		3d	4s	4p	4d	5s		
21	Sc	1	2				[Ar]	44.96
39	Y	10	2	6	1	2	[Kr]	88.91

As a result, several lanthanide ions show sharp line like spectra of free atoms or ions. Each lanthanide ion shows characteristic absorption and emission spectra and it can emit in the near-UV, visible, near infrared (NIR) and infrared (IR) regions of the electromagnetic spectrum upon irradiation with ultraviolet radiation. For instance, Sm³⁺ emits orange light, Eu³⁺ red light, Tb³⁺ green light, and Tm³⁺ blue light. Nd³⁺, Er³⁺, and Yb³⁺ are well-known for their near-infrared luminescence, but other lanthanide ions (Pr³⁺, Sm³⁺, Dy³⁺, Ho³⁺, and Tm³⁺) also show transitions in the near-infrared region. Most of the emitting lanthanide ions are luminescent, characterized by high color purity and are very attractive for technical applications, while the La³⁺ and Lu³⁺ are not luminescent in equal degree, and thus not useful in any optical applications. The luminescence intensity of a lanthanide ion is dependent on the quantum yield (Φ).

Figure 1, shows the energy level diagram of aqueous lanthanide ions, and explains the energy gaps, [19]. Judged by the energy gap, Eu³⁺, Tb³⁺, and Gd³⁺ ions have the strongest luminescence. Eu³⁺

and Tb^{3+} are often used in bioanalytical applications. In addition to that intense emission in the visible wavelength, these emission have a particularly long lifetime [20].

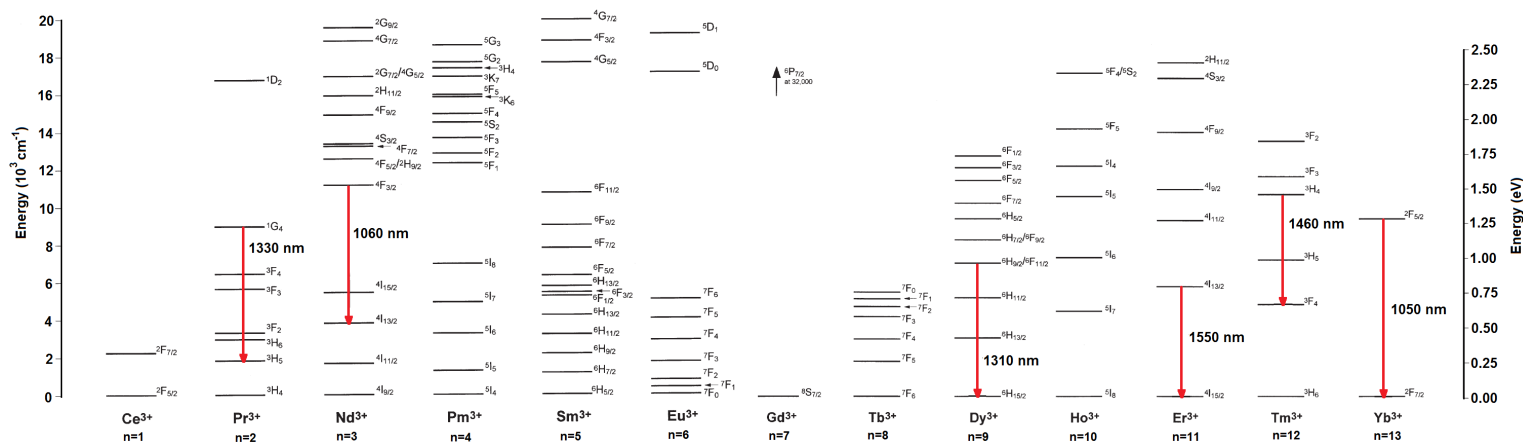


Figure 1 A diagram depicting the approximate energy levels for aqueous lanthanide ions [21].

Lanthanides with exceptional photoluminescent properties have been used in a broad range of applications in fields such as X-ray crystallography, magnetic resonance imaging (MRI), optics, nuclear magnetic resonance (NMR) spectroscopy, lighting, metallurgy, bio-organic chemistry, medical diagnostics, and imaging [22].

1.1.2 Photophysics of lanthanide ions

1.1.2.1 Electronic energy levels

The number of electronic levels formed by $[\text{Xe}] 4f^n$ and electronic level is 3003 in Eu^{3+} and Tb^{3+} [23]. Depending on the number of electrons in the 4f orbitals, there are many ways to distribute these electrons. Figure 2, describes the interactions leading to different energy levels such as in Eu^{3+} . The electronic configuration first is divided into terms because of the repulsion between the electrons within the orbitals. This interaction is termed Coulombic interaction. The terms are then split into J-levels, because of spin-orbit coupling, which is relatively large (10^3 cm^{-1}) because of the heavy lanthanide. These represent the free ion levels and are described by the term symbols S, L, and J with the formula $^{2S+1}L_J$, where $2S+1$ represents the total spin multiplicity, L is the total orbital angular momentum, and J the total angular momentum of the f electrons. Because of the 4f

orbitals are shielded by the filled electrons in the 5s and 5p sub-shells, the transitions are sharp between these levels. When the lanthanide ion is in a coordinating environment, (such as an inorganic crystal or an organic ligand), the J-levels are split into sublevels because of the electric field of the matrix. This splitting is usually small (10^2 cm^{-1}) depending on the spectral resolution of the spectrometer and in the main emission bands of the lanthanide ion [24].

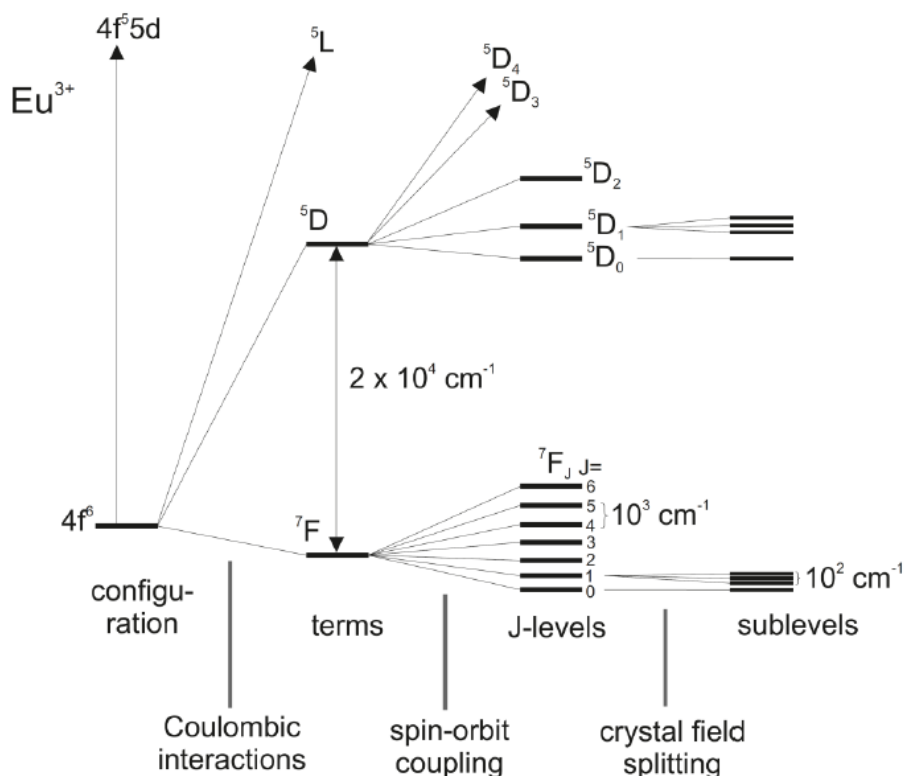


Figure 2 Diagram representing the interactions leading to the splitting of the electronic energy levels of a Eu^{3+} ion. In the diagram, energy increases when going up [2].

1.1.2.2 Radiative transitions

The absorption and emission light results from two main types of transitions: the parity-allowed magnetic dipole (MD) transitions and the parity-forbidden electric dipole (ED) transitions. Most absorption and emission light of lanthanides in complexes involves redistribution of electrons within the 4f sub-shell (intraconfigurational f–f transitions) therefore (ED) transitions. For example the emission bands of the $\text{Eu}^{3+} \ ^5D_0 \rightarrow \ ^7F_1$ transition are allowed as MD transitions, while the emission bands of Tb^{3+} require both, ED and MD mechanisms because the intensity of ED transitions in lanthanide ions are depending on the ligand field [2]. Hypersensitive transition means

the relative intensities emissions are very sensitive to the detailed nature of the ligand environment. In Eu^{3+} , this is $^5\text{D}_0 \rightarrow ^7\text{F}_1$ and $^5\text{D}_0 \rightarrow ^7\text{F}_2$. Both MD and the ED transitions of lanthanide ions are weak compared to the “fully allowed” transitions of organic chromophores which causes long lifetimes to milliseconds in lanthanide complexes which depend on the lanthanide and matrix [2]. Some transitions require both MD and ED. Further, Eu^{3+} firstly accepts energy through its $^5\text{D}_1$ and $^5\text{D}_2$ levels above the emissive $^5\text{D}_0$ level [25]. Tb^{3+} directly accepts energy by the $^5\text{D}_4$ emissive level and decay to several $^7\text{F}_n$ -levels.

1.1.2.3 Non radiative decay

The excited states in the lanthanide ions do not decay by radiative processes only. If the excited state and the next lower state energy gap are relatively small, luminescence will be in strong competition with the non-radiative decay of the excited state and depend on the number of matrix vibrations. In glasses and crystals the electronic excitation energy can be dissipated by vibrations of the matrix, a process known as multiphonon relaxation [26]. It can occur through coupling of the lanthanide energy levels with the vibrational modes in the direct surrounding of the lanthanide ion. The high energy O-H vibrations are very efficient quenchers for lanthanide luminescence. Therefore water molecules are avoided from the first coordination sphere of the lanthanide complexes. A similar relaxation process is more pronounced when lanthanide complexes carry organic ligands. In organic media suitable high-energy vibrations are more common [27]. The efficacy of matrix vibration mediated nonradiative relaxation is inversely proportionall to the number of vibrations quanta (phonons) required to bridge the gap between a given energy level and the next-lower one (radiative emission will efficiently compete with the non-radiative relaxation processes) [22].

Lanthanide ions usually require indirect excitation, named the “antenna effect”, or “sensitization of the metal-centred luminescence” because most of the transitions of the Ln^{3+} ions are related to the redistribution of electrons within the 4f sub-shell (intra configurational f–f transitions). This is a direct excitation of the lanthanide ions only producing low levels of luminescence (the weak f–f

transitions have absorption cross sections in the order of $1 \text{ M}^{-1} \text{ cm}^{-1}$), [19],[22]-[25]. This means the ion needs to form a complex with a sensitizing structure, such as an organic ligand containing a light absorbing chromophore structure.

1.1.2.4 The antenna effect

The lanthanide ions (f-f transitions) have very weak absorption coefficients (ϵ), which makes direct photo-excitation of the lanthanide ions difficult. However, this can be overcome by using the large absorption cross section of the organic chromophores and the energy transfer from organic chromophores to lanthanide ions (see figure 3).

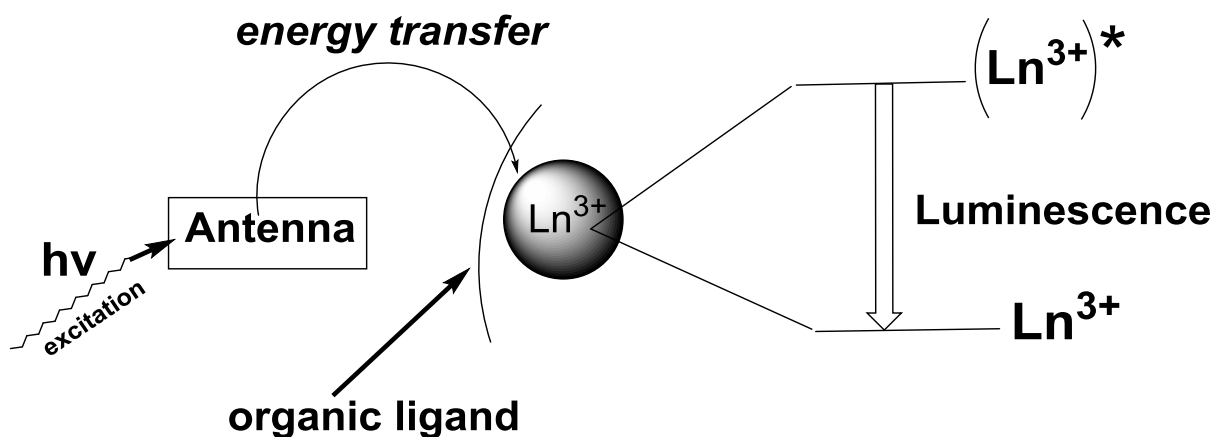


Figure 3 General architecture of luminescent lanthanide complexes.

Thus, in order to design highly luminescent Ln^{3+} complexes, Weissman [12], first noticed the sensitization process in which the energy transfer takes place from coordinated ligands to the central metal ion.

Luminescent lanthanide complexes consist of a lanthanide ion encapsulated in one or more ligands. Figure 3 shows that the organic chromophore ligand contains a light-absorbing group. Such a group is generally referred to as the antenna chromophore, in analogy to the light harvesting centra in photosynthetic reaction centers. The photonic energy absorbed by this antenna can be transferred to the encapsulated lanthanide ion, thus circumventing the photoexcitation bottleneck posed by the small absorption cross-sections of the lanthanide ions.

The β -diketonate complexes are known to be very efficient sensitizers for the lanthanide ions [28],[29]. Organic ligands coordinated to lanthanide ions have a twofold beneficial effect, they not only increase the light absorption cross section by “antenna effects” but also protect metal ions from vibrational coupling [30].

1.1.2.5 Lanthanide ion sensitization

Lanthanide ion sensitization occurs, when the ligand coordinates with the lanthanide. This process protects the ion from the quenching effects of the aqueous matrix. Lanthanide luminescence is quenched through nonradiative relaxation processes, especially O–H vibrations (vibrational quenching). Water should be removed from the inner and the outer coordination sphere of the lanthanide ion [31]. Because of the large energy gap the terbium is not exposed to the quenching by O–H vibrations compared with the other lanthanides [17]. Terbium complexes may possess an energy back-transfer route from the emissive 5D_4 level to an energetically close-lying ligand triplet state, which causes quenching of the luminescence and enhanced sensitivity to environmental conditions [32]. An energy difference of approximately $2500\text{--}3500\text{ cm}^{-1}$ is required to prevent this kind of energy back-transfer [24].

1.1.2.6 Ligand and lanthanide ion excitation

The mechanism of energy transfer from organic ligands to the lanthanide ion involves three steps: First, strong absorption from the ground singlet state (S_0) to the excited singlet state (S_1) of the ligand. Then excited singlet state (S_1) decays non-radiatively to the triplet state (T_1) via intersystem crossing, and finally the non-radiative energy transfer pathway from the T_1 state of the ligand to excited states of the Ln^{3+} ion to emit light [1]. In some cases the direct energy transfer from the S_1 singlet state to the excited Ln^{3+} levels is also observed.

A simplified scheme of these energy transfer processes, e.g., a Jablonski diagram, can be used to explain the processes related to lanthanide luminescence. This is illustrated in the figure 4 below.

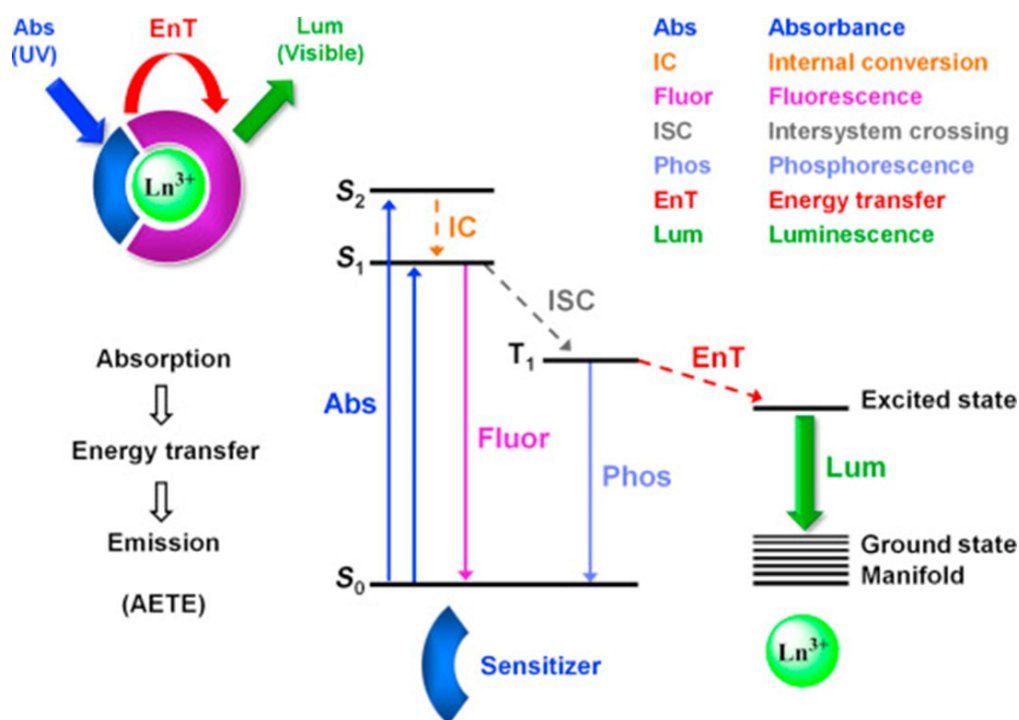


Figure 4 Jablonski Energy Diagram of Absorbance Energy Transfer Emission (AETE) mechanism for a Ln^{3+} complex [33].

Most lanthanide complexes are excited in the near-UV range at wavelengths around 350 nm. The absorption of light by the lanthanide complex is a very fast process in the range of 10^{-15} s. It occurs from the ground state (low energy) to an excited singlet state (high energy). Internal conversion (IC) happens on the time scale of 10^{-12} s. From the original excited singlet energy state of the ligand, electrons vibrate or rotate down to excited vibration levels, or to the lowest excited electronic levels. Then, intersystem crossing (ISC) happens within a time scale of 10^{-13} s. The electrons relax from the excited singlet state (S_1) to the excited triplet state (T_1 lower energy), and from the excited triplet state (lower energy) through intramolecular energy transfer to the excited energy levels of the central ion. The singlet state is short lived, and the process is not efficient [20],[34].

There are two main mechanisms for the intramolecular energy transfer from excited triplet state (lower energy) to the central ion: the Dexter (electron exchange) mechanism and the Förster (dipole-dipole) mechanism [35]. The Dexter mechanism does require physical contact between the ligand and the central ion and includes electronic exchange between two components [36], while in the Förster mechanism does not require physical contact between the two components because the

triplet state transition dipole moment associates with the dipole moment of the 4f orbitals [5],[37]. In addition, there are other mechanisms, the metal to ligand charge-transfer (MLCT) from chromophores containing d-transition metal ions [38], and the ligand to metal charge-transfer (LMCT) when energy is transferred to the excited 4f-states of the lanthanide ion [39]. Lanthanide ions display f-f transitions and charge transfer transitions also display a third type of electronic transitions: the f-d transitions, meaning the promotion of a 4f electron into the 5d sub-shell [40].

1.1.3 Coordination chemistry

The study of coordination compounds or complexes has started in the nineteenth century with scientists such as Werner [41] who resolved the link between metal oxidation state and coordination number and developed the coordination chemistry.

The physical properties of a metal complex can be affected by the type of ligand. Ligands may be simple monoatomic structures, such as halides or large macromolecules with many coordination sites. The denticity is known as the number of sites on a molecule that are capable of coordinating. Monodentate ligands are compounds with one coordination site, such as pyridine, while polydentate ligands are compounds with more than one coordination site. The physical properties of lanthanides are unlike those of the d-block metals. These properties are very similar and uniform across the row.

Lanthanides typically form eight or nine coordinate species, especially in aqueous solution where water molecules often coordinate to any sites around the ion. The complexes also exhibit rapid ligand exchange, except in the case of multidentate ligands, with water coordination residency times of around 10^{-9} s. Essentially, this means that the rate of exchange is determined by the diffusion of water molecules is the inner coordination sphere. This means that monodentate ligands are extremely unstable and highly kinetically inert lanthanide complexes can only be obtained through the incorporation of the ion into a macrocycle-based or rigid polydentate ligand.

1.1.4 Luminescence quenching

This non-radiative process occurs if a molecule in an excited state releases energy to a quencher and subsequently returns to the ground state [42]. Quenching can occur where the excited

states can be very short lived due to the efficient cascade of energy transfer from one component to another [43].

Quenching can also take place in an intermolecular manner through second-order rate kinetics. It causes decrease of the fluorescence intensity of a substance through either energy-transfer, complex formation, excited state, O-H vibrations, N-H and C-H vibrations [44].

1.1.5 Quantum yields (Φ)

Quantum yields (Φ) is the ratio of the number of emitted photons (radiative) in relation to the number of photons absorbed as outlined equation (1) [24]. The quantum yield is also related to the extent of the energy gap between the lowest excited energy level of the ion (called the emissive energy level) and the highest sublevel of its ground state multiplet

$$\Phi = \text{number of emitted photons} / \text{number of absorbed photons} \quad (1)$$

1.2 Optical wide-range pH sensors

The measurement of pH is still one of the most vital analytical methods in laboratory routine, research and measurements in the field for e.g. 1) pH is used as a quality parameter in clinical assessment of blood, body fluids, the freshness of food, drinking water and for treatment of industrial waste water. 2) pH is used to find the optimum reaction conditions in bioreactors, for precipitation of heavy metal ions from waste water and in industrial fermentation. Therefore, there are continuous attempts to find novel techniques for pH detection [45]. Nowadays, pH values are most often determined by using electrochemical sensors such as the pH glass electrode [46] or pH test paper strips or and optical pH-sensors.

Earlier reviews on optical pH sensors have been published by Wencel, et al. [80], Wolfbeis et al. [81], Wolfbeis et al. [82], Lin et al. [83], Bilro et al. [84], Wolfbeis et al. [85], Seitz et al. [86], Janata et al. [87] and others. Recently, authors try to extend the measurement range of optical pH sensors. By this they want to overcome one major drawback of optical pH sensors using an equilibrium between a single protonated and unprotonated couple of indicator species. Due to the mass action law, this results in sensors which in most cases do not cover more than 3-4 pH units. As

glass electrodes (as the electrochemical competitors) offer a detection range that is typically larger than 12 pH units, there is a huge demand for optical wide-range sensors for pH because they offer some advantages with respect to miniaturization, remote sensing, imaging, sensing in-vivo, in the field or by non-educated staff that can hardly be reached by ion selective electrodes.

In this chapter the scientific literature on optical wide-range sensors for pH is shown that has appeared over the last two to three decades. They are ordered with respect to the detection methods and with respect to the sensor layouts. Initially a concluding overview over pH measurement by pH-electrodes is given mainly with the glass electrode. In the following sections their major properties are compared with those of the various optical detection methods. After some concluding remarks, an outlook is given on which sensing schemes seem to be promising for which field of application if detection ranges should be further extended.

1.2.1 Theoretical Definition of pH that Uses the Hydrogen Ion Activity

In 1920, Sørensen's definition of pH, i.e. that $\text{pH} = -\log_{10}[\text{H}^+]$, was later revised, as further research demonstrated that pH is more related to hydrogen ion activity than hydrogen ion concentration. As a result, the new definition of pH is $\text{pH} = -\log a_{\text{H}^+}$ where a_{H^+} is the hydrogen ion activity. This is derived from Lowry's recognition [47] of the activity of the hydronium ion instead of the hydrogen ion as the key to pH. The activity is an effective concentration of hydrogen ions, rather than the true concentration; It considers that other ions surrounding hydrogen ions will protect them and affect their ability to participate in chemical reactions. These other ions effectively change the hydrogen ion concentration in any process that involves H^+ .

1.2.2 The Experimental Definition

IUPAC has endorsed two pH scales based on comparison with a standard buffer of known pH using electrochemical measurements:

a) the British Standard Institution (BSI) scale has one fixed point, which is the reference buffer. The pH of a potassium hydrogen phthalate solution with $b = 0.05 \text{ mol/kg}$ was set to be $4.000 + (T - 15)2 \cdot 10^{-4}$, where T is the temperature. Any other standard solutions are derived by measurement with

a reference electrode and a hydrogen electrode. The signal includes a residual, non-eliminable diffusion potential. This scale is predominantly used in Great Britain and Japan [48].

b) the National Bureau of Standards (NBS) scale uses several fixed points [49]. The fixed points are set by so-called primary pH standard solutions. The signal is determined with chains without electrochemical transport and is therefore free of a noneliminable diffusion potential. This scale is adopted by most national standards, e.g. Germany's DIN 19266.

1.2.3 The glass electrode for wide range pH sensing

Nowadays, the pH glass electrode is the most common sensor for a wide-range pH measurement. In 1889, Nernst [50] worked in thermodynamics and invented the hydrogen electrode for $[H^+]$ for the first time. Cremer [51] studied the electric potential difference between a glass and an aqueous solution and plotted the electrical response of glass membranes to variable hydrogen ion concentrations in 1906. Then, Haber and Klemensiewicz [52] used the first glass electrode in 1909 based on bases Cremer's detection principle and determined the electrochemical signals based on $[H^+]$. In 1924 Schiller [53] found the magnitude of counter electric magnetic fields and applied potential difference to be same. Horovitz and Zimmermann [54] suggested that a certain proton concentration must be reached before the glass acts as electrode for H^+ . Few years later, MacInnes and Dole [55] found that the most suitable glass for a pH electrode had the composition $22 Na_2O \cdot 6 CaO \cdot 72 SiO_2$ (Corning 015 glass). In 1937 Nicolsky [56] proposed the ion exchange equilibrium theory and worked on the thermodynamic description of the glass electrode. However, Haugaard [57] later concluded that thermodynamics alone cannot tell enough about the mechanism of the building of the glass boundary potential. In the 1960s, Durst [58] summarized the still accepted common knowledge that the response of the glass membrane occurs as a result of an ion exchange process which takes place in the gel layer of the glass membrane thereby inducing a phase boundary potential. This governs the pH response of the electrode but not a diffusion of hydrogen ions through entire glass membrane. Recent literature mostly supposed that ion exchange was the real physicochemical process responsible for the potential formation. In (1974) Baucke [59] developed

new techniques to increase sensitivity and resolution of glass electrodes. In (1980) Dole [60] proposed steaming as a method of cleaning and offered a modified theory of the glass electrode by deducing an equation which fits accurately to the response in alkaline solution. Among the various types of pH measuring electrodes, the pH glass electrode nowadays is one of the most common types for highly accurate pH measurements or for studying of (de)protonation, coordination equilibria in aqueous solution (i.e. stoichiometry) [61]. The glass pH electrode is not as cheap as pH stripes but moderately expensive, and offers some advantages such as excellent electrode performances with respect to slope, sensitivity, selectivity to protons, limit of detection, reliability, distinguished response characteristics, long-term stability, fast response time, insensitivity vs redox systems and width of the dynamic pH range [62]. However, glass pH electrodes have some disadvantages such as bulky size and high resistance, they are prone to membrane pollution and instable in solutions containing fluoride and can show alkaline and acid errors. They may be a source of electromagnetic interferences in an in-vivo measurement (cell) and (due to mechanical frailty) unsuitable to be integrated into microfabricated electrochemical sensing systems for biological, industrial, environmental, and security applications [63], [64]. Therefore, several alternatives have been suggested to the glass membrane electrode such as ion-sensitive field effect transistors, metal oxide electrodes, and the quinhydrone electrode. The interference of fluoride could be compensated, recently [65] by employing a 5,17-bis(4-benzylpiperidine-1-yl)methyl-25,26,27,28-tetrahydroxy-calix[4]arene as a ionophore in a polyvinylchloride (PVC) pH-sensing membrane. In fig. 5 two calibration curves of the measured potentials were plotted against the pH value from 1.9–12.9. The calix[4]arene electrode offers some advantages such as being inexpensive and easy to prepare. It has a wide linear working range and an almost Nernstian slope, a good selectivity and reproducibility for H^+ ions, a broad pH working range and a quick response time of 6–7 s. The proposed calix[4]arene electrode has a wider linear working range and exhibits a better near-Nernstian slope of $58.77 \pm 1.1 mVpH^{-1}$ which is more suitable than previous literature [66],

[67]. However, such electrodes might suffer from limited selectivity because they show reversible anion binding due to the ability of the protonated calix[4]arene by hydrogen bonds [68].

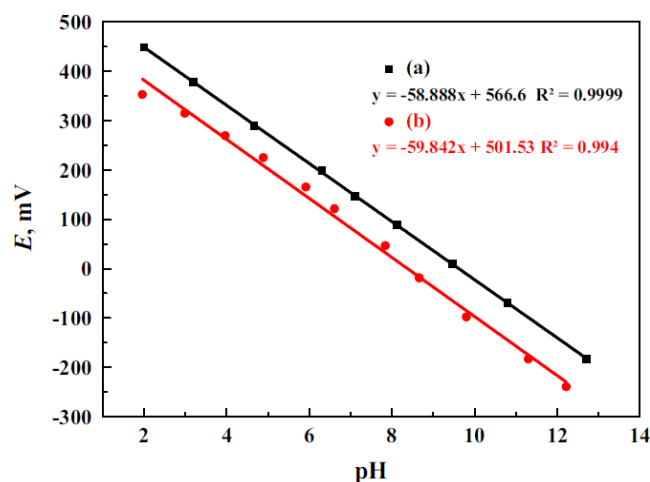


Figure 5 Calibration graphs of the proposed pH sensing membrane electrode plotted by the data obtained from pH ion meter and (b) potential graph [65].

Compared with other electrodes [69], the response times are comparable or shorter and the electrode gives a fast response, and has a long life time at least 12 months.

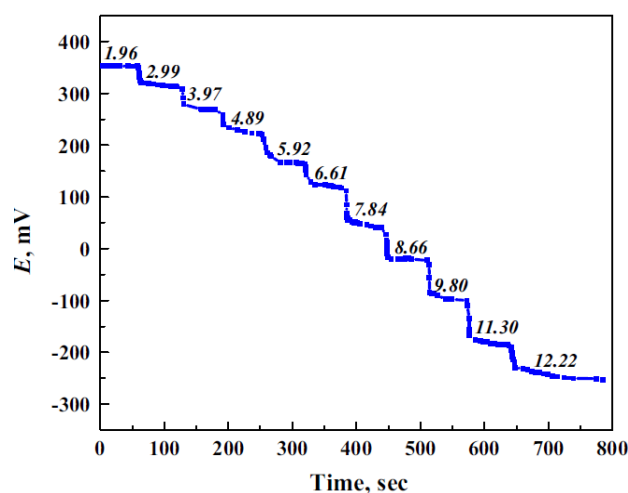


Figure 6 Dynamic response of the proposed electrode for step changes in pH (1.9–12.22) [65].

Jović et al. [70] fabricated, characterized and applied sensitive pH sensors based on a nano-assembly of iridium oxide (IrO_2) nanoparticles and polydiallyldimethylammonium (PDDA) polymer layers obtained via Layer-by-Layer Inkjet Printing (LbL IJP) methodology. LbL assemblies were composed of positively charged PDDA and negatively charged IrO_2 citrate-

stabilized nanoparticles in various pH (2.9–10.37). This method is suitable for the production of thin nanofilm pH sensitive bilayers which are inexpensive, flexible, offer a fast response time, excellent reproducibility and near-Nernstian sensitivity. Fig.7 shows data of the pH-sensing properties and the reproducibility study. The pH electrode showed a linear response in the examined pH range. Compared with earlier literature [71] on oxidized Ir electrodes, the pH-sensing properties of IrO₂ films are dependent of the structure, composition and oxidation state, which are impacted by the fabrication method. The response was rapid and stability was reached after 2–3 s. The good reproducibility of the inkjet printing processes was assessed via the potential – pH dependence of five different 5-bilayer electrodes of the same batch (vs. Ag/AgCl (3 M KCl) reference electrode) using acid-to-base and base-to-acid measurements. Compared with the earlier electrodes of this type [72] the LbL IJP electrode shows excellent reproducibility and a top-class reversibility of the response.

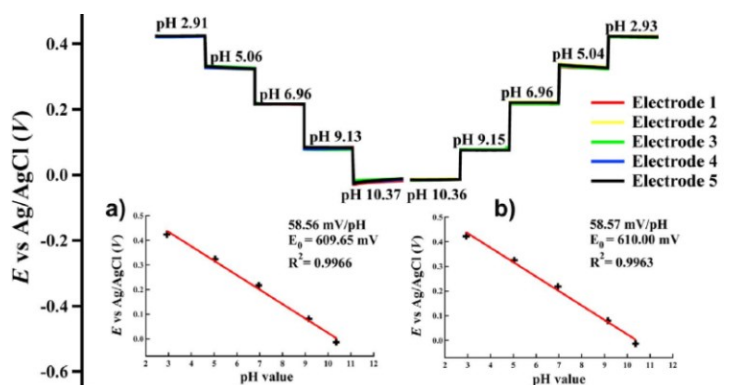


Figure 7 Acid-to-base and base-to-acid pH measurements of the different 5-bilayer IJP electrodes from the same printed batch. Inset plots represent the average potential –pH dependence for a) acid to base and b) base to acid direction. (the error bars represent the standard deviation of five different electrodes; bars are similar to the data symbols employed) [70].

Electrode-based pH sensing still has several drawbacks. Electrodes are prone to membrane pollution and a source of interference in in-vivo cell measurements and cannot be minimized or changed to sub- μm size. This is a disadvantage when pH detection in very small volumes such as cells or cell organelles is required. Additionally, a reference electrode is required. Furthermore, pH electrodes show weak performance in both extremes of the pH scale, especially in the highly

alkaline region because of the alkaline error. Despite the high selectivity of glass electrodes to hydrogen ions, particularly Li^+ , Na^+ and K^+ can induce errors in pH measurements in concentrated solutions at $\text{pH} > 9$. At high pH, the hydrogen ion activity (and hence, concentration) is low. Then, protons in the outer gel layer of the glass membrane may be exchanged by the cations. As a result, erroneous potentials across the glass membrane and thus erroneous pH will be acquired. This leads to lower pH value measured than is actually present in the sample. pH electrodes with special glass membranes for use in high alkaline media are therefore offered [73].

In highly acidic solutions the acid error may occur. At very low pH values (typically $< -0,5$) acid molecules are absorbed by the gel layer leading to a decrease in the hydrogen ion (H^+) activity in the gel layer. The pH measurement, therefore, shows a higher pH value than actually present in solution. Due to its occurrence at only very low pH this error is rarely relevant in practical applications and further reduced in lithium silicate glasses [74].

Additionally the fluoride and the phosphate errors have been described more recently [75]. They may occur, if La_2O_3 -containing membrane glasses are employed in presence of on the said anions. These errors arise due to the formation of lowly soluble LaF_3 and LaPO_4 at medium to high pH values at the membrane surface after about 1 h induction time. Potential deviations until -35 mV are possible and remain until long-term measurements at pHs below 5 are performed.

The drift of the diffusion potential is a common source of error, if a Ag/AgCl reference electrode is used in KCl. Dilution of KCl in the porous plug induces a precipitation of AgCl or Ag(s) (if the sample contains reduction agents) inside the porous plug. Both precipitation reactions lead to a drift of the diffusion potential and hence, a drift of the pH detected. This can be compensated by recalibration about every second hour. Finally, different temperatures of calibration and sample measurements may induce erroneous pH reads, as well as a swelling time of less than several hours of a dry electrode in water, before calibration is performed. One should be patient until taking pH in solutions of low ionic strength because the equilibrium at the electrode might require several minutes to form [76].

All these interferences or sources of potential errors show that there is an increasing need for alternative ways to determine pH. One such alternative is the optical pH sensor (optode). pH optodes are nowadays widely used for pH-measurement and can be based on the change of a wide variety of properties of (mostly visible) light such as absorbance, fluorescence intensity or lifetime, energy transfer, reflectance and refractive index.

1.3 Optical sensors for wide range pH sensing

Optical and electrochemical sensors can be regarded as the two groups of sensors with the highest importance. In the earlier years of optical chemical sensors, optical pH sensors represented a group of chemical sensors that are complementary to glass electrodes. This is outlined in the following table where can be seen that many desired properties that are typical for optical sensors are difficult to be achieved with electrochemical sensors (i.e. a glass electrode) and vice versa. Moreover, some merits are given that may induce unwanted problems when using an optical or electrochemical sensor. The reader may decide on the usefulness of those for his proprietary use depending on his individual requirements.

Table 2 Comparison of the properties between optical sensors and electrochemical sensors (i.e. a glass electrode).

Figures of merit of pH Electrode	Figures of merit of Optical Sensors	Disadvantages of pH Electrodes	Disadvantages of Optical Sensors
good sensitivity/resolution and wide dynamic range (pH electrodes linear from pH 1 to 13)	very good sensitivity/resolution over sometimes smaller dynamic range (yet, pH 1-13 already published)	poor performance at extreme pHs	ambient light may interfere
small power requirements	no electrical power required	difficulties in remote sensing	photobleaching or leaching limited long-term stability due to of the immobilized indicator
activities rather than concentrations are measured	concentrations rather than activities are measured	source of electromagnetic interferences in an in-vivo measurement (cell)	surface potentials caused by charged sensor surfaces affect the sensor signal with varying ionic strength
miniaturization involves several steps	easy miniaturization		
additional reference element required	no requirements for additional reference element		
sensitivity to electrical fields	not subject to electrical interferences		
	insensitive towards magnetic fields and high pressure		
	light can transmit more information than electrical signal		
	multianalyte sensor arrays easier achieved		
	non-invasive		
	easy fabrication as disposable sensors		

The lack of the necessity of a reference electrode and the electrical safety are among the main reasons for an increasing need for alternative devices for pH measurements such as optical pH sensors (so called pH opt(r)odes). If highly charged indicators are used, even small changes in the IS can compromise sensor performance [77]. Therefore, such sensors should be used at constant IS only. Interferences of certain organic matter (in real samples) may limit the capabilities of both, electrodes and optical sensors because blocking of the glass membrane of electrode may occur or additional scatter that can compromise an optical readout. Optodes are considered the most long-standing and the best techniques for pH measurement and are further used in chemical and biological environments in solution and the gas phase, for monitoring of biochemical reactions and for physical applications such as measuring pressure, temperature, electric current and magnetic field [78]. pH optodes are based on changes of optical properties such as absorbance, fluorescence, luminescence, chemiluminescence, energy transfer or reflectance by measuring the intensity of light in various regions of the spectrum (UV, Visible, NIR, IR). Moreover, related properties such as light scattering, luminescence lifetime, refractive index, diffraction and polarization may vary upon changes of pH [79], [80]. pH optodes are more beneficial due to their flexibility, small size, low cost, fast response and light weight. Due to their electrical safety they may enable work in presence of flammable and explosive compounds and are suitable for continuous use in-vivo (e.g. in the blood stream) [81]. Moreover these sensors can be used in hazardous media without compromising their accuracy and have the ability to provide multiplexed or distributed sensing [80], [82], because of their small dimensions (down to μm size). They are suitable for remote sensing (even over distances of kilometres) and disposable use, which is typical for in-situ applications [83], [84], [85]. Unlike electrical sensors, pH optodes can be used for in-vivo measurements because of their immunity to electromagnetic interferences. Besides, optodes can monitor a broad range of parameters including pressure, temperature, and vibration [85]. This lead to the use of optical sensors in various fields such as chemical, biological, medical and telecommunication industries and in engineering research. Also pH optodes exhibit disadvantages such as leaching or

photobleaching of the optical probe due to limited long-term stability. Sometimes a poor selectivity and a limited dynamic range [86] is found. The response of pH optodes is a function of the concentrations of the acidic and basic forms of the indicator [87], which follows the mass action law (and associated with it, the Henderson-Hasselbalch equation) but not the activity of the hydrogen ion. Most optical pH-sensors consist of a pH-sensitive dye (i.e. a pH-indicator) immobilized in a polymer matrix which has to provide suitable mechanical and adhesive properties to prevent the indicator from leaching. Moreover, the polymer should be polar enough to permit a rapid access of the protons from the bulk solution into the membrane, so to provide a quick optical response of the sensor.

1.3.1 Absorbance and reflectance-based pH sensors

Most optical and fiber-optical pH sensors transduce reversible changes of the structure of the indicator that are induced by pH into changes of spectroscopic phenomena such as absorbance [88], and reflectance [89]. Absorbance or reflectance methods benefit from the fact that instrumentation is inexpensive and simple to use. Unlike luminescence intensities, absorbances measured by photometry do not vary from instrument to instrument because the ratio of transmitted to incident light is always detected. Furthermore, the change of absorbance and reflectance acquired by the instrument correlates to the color changes seen visually by the eye. This favors the use of such kind of sensors also by non-trained lab staff. On the other hand, both methods are not very sensitive and therefore require the use high concentrations of the pH indicator.

One of the first absorbance-based fiber-optical pH sensors for the physiological pH range was developed by Peterson et al. [90] in 1980. It was based on microspheres of polyacrylamide containing phenol red and smaller polystyrene microspheres (for light scattering) and responded in a pH range of 7.0 - 7.4 with almost 0.01 pH unit resolution. Microspheres have the merit that they can adsorb indicators on their huge surface or permit chemical bonding of pH indicators on the surface (and eventually inside the microsphere) to reduce leaching of the indicator. Further, the indicator may be embedded inside the polymer of the microsphere. All those methods lead to a

higher concentration of the indicator in the sensor membrane which is beneficial for enhancing the resolution in photometry. A sensor using cellulose acetate gave a wider detection range [91]. In 1984, Kirkbright et al. [92] designed a fiber-optical probe based on bromothymol blue to demonstrate the use of colorimetric indicators in sensors with a working range from pH 7-11. Edmonds et al. [93] used XAD-2 (styrene-divinylbenzene ion-exchanger copolymer) porous microspheres to absorb bromothymol blue as the indicator to optically probe pHs from 4-8 with a response time of 5 min. The suitability of four acid-base indicators immobilized on the same Amberlite XAD-2 resin for fibre-optic pH sensors was evaluated and an up to 3 pH units reflectance response was found [94]. Zemin et al. [78] compared the covalent immobilization of combinations of phenol red phenol blue and bromothymol blue on polyacrylamide microspheres embedded in a polytetrafluorethylene film. They fabricated a wide-range optical pH sensor that responded from pH 7- 10 within 2 min.

The use of only one indicator inside a sensor membrane usually leads to a restricted measurement range due to the ratio of protonated and deprotonated form of the indicator being dependent from the mass action law [95]. An example where the single pH indicators congo red (pK_a 3.7) or neutral red (pK_a 7.2) [96] were immobilized in a cellulose acetate membrane is a good example. The linear range of the sensor with congo red is pH 4.2–6.3 and the sensor with neutral red responds linearly from pH 4.1–9.0. Response time is about 20 s, the reversibility of the sensor is good and a 60 days long-term stability was found. Very similar optodes were published recently [97], [98]. A much wider range of pH response was found by bonding of a 1:1 mixture of neutral red and thionin (with different pK_a s) to an epoxy activated agarose film coated glass slide (ACGS). This yielded a sensor capable to monitor a pH range of 0.5–12, with two different slopes of the calibration plot. A fast response occurred within 1–2 min and the long term stability was at least 3 months with no leaching. The ionic strength of a sample up to 0.5 molL^{-1} did not significantly alter the sensor response. The reproducibility from 6 replicated pH measurements was better than 0.20% R.S.D. [99]. An autonomous and fully automated system for determination of pH within a

microfluidic chip coupled with an LED and a photodiode was constructed and validated for the pH range 4–9. The combination of phenol red, chlorophenol red and bromphenol blue gave an indicator mixture that is stable for > 8 months. The accuracy was good ($\text{RSD} \leq 2.82\%$) and the pH found in blind samples compared to the ones obtained by an accredited laboratory ($\leq 5.96\%$ relative error) [100]. Hampshire et al. [101] developed optic a fiber sensor to detect the pH in the gastric tract of a dog in a range of 0.5- 7. The sensor comprises two absorbance indicators with three pK_a values immobilized on polyacrylamide microspheres. Those were deposited on a plastic optical fibre. A precision better than 0.1 pH unit and an up to 3.5 min response time is found with a two wavelength measurment. The sensor is long-term stable with 0.2 pH unit drift over a 24 h and an interference of coloured or other substances or ionic strength in gastric juice samples was not found. Instead of using two or more pH indicators in one and the same sensor foil, the use of a dye with more than one deprotonable group on the same chromophore may be considered to construct a sensor. This principle is attractive for widening the detection range of a pH sensor because those dyes commonly have several pK_a s, and, associated with it, several colors. The pH-dependent equilibria between those are then used to measure pH over a wider range. A planar pH sensitive film was prepared by immobilizing purple cabbage pigment (which contains mainly an anthocyanin dye) as pH indicator in a sol–gel via dip-coating onto glass slides [102]. The sensor showed good reversibility between pH 2 and 7, a response time of 2 min and a linear range from pH 2 - 11. Another sensor using anthocyanines extracted from grapes was used in a novel green optical pH sensor [103]. Upon immobilization of the red grape extract on an optically transparent agarose biopolymer a wide range pH from 1–10 was covered. The response time was 3 min and the repeatability better than 0.3 % (RSD) and with no evidence of dye leakage.

The various pK_a s of bromopyrogallol red (BPR) indicator was used to construct sol-gel optodes in a silica matrix that responded reversibly from pH 3-9 within a minute, also in real samples [104]. This range is similarly wide as published in previous literature [105] for a sensor made with malachite green oxalate and bromocresol green indicators immobilized in a

triacetylcellulose membrane. It showed a faster response time about 10 s (compared to the former sensor) and both have a long lifetime (2 and 10 months). Another optical sensor employing a dye mixture on an activated triacetylcellulose membrane used the Giemsa indicator mixture to yield a membrane that is stable over 6 months of storage in water/ethanol. It has a 2 min response time and features a wide linear range of pH 3–12 [106]. Another research team used mixed the indicators m-cresol purple / bromocresol green in a sol-gel membrane [107] and obtained an optical pH sensor with a wide working range towards the acidic range. It responds from pH -1.04 - 8.70 and the spectra were modelled by an artificial neural network (ANN) with back-propagation training algorithm. The ANN could then be used to predict pH values from spectra from unknown samples. An excellent reversibility, no leaching and a rapid response time of less than 2 min were found. In 2013, Lee et al. [108] developed a fiber-optic pH sensor based on a sol-gel film with immobilized neutral red (NR). The film responds with color changes from red to yellow in the pH range of 5–9, due to two different absorption peaks, one at 536 nm and one at 461 nm. It can also be read out ratiometrically at those two wavelengths. Ratiometric evaluation of sensors can be an advantage to reduce instrumental drifts, misalignment of optical fibers, light scatter by the sample, dye leaching or inhomogenous dye loading [109]. The sensor shows good reversibility, reproducibility and a 20 s response time. A novel luminol derivative enabled double-wavelength photometric (A_{433} and A_{529}) and visible pH detection. A visible colour change from purple to bright yellow occurs over a wide range from pH 4.0-11.0. It responds in less than a few seconds and was demonstrated be low-toxic because it works in mouse fibroblast cells with pK_{a1} and pK_{a2} of 5.84 and 10.36, respectively. A pH dipstick with this indicator successfully detected the pH in some fruit juices.

Sbinohara et al. [110] developed the earliest pH sensor with a polyaniline (PANI) pH-sensitive thin film to be used at pH from 3-7. Unlike in other sensor concepts, the pH-dependent inherent absorbance of the polymer itself delivers the measured signal. A change of pH is associated with color changes from the green to the blue emeraldine base. In 1997 Wolfbeis et al. [111] used substituted PANI polymers which change colours as a function of pH and permitted optical pH

sensing with pH 1-12. In Fig. 8 absorbance spectra of PANI are shown which have two maxima at wavelengths around 600 nm (emeraldine base) and 810 nm (emeraldine salt) at various pH. PANIs offer many advantages like a simple sensor fabrication and a wide dynamic range because these polymers are basic polyelectrolytes with multiple pK_a values. The reproducibility is high, the response is rapid (60 s) and the detection in the near-IR region (840 nm) is less prone to spectral and light scattering interference. The activity of the immobilized enzyme urease could be monitored with the resulting films to detect urea. However, PANIs can have drawbacks such as interference from reducing and oxidizing agents, and the need for pre-/reconditioning (in 0.1 M HCl) before/after each measurement upon changes of pH. Sensors with PANI coated on polysulfone were also published [112].

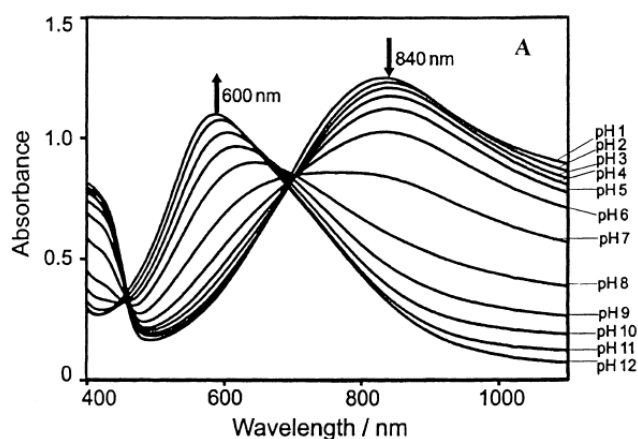


Figure 8 Variation of the absorbance spectra of polyaniline film (PA-1) with pH at 600 and 840 nm [111].

The pH-sensitive polymer (PANI) was also embedded into a microfluidic device as a coating inside a channel to for dynamic pH imaging and mapping (pH 2-8) [113]. The PANI layer showed an increasing absorption at 605 nm and a decreasing absorption at 832 nm with higher pH. pH gradients inside a channel can be detected by means of imaging and even changes of the pH of a sample travelling along the microfluidic can be detected on-line.

In 2011 Martinez-Olmos et al. [114] used a sensor array of four membranes containing acid-base indicators to cover almost the full common range of pH (0-12) by a evaluating the H (hue) coordinate of the HSV colour space. A handheld photometer was designed with OLED

illumination, photodiode array for red, blue, green (RGB) evaluation of the transmitted light, microcontroller and a programmed user interface for operation by a PC. Compared with the disposable optical sensor array that was published by the same group previously [115], [116], the current one has more simple electronics, less sensor membranes (4 instead of 11) and no scanner to acquire the colour change. The proposed system was used to determine real water samples (tap and river water from Granada, Spain). Moreover, a detailed study on three mathematical approaches for prediction of pH from the hue values of the sensing elements of the array was conducted [117].

In 2006 Egawa et al. [118] used poly-allylamine (PAA) polymer as a polycation to immobilize the anionic brilliant yellow (BY) azo dye inside layer-by-layer (LBL) pH sensitive films. BY is an azo dye used as a pH indicator in the neutral region and monitored by UV-VIS spectroscopy upon change of pH from 10 - 5 and vice versa. BY shows similar spectral properties in solution and inside the sensor film and a slightly changing pK_a value (8.16 and 8.37). The absorption maxima at pH 5 and pH 10 are 408 nm and 490 nm, respectively, with an isosbestic point at 442 nm (figure 9). The response time varies between seconds and 100 s depending on the basic to acidic response or vice versa.

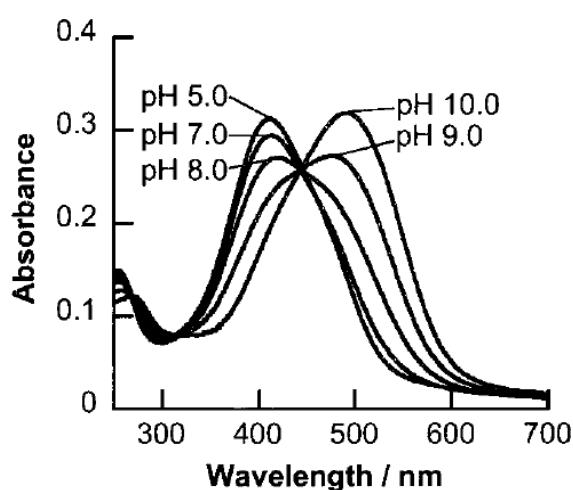


Figure 9 Absorption spectra of (PAA/BY)5PAA multilayer sensor in different pH solutions [118].

Another layer-by-layer sensor was published by Raoufi et al. [119] with anionic BY as a pH indicator showing a wavelength shift with pH change. Here, PAA serves as a cross-linker between

the layers and was deposited on the end of a bare silica core of an optical fibre. The wavelength shift of up to 50 nm permitted determination of pH in a range from 6.2 – 9.4. In 2002 Arregui et al. [120] used the Liquicoat[®] metal alkoxide colloidal solution (with about 7 % silica content; Liquicoat[®] serves for the deposition of anti-reflective coatings on displays) which is an alternative to sol–gel coatings, for the fabrication of optical sensors with an expanded operation range (pH 1-6). Liquicoat[®] solutions were mixed with an universal indicator solution and deposited on microscope glass slides. The sensors were fabricated by dipping into the sample and mounting a stack of up to 6 slides after they had been baked at 250°C for 2 min for three times. Fiber-optic detection revealed well repeatability, excellent stability and a response time of less than 90 s. This principle was used to construct evanescent field fiber-optical sensors by removing the cladding of a multimode fiber to substitute it with 20 layers of Liquicoat[®]. In fig. 10, the spectral response of the evanescent optical fiber sensor to various pH from 1- 6 is presented.

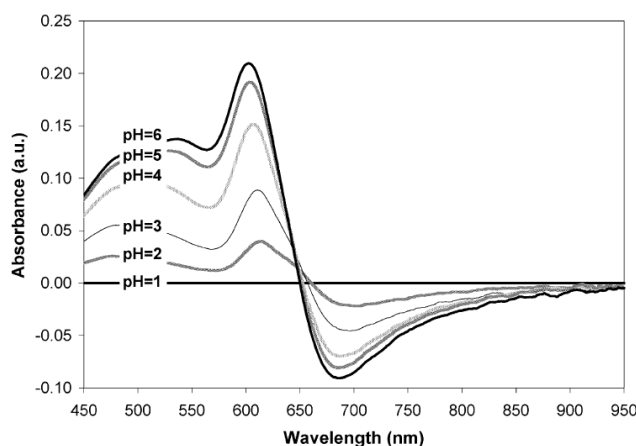


Figure 10 Spectral response of the optical fiber sensor respect to the pH. The spectral reference (absorption=0) was taken at pH1[120].

This completely different concept of a pH sensor is based on a no-core fiber segment into which phenol red is immobilized inside a sol–gel [121] (see figure 11).

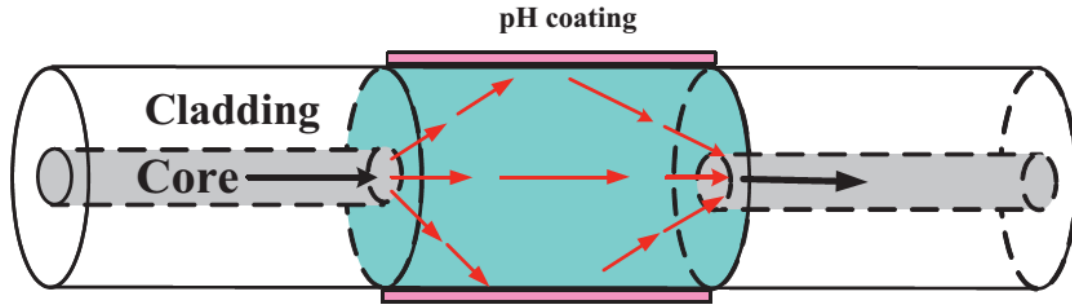


Figure 11 Schematic of a no-core optical fiber with pH coating [121].

A no-core fiber section inside an optical fiber can enhance the fraction of power of the evanescent wave at its end. Hence the surrounding environment can contribute to the effective refractive index of the no-core fiber, if there is an interaction between the evanescent wave of the excited modes and the surrounding environment. As a result, a different optical output power in the couple-back mode from the fiber is detected and analyzed with the beam propagation method. The sensor showed a large dynamic range from pH 1 and 13, the response time is 60 s, but the durability is 2 days, only. Very recently, Singh et al. described [122] the fabrication and characterization of another highly sensitive no-core fiber (NCF) pH sensor using a smart hydrogel. The NCF section which is a polyacrylamide hydrogel is placed between the two ends of single-mode fibres. The swelling of the hydrogel yields minima of the transmission of the hydrogel that shift with pH. The new sensor offers advantages such as high sensitivity of 1.94 nm/pH for a wide range pH from 3 - 10, a good linear response in both the acid and basic range, high sensitivity over a wide range of pH 3 – 10 and a fast forward response time ($t_f=10$ s) and back response time ($t_b=15$ s). Those are faster than the ones of similar sensors of the same detection principle published previously [123], [124], [125] which also show similar detection ranges. A good stability, repeatability and reproducibility are achieved. In fig.12, a stability test of an NCF pH sensor over 80 min at pH_s of 4, 6, 8 and 10 shows only a very small drift which proves an excellent stability.

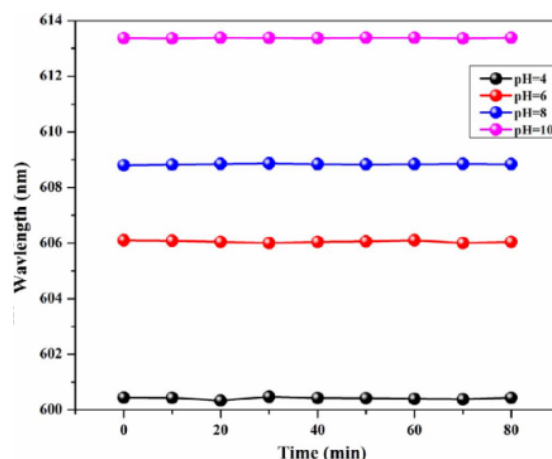


Figure 12 Stability curve of no-core pH sensor for both acidic basic [122].

A recent article reported a long-period fiber grating (LPFG) onto which a thin layer of a smart hydrogel was deposited. From the shift in the resonance wavelength a pH range from 2– 12 was accessible with a sensitivity of ~ 0.66 nm/pH and a response time of less than 2 s [126]. Another no-core fibre optic pH sensor was prepared by immobilizing a mixture of three pH indicators (cresol red, bromophenol blue and chlorophenol red) onto the unclad fibre surface using a sol–gel matrix. A broad response to pH values between 4.5–13.0 was found, with a response time of 5s. Reversibility and repeatability of the response was limited to few cycles due to cladding failures [127].

1.3.2 Luminescence-based pH sensors

As discussed in the previous chapter, also most luminescent optical pH sensors are based on the pH dependent change of the optical properties of certain indicator molecules immobilized on/in certain solids [128]. Luminescence is especially suitable for optical sensing because of its high sensitivity, selectivity, and due to the emission being evenly emitted in all directions. Unlike absorbance or reflectance, there are more measurands available from luminescent sensors. In principle, luminescence not only offers emission intensity to be detected but, also luminescence quenching, luminescence lifetime, luminescence polarization, energy transfer efficiency or the shift of the wavelength of an emission maximum or the intensity ratio of two emission bands may be acquired. In many schemes, an embedded fluorophore undergoes either a spectral or intensity

change upon reversible protonation/deprotonation. One of the first fluorescence based optical pH sensors by Wolfbeis et al. [129] in 1986 showed two setups of optical sensors for continuous measurement of near-neutral pH values. The sensors are based on glass-immobilized fluorescent pH indicators and allow the determination of pHs the range from 5-8.12 with 1-hydroxypyrene-3,6,8-tirsulphonate (HPTS) (see fig. 13) and 4.4-9.6 with 7-hydroxycoumarin-3-carboxylic acid (HCC) (see fig. 14).

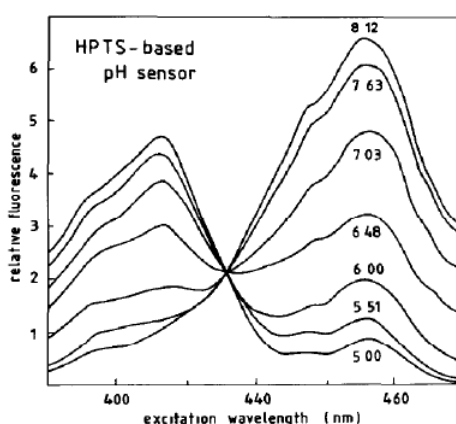


Figure 13 Excitation spectra of glass-immobilized HPTS at various pH values (phosphate buffers, 23 °C, emission taken at 520 nm.). The shoulder at 455 nm. Is assigned to a Raman band [129].

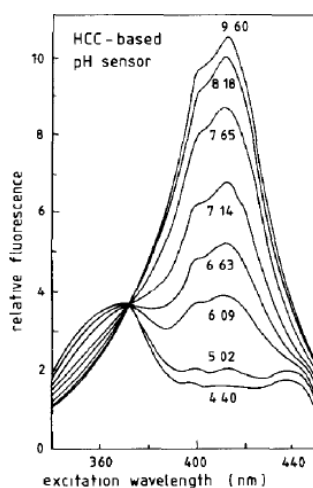


Figure 14 Excitation spectra of glass-immobilized HCC at various pH values (phosphate buffer, 23 °C, emission taken at 460 nm.). The shoulder at around 400 nm. Is assigned to a Raman band [129].

The sensor shows a precision of ± 0.01 units and response times (t_{99}) are about 1 min (see fig. 15). Adverse effects of ionic strength are eliminated by silanization of the glass surface. Attaching the sensing layers to the end of a bifurcated optical light guide provides a device for remote sensing of pH.

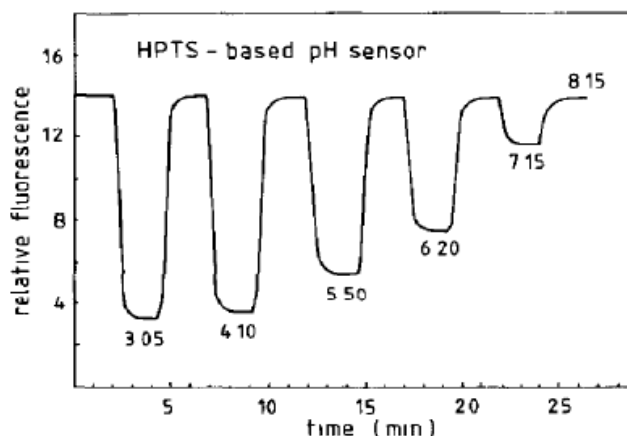


Figure 15 Response of the HPTS-based sensor towards changes in pH. The upper level corresponds to pH 8.15. Excitation at 465 nm. Emission taken at 520 nm. [129].

Another sensor was published where HPTS was just embedded into a sol-gel as an ion-pair with hexadecyltrimethylammonium bromide (CTAB) [130]. The pH range and response times and reversibility closely resemble the data from the previous paper, yet a higher dependence of the pK_a of ionic strength was found. Qin et al. [131] show an example of a ratiometric fluorescence pH sensor. For this purpose, a pH-sensitive porphyrin derivative served as the indicator dye and a pH-insensitive benzothioxanthene derivative as a reference dye for fluorescence ratiometric measurement of pH from 1.5-9. Ratiometric fluorescence evaluation of sensors can be an advantage to compensate for misalignment of optical fibres and inhomogeneous dye loading and to reduce instrumental drifts, light scatter by the sample or the sensor material, dye leaching [109]. To prevent leakage, both dyes were copolymerized with the sensor cocktail on a silanized glass surface. The fluorescence intensity ratio varied linearly as a function of pH 1.5 to 5.0 and the sensor featured a rapid response time (60 s) and one month lifetime. An application to real samples was demonstrated with waste water and water samples containing heavy metal ions. Another paper focuses more on the general design of a whole instrument for pH ratiometric fluorescent measurements [132]. The sol-gel matrix houses mercurochrome (a xanthene dye) as pH indicator and is placed at the end of a fiber. A blue light-emitting diode excites green fluorescence emission and a ratiometric measurement accesses a pH range of 4-8. The applicability of this device was tested for its performance in pH analysis in tap and bottled water [133]. A new 10-(4-aminophenyl)-5,15-

dimesitylcorrole was found to serve as an indicator with three deprotonation steps. Upon immobilization in a sol-gel the pH sensor was found to respond over a pH range 2.17–10.30 [134]. The response time is two min and the wet stability is one month. Temperature does not show obvious effects from 0-50°C.

Two ways of for fast and easy covalent immobilisation of naphthalimide indicators on a thin film of an amine-containing polyethylene glycol are shown to have little effect on the detection range from pH 5-9 and the pK_a of the naphthalimide [135]. Double layer spin-coating of quantum dots (QDs) with 525 nm and 605 nm emission and a mixture of neutral red and methyl yellow in the other layer resulted in sensor membranes in which the QD emission is transmitted depending on the pH-dependent absorption of the indicator couple [136]. The QDs are excited at 400 nm and the dynamic range of the optode is from pH 4-10. The ratiometric response of luminescence to pH is stable over 6 months. The evaluation of the ratiometric response with chemometric methods can serve to extend the calibration range of a sensor compared to the ratiometric method. This was demonstrated by optical pH sensing with aminofluorescein [137] where the pH value influences the spectrum in a complex way. The fluorescence spectra are reduced to a few data points and hence, no high-resolution spectral sensors are necessary. Reducing the resolution of the fluorescence spectra from 0.2 to 10 nm increased the error of the calculated pH values from 0.07 to 0.13 pH units, only. Novel iminocoumarin derivatives were shown to be useful pH indicators after covalent immobilization on the surface of various types of amino-modified polymer microbeads. The embedding of a mixture of microbeads of two indicators (having different pK_a s) into a hydrogel matrix yielded sensor membranes with high brightness, excellent photostability and compatibility with light-emitting diodes and a wide detection range from pH 1–11 [138]. Novel water-soluble, multicolor fluorescent graphene quantum dots of 11 nm size were reported as a new material that shows both a visible color change and luminescence response to pH from 1- 14 [139]. The luminescence response to pH shows either increasing intensity between pH 1-7 or decreasing luminescence between pH 7-14. The luminescence of the GQDs was also found to be responsive to temperature changes,

demonstrating the great potential as a dual probe of pH and temperature. However, this temperature sensitivity requires strict temperature control if pH detection is done in real samples (e.g. biological fluids). An optical fiber-optic pH sensor coated with CdSe/ZnS quantum dots (QDs) and oxazine 170 perchlorate (O170) in an ethyl cellulose layer provided pH sensing in the pH range 0.9-12.2. LED excitation at 405 nm yielded a ratiometric response at 575 nm and 655 nm. The sensor has a linear relationship with pH in the 0.9-12.2 range. This makes the inexpensive pH sensor insensitive to fluctuations of the intensity of the excitation source. Unlike when using a single ratiometric fluorophore, leaching or photobleaching of the organic dye will potentially not be compensated for [140]. N-doped carbon quantum dots (NCQDs) with a quantum yield of up to 36.3% respond to pH by luminescence decrease in a broad range pH from 5-13.5 due to protonation of pyridinic nitrogen atoms on dots (shown in fig.16). The luminescence intensity peaks at 400 nm and Ag^+ and Fe^{3+} ions respond in μM and nM concentration with an increase or decrease in aqueous solution, respectively. NCQDs display low toxicity to cells and bioimaging experiments reveal NCQDs to be superior to Carbon quantum dots CQDs with respect to photobleaching [141].

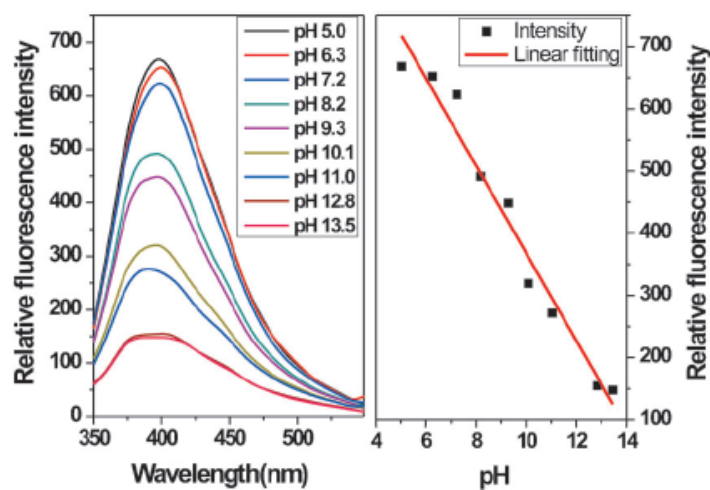


Figure 16 Fluorescence intensity versus pH values and the resulting linear relationship [141].

The dual lifetime referencing (DLR) scheme is shown to provide a referenced readout of pH via lifetime measurements, either in the frequency or the time domain. Here, an analyte-insensitive long-lived Ru-luminophore with μs -decay times is added to the sensor cocktail with the analyte-

sensitive fluorophore (here, the pH indicator having a decay time in the nanosecond range). If both, absorption and emission spectra of those indicators overlap and all probes are excited with one single light source and luminescence is detected simultaneously, the combined luminescence intensity is converted into a phase shift (in frequency-domain DLR) which is then related to analyte concentration. A linear relation exists between the cotangent of the phase shift and the fluorescence intensity of the pH indicator. Frequency-domain DLR is one of the best referencing schemes that exist because it compensates interference from drifts of the light source and the detector, a misalignment of optical fibres and of other optical components, light scatter by the sensor material and partially inner filter effects and inhomogeneous dye loading of the sensor membrane [109]. Aromatic fluorescent Schiff bases were proposed as pH sensing fluorescent probes for the alkaline pH range 7.0–12.0. They can be excited at around 570 nm and exhibited quantum yields until 37 % when embedded in PVC membranes. The response times vary between 3–13 min and a slight cross sensitivity to Hg^+ and Fe^{3+} , respectively, was seen [142]. Another concept is to use metal-ligand complexes or lanthanide complexes to obtain luminescent pH probes. Those complexes have the merit that by attaching various ligands with various functional deprotonable groups (and hence various pK_{a} s) a wider pH range becomes accessible [143]. Potential candidates for such luminescent probes are complexes of Ru^{2+} , Re^+ and Os^{2+} and Eu^{3+} , Tb^{3+} , Dy^{3+} and Sm^{3+} . The first three metal ions offer six coordination sites in an octahedral coordination geometry whereas the lanthanide ions even provide 8-9 coordination sites [144]. Attaching a common bidentate ligand would then provide 3-4 ligands to be used with different pK_{a} s. The advantage of this concept is that only one excitation and detection wavelength are required for detection of pH, unlike in schemes which use dye mixtures which often require several excitation and emission readouts. This facilitates the pH readout and retains the possibility to include another luminophore for referencing into a sensor membrane e.g. to use the common DLR scheme [109]. A further advantage is that the synthetic effort to obtain various ligands is much less (many ligands can be purchased) compared to the many steps required to prepare several derivatives of the same class of dyes (to retain excitation

and emission wavelengths). Therefore, this multi-pK-ligands-complex scheme can open a gate for new wide-range optical pH probes and sensors. One of the few examples uses a Ru^{2+} complex carrying two different polypyridyl ligands with CO_2H and phenolic OH as different deprotonatable groups. This results in a broad pH sensing range from 3-9 [145]. The concept of using indicators from the same class of dyes, yet with various substitution patterns was shown for asymmetric perylene bisimide (PBI) dyes. They carry one amino functional substituent to warrant response to pH and the emission follows a photoinduced electron transfer (PET) scheme. Another substituent enhances solubility of the overall very nonpolar chromophore in polar solvents. Upon embedding PBIs in hydrogels, luminescence quantum yields >75% are detected in the protonated state [61]. If dyes with different substitution patterns are embedded inside the same membrane, sensors with a working range of pH 4-8 were obtained. Their similar spectral properties permitted a joint readout but the response time can be up to 5 min. Ionic strength was found to have very little effect on the sensor membranes. Lobnik et al. [146] co-immobilized non-fluorescent bromothymol blue with a luminescent europium 4-trifluoromethylcarbostyryl complex in a sol-gel membrane which responded to pH from 5-9. The pK_a was 7.29 at an ionic strength 0.1 M and 6.05 at an ionic strength of 1.0 M (KCl). Borisov et al. [147] presented a new class of functionalized rhodamines the pH-sensitivity of which arises from an intramolecular photoinduced electron transfer process (PET) originating from piperazine groups. The chromophore can be coupled covalently to thiols (mercapto groups) via a pentafluorophenyl group in the 9-position of the xanthene core. Luminescent sensor membranes were shown based on silica beads (pH 3-8) and Poly-HEMA (pH 4-8) with 2-3 min response times. The photophysical properties of the indicators closely resemble those of common rhodamines and the sensors have a high brightness (quantum yield of 0.6), and can be used in very beneficial dual lifetime referencing sensing schemes. Those have the advantage that they are immune to most of the common instrumental sources of interference, as outlined earlier [109] Eight tetraaryl aza-dipyrromethene 4,4-difluoro-4-bora-3a,4a-triaza-s-indacene (aza-BODIPY) dyes that can detect pH through a PET have been proposed with pK_a values between 7.2 and 11.4. The fluorophores show

pronounced changes in the emission 700 nm and the sensor foils produced show good brightness, excellent photostability, and modest quantum yields between 0.02 and 0.18. Their high potential for a variety of biotechnological, biological and marine applications is shown by dual lifetime referencing detection of the pH-gradient from the moth into the gastric cavity (i.e. the stomach) of a coral [148]. As a new material conjugated polymer nanoparticles were synthesized where a polyfluorene-based polymer was appended with thiophene units carrying pyridyl moieties incorporated in the backbone of polymer chains. An optically transparent amphiphilic polymer dispersion displayed a pH-sensitive fluorescence emission from pH 4.8–13. This is accompanied by a distinct change of the luminescence lifetime in the ps range. The pH sensing capability of the material is due to the reversible protonation/deprotonation of pyridinic nitrogen atoms. Fluorescence at around 470 nm decreases with increasing alkalinity [149]. A series of PET pH indicators based on a naphthalimide core, a spacer and various aniline or phenol electron donors were combined in various ratios in D4 hydrogel. This yielded a series of novel optical sensors with a working range up to pH 1–14. A useful feature is that all indicator dyes inside the sensor membrane have the same excitation and emission maxima. This enables the use of simple equipment with only one excitation source and one emission wavelength. A further desired feature is that the emission intensity of all indicators shows a decrease of emission at higher pH which facilitates the combination of many dyes in one sensor membrane. The sensors show excellent stability, reversibility over many cycles and 60 s response times [150]. Similarly, 8 new azo-BODIPY indicators with pK_a values from the acidic to the basic range were used to fabricate sensors in D4 hydrogel that respond from pH 2-9 by combining four of them in the same sensor foil. Their advantages are longwave absorption/emission bands in the red/near-infrared (NIR) spectral region where autofluorescence from real (biological) samples is low and inexpensive LEDs can be used for luminescence excitation. High molar absorption coefficients ($\sim 80\,000\text{ L M}^{-1}\text{ cm}^{-1}$) and good quantum yields ($\sim 20\%$) and high photostability are further favourable properties of the new indicators [151]. A set of even 17 BODIPY derivatives as pH indicators were presented to cover the

1-13 scale for pH measurement in aqueous solution. By combining 12 of them with 4 four reference dyes on an array pH can be determined with LED excitation in a home-made inexpensive device that is attached to a smartphone. An App based on Andriod software converts luminance and hue into pH values together with two reference values obtained from a calibration. In the hydrogel mixture on the pH dipstick all dyes show very similar spectroscopic properties such as excitation/emission wavelengths and quantum yields of >55 %. Unlike common pH indicator paper the dipsticks can be reused up to 10 times [152] with a precision of ± 0.2 pH units. This makes the whole setup well-suited for use by non-experts and in-field use. The conjugation of a tetraphenylethene (TPE) and an N-alkylated cyanine yielded a red-emissive zwitter ionic hemicyanine dye, named TPE–Cy. TPE–Cy shows a aggregation-induced emission (AIE) behaviour at pH 5-14 which means that by motions of a conformationally twisted and strained molecule exciton emission is annihilated through nonradiative decay. In the aggregate state (upon change of pH) these motions are restricted and radiative decay (i.e. strong emission) is detected. The dye has a large Stokes' shift (>185 nm) and this prevents concentration quenching. TPE–Cy is able to sense pH in various ways. Either photometric (pH 9-13) or fluorimetric via different emission colours and intensities. The red emission at 630 nm is strong to moderate at pH 5–7, weak to no emission is seen at pH 7–10, and no emission to strong blue emission at 480 nm is detected at pH 10–14 [153]. The colour change induced by pH-switching is reversible and well reproducible. Various 1,4-diketopyrrolo-[3,4-c]-pyrroles were proposed as fluorescent pH-indicators for a pH range from 5-12. At high pH (>9), the dyes exhibit changing absorption and fluorescence spectra due to deprotonation of the nitrogen atoms of the lactam rings. Their pK_a value varies up to 1.5 in various hydrogels and also sensor beads were presented. A planar foil doped with these nanoparticles was shown to enable a ratiometric red to green readout with an RGB camera from pH 5.4-9.6. The dye showed moderate photostability [154]. The surface curvature distribution on hollow mesoporous silica–dye nanoparticles can be a means to widen the working range of optical pH sensors. This was shown by particle sensors monitoring the intracellular pH via ratiometric fluorescence. For this

purpose, pH-sensitive fluorescein isothiocyanate and rhodamine B isothiocyanate as reference dye were embedded into those silica nanoparticles which permitted monitoring of the intracellular pH between 4.5 and 8.5 by confocal fluorescence microscopy [155]. Upon tuning of shell thickness and of the pore size distribution or the size of the nanoparticles (by sonication) the pH range could be extended up to pH 3.2-9.0 [156]. Photochemical cross-linking of a triblock copolymer containing poly(coumarin methacrylate) yielded polymeric core-shell-corona nanomicelles with a broad pH measurement range from pH 3.4-8.0. Binding of pH-sensitive fluorophores (Oregon green 488, 2',7'-bis-(2-carboxyethyl)-5-(and-6) carboxyfluorescein) and Alexa 633 as a reference dye provide the enhanced sensing range due to a variety of microenvironments of the respective fluorophore. The particles are suitable for ex vivo cellular measurements, however two different excitation wavelengths are necessary for the ratiometric readout of the pH [157]. Among the new 2D materials, also metal-organic frameworks (MOF) have been used for sensing of pH. MOFs are hybrid materials made from organic linkers and metal ions or clusters and can be made luminescent by embedding luminescent ions or ligands. UiO-66-NH₂ contains clusters of 6 Zr atoms (Zn₆O₄(OH)₄) and the linker 2-aminoterephthalic acid and is easily synthesized. The introduction of indole groups at the linker provides increased framework chemical stability under basic conditions, Therefore, sensing from pH 1 up to pH 12 is possible. By using the fluorescence of the MOF and the 380 nm emission of polystyrene cuvettes, the pH of several buffers could be determined with good precision [158]. Another modified MOF for pH sensing was created by encapsulating Eu³⁺ cations with a dicarboxy-4,4'-bipyridine. With a good chemical resistance to both acid and alkaline pH, a detection range from 1.06-8 was found using the emission of Eu³⁺ at 615 nm. Fluorescence imaging of the pH in PC12 cells with the MOF was tested in vivo. This shows that MOFs can be promising materials for fluorescent pH sensing in vitro and in vivo [159]. Gold/silver core-shell nanoparticles with p-aminothiophenol (pATP) decorated multiwalled carbon nanotubes yielded pH-sensitive particles with a wide dynamic range (pH 3.0-14.0). The pH is derived from the ratio of surface-enhanced Raman scattering (SERS) signals of p-aminothiophenol (pATP) molecules. The

particles show biocompatibility and low cytotoxicity, as derived from intracellular pH measurements with a pH resolution of 1.0 pH unit [160]. The so-called “counterion-induced vesicle (CIV) formation” is a strategy where an EDTA counterion induces spontaneous formation of stable vesicles from imidazolium salts in aqueous media. The counterion-induced vesicles (CIVs) feature spontaneous formation and simple preparation and can further chelate europium (III) ions. Depending on the protonation state of the carboxylic acid groups of the EDTA the europium emission in aqueous media is modulated with a linear response from pH 3-11 [161]. This concept was expanded by covalently embedding three pH-sensitive fluorophores (difluoro-Oregon Green, Oregon Green 488 and fluorescein) and one pH-insensitive Alexa 568 into a nanoparticle hydrogel matrix [162]. These quadruple-labelled nanosensors featured pH-sensitivity from 1.4-7.0 which covers the physiological pH range in all living cells. Other ions at physiological concentrations do not interfere. The positive surface charge of those nanosensors promotes uptake into HeLa cells. The pH in lysosomes where the particles were localized was found to be 4.6 ± 0.1 and modulation of pH could be followed by fluorescence microscopy imaging. These measurements were consistent with earlier measurements [163] and the identical nanoparticle matrix in both papers points to a low cytotoxicity of the nanosensors. In 2016 Yao He et al. [164] demonstrated that fluorescent silica nanoparticles (SiNPs) with pH-sensitive dopamine (DA) and pH-insensitive rhodamine B isothiocyanate can yield particles with a ratiometric luminescence response from pH 4-10. Their minimal toxicity enables pH sensing in cells where their bright fluorescence and high photostability further facilitates fluorescence microscopy measurements. Hence, detection of lysosomal pH changes governed by nigericin in live HeLa and MCF-7 cells could be followed over 30 min. Therefore, real-time sensing of pH in living cells seems feasible. A Förster resonance energy transfer (FRET) system with a europium complex as the donor and carboxynaphthofluorescein as a pH sensitive acceptor forms a couple that responds to pH from 3-9. This probe either offers ratiometric luminescence intensity-based readout of pH or a referenced lifetime-based readout of the pH. The large Stokes' shift about 250 nm is advantageous for measurements in real samples to

suppress scattered excitation and background luminescence. It is even more advantageous to use the long μs decay times of the lanthanide complex because this enables delayed measurements when the background fluorescence has decayed to 0 after few ns. This was demonstrated by successful pH measurements in urine samples [165]. In 2016 Zhao et al. [166] synthesized carbon nanoparticles (N-CNs) that have nitrogen-rich functional groups as fluorescent pH indicator. The sensor has a broad working range from 3.0- 12.0. The N-CNs exhibited blue photoluminescence with an absolute quantum yield (QY) of 11.0%. The mechanism responsible for the pH-sensitive properties involved photoinduced electron transfer (PET) from aniline groups to the N-CNs. The as-prepared N-CNs exhibited low cytotoxicity and excellent biocompatibility with cell viabilities of more than 87% in pH fluorescence imaging of live T24 cells. In 2017, Szita et al. [167] demonstrated and developed real-time pH monitoring of the progression of an enzymatic reaction in a microfluidic side-entry reactor to improve the conversion yield of inhibition-prone enzyme reactions. Two different types of optical pH sensors were integrated, each with a different dye, at several positions in the reactor channel which enabled pH monitoring over a broader pH range 3.5 - 8.5. The new sensor showed high reproducibility and was heat stable to sustain the temperatures typical for thermal bonding of microfluidic devices. This robustness greatly facilitates their integration into enclosed microfluidic devices. In 2018, Liu et al. [168] developed and present three near-infrared ratiometric fluorescent probes for pH. The probes show ratiometric fluorescence responses to pH changes from 7 to 3 in buffers and in live cells. The last probe displays well-defined dual emissions and excitations and achieves remarkable ratiometric changes of the signal-to-background fluorescence ratio up to 238-fold.

1.4 pH sensors in real samples

Some of the reviewed pH sensors have been used in real environments. Martinez-Olmos et al. [113] used different real water samples (14) (tap and river water) and compared the accuracy of their pH sensing array with the accuracy of a glass electrode. The correlation coefficient showed a high positive correlation between the real and predicted data. Lu et al. [169] measured

photosynthetic activities of cyanobacterial cell cultures (*Synechocystis* sp. PCC 6803) during the exponential and stationary growth phases by monitoring pH and O₂ measurements in a cell suspension by using multianalyte sensor films [170]. The photosynthetic activity in the exponential phase (and the of the pH) was higher than that in the stationary phase. Wolfbeis et al. [171] used luminescent pH nanosensors in a conventional layer of agarose gel for fluorescence imaging. The growth of *Escherichia coli* (*E. coli*) on a pH-sensitive agarose film in a Petri dish was determined. The green luminescence (under 405 nm illumination) emitted by the pH probe is very sensitive to pH value while the red luminescence of 5,10,15,20- tetrakis(pentafluorophenyl)porphyrin (TFPP) is not sensitive to both pH and oxygen at different concentrations. TFPP was chosen because fluorinated porphyrins are resistant to oxidation by reactive species [172]. On encapsulation of the TFPP in the hydrophobic core of the particles, they are well protected from interferences by potential quenchers [173]. Thus, the color tint of the red and green emission undergoes a distinct change from red to green when pH values are increased stepwise from 5.5 to 9.0.

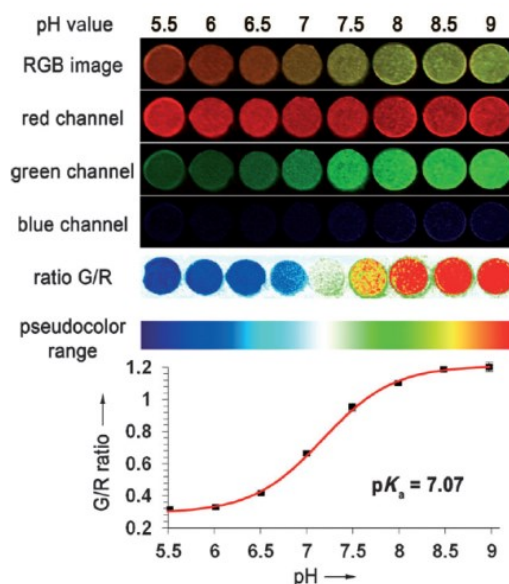


Figure 17 Optical response of the pH-sensitive agarose Petri dish [171].

Rerolle al. [174] designed simple and low cost spectrophotometric an absorption-based microfluidic device for the autonomous measurement of seawater pH. The device consumes less than 30 mL of

indicator over one month. The device is not a sensor in the strictest sense, and installed on a research vessel and measured the shelf water pH in the North Sea, the northern Atlantic ocean acidification, and the Bay of Biscay.

1.5 Response time & lifetime

The response time represents an important feature for the performance of a specific sensor. The sensor response time is defined as the time required for the sensor output to reach 95% or 99% respectively, of the change from its starting value to the final settled value [175]. It is important an factor in analytical applications and it depends of the structure and type of materials, thickness of the sensing layer, the amount of indicator, temperature and fabrication scheme of the sensor membrane [176]. The buffer capacities of the sensing layers should be small relative to the buffer capacity and the amount of the sample reacting with the sensor. The sensors showed response times ranging from a few seconds to several minutes. Klimant [61] showed memberanes with reversible and fairly fast (t_{90} is 5 min on going from pH 6 to 4.3 and <30 s in the reverse direction) response times. Longer response times (>1 h) for thin ($2\text{ }\mu\text{m}$) sensing layers are disadvantageous for online monitoring but a long lifetime of the membrane of 1 month (see fig.18) was found.

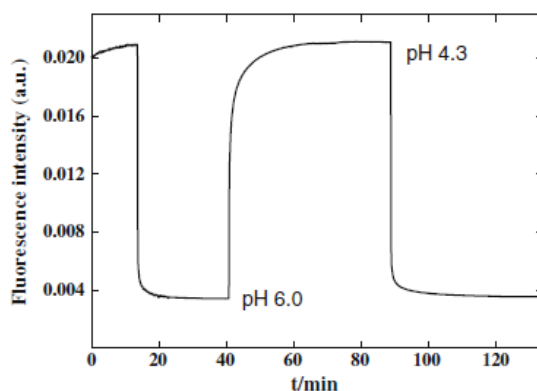


Figure 18 Response curves of 2b in D4 (dye content 1%, layer thickness $5\text{ }\mu\text{m}$) to dynamic changes of pH [61].

Noroozifar [105] showed a faster response time of an optode about 10 s in the pH transition interval between 1.34 and 5.01 at 624 nm (see fig.19). This sensor has an even longer lifetime (10 months) which is similar to a pH electrode. Another optical sensor employing a dye mixture on an

activated triacetylcellulose membrane used the Giemsa indicator mixture, to yield a membrane that is stable over 6 months of storage in water/ethanol. It has a 2 min response time and features a wide linear range of pH 3–12 [106].

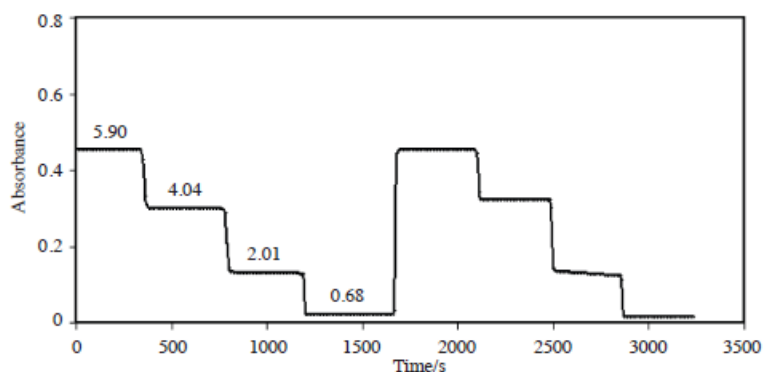


Figure 19 Response reproducibility of the membrane at 624.0 nm for the alternative change in pH from 5.90 to 3 different pH values of 4.04, 2.01, and 0.68, respectively. (Conditions for preparation of membrane, solution contains 0.0375m/v MGO, absorbance at 625 nm, respectively, preparation time, 2 min. and preparation temperature, 60 [106])

1.6 Precision of pH measurements

A light precision of pH measurements in the pH range 7.995 - 8.210. The system featured a short term precision of 0.001 pH unit ($n = 20$) and an accuracy within the range of a certified Tris buffer (0.004 pH units). Over five weeks of deployment of the instrument at the sea (see table 2) [174].

Table 3 Precision and accuracy of certified Tris buffer measurements [174].

Average discrepancy between certified pH and measured value for Tris buffer ($n = 20$)	Precision (pH unit) of replicate Tris buffer analyses ($n = 20$)	Date of analysis
0.0007	0.0007	11/06/2011
0.0021	0.0009	23/06/2011
0.0025	0.0011	07/07/2011

1.7 Repeatability & reproducibility of pH measurements

By intensity measurements, the response stability of the pH sensors over time is depending on the stability of the light source and the photo degradation of the dye. Most review literature reported show excellent reproducibility measurements. pH electrodes are highly reproducible with sensitivities of -77.6 ± 2 mV/pH and potential drifts of 2–3 mV/month (static solution) [72]. This is

a similar level as the [134] the optode in fluorescence intensity values at 656 nm during alternately pumping buffer solutions of pH 2.17, 4.96 and 8.08 with the standard deviations were found to be 114.7 ± 0.9 ($n = 5$, pH = 2.17), 132.8 ± 0.8 ($n = 5$, pH = 4.96) and 149.3 ± 0.6 ($n = 5$, pH = 8.08), (show in fig.20).

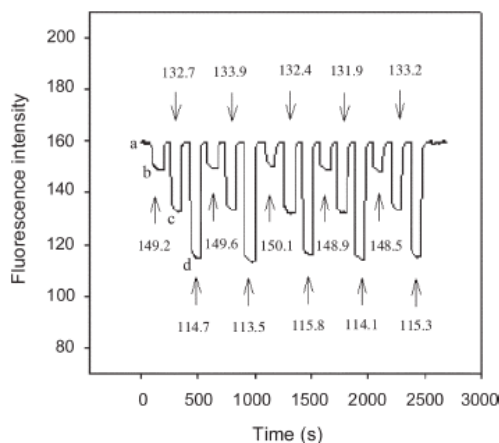


Figure 20 Fluorescence responses vs. time by alternately pumping different pH buffer solutions (a) 11.02; (b)8.08, (c) 4.96, (d) 2.17. The fluorescence intensities are in arbitrary units given by the time scanning, Mode of the Hitachi F 4500 instrument [134].

1.8 Effect of ionic strength

Ionic strength causes pH errors which depend on the type of indicator and matrix which is used. When the salt composition of the sample solution differs significantly from the calibration solutions or when it changes during measurements the resulting errors can be particularly significant. Due to the effects of salt composition of the sample, pH optodes performs best under well-defined sample conditions [87]. Wolfbeis and Offenbacher [177] described surface chemistries of pH sensors with different sensitivities towards changes in ionic strength by immobilizing 7-hydroxycoumarin-3-carboxylic acid covalently onto porous glass supports with different surface chemistries. In the first sensor, the indicator is embedded in an uncharged micro-environment. This sensor is highly sensitive towards changes in ionic strength. In the second sensor, the indicator is embedded in a highly charged environment. This sensor is less sensitive towards changes in ionic strength in the range of 100- 200 mM and practically independent of ionic-strength variations of the sample.

While Wolfbeis and Mohr [95] showed sensor with almost no effect of IS. Fig. 21 shows the pH titration of a sensor membrane with various concentrations of sodium sulfate added to the buffer (consists of 0.04 M sodium acetate, 0.04 M boric acid, 0.04 M sodium dihydrogen phosphate). The pK reduced from 7.64 to 7.45 on going from 0 to 1.0 M sodium sulfate. The effect of IS on the pK , is more expressed at low IS. Here, the shift is 0.09 units on changing from 0 to 0.1 M sodium sulfate, and 0.1 units on going from 0.1 to 1.0 M sodium sulfate (see Fig. 21).

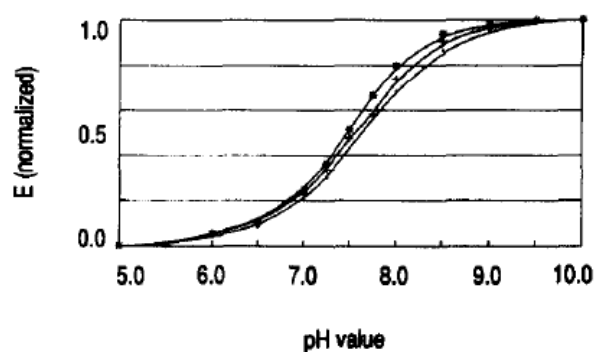


Figure 21 pH titration plot of membrane M-3 in the presence of 0, 0.1 and 1.0 M sodium sulphate (absorption measured at 560 nm.), showing the effect of ionic strength [95].

Ertekin et al. [142] show the effect of ionic strength on the PVC doped Schiff bases in 135mM NaCl containing 0.005 M phosphate buffer which covers the physiologically important salinity level. The pK_a values of the indicators were found to be 10.25 ± 0.07 and 9.17 ± 0.04 , respectively. In clinically important salinity levels, the pK_a of one dye exhibited an increase of 0.37 pK_a units with respect to its original value. In contrast, the pK_a of the other dye decreased from 10.30 to 10.25.

1.9 Aim of work

The ultimate goal of this work was to design new low-cost optical luminescent pH sensor membranes and a sensor microtiterplate containing lanthanide complexes for continuous quantitation of pH over a wide range. These sensors should overcome the typical drawbacks of classical optical indicator dyes with a dynamic range of up to 3 pH units only (due to the mass action law) and of electrochemical sensors which cannot be miniaturized to μm -size or enable

imaging over larger areas (e.g. in cell culture). We therefore introduced a new design concept for wide-range pH indicators and sensors that employs lanthanide complexes with ligands that have various pK_a s. Hence, a wider pH range becomes accessible.

1.10 References

- [1] J. C. G. Bunzli and C. Piguet, "Taking advantage of luminescent lanthanide ions," *Chem. Soc. Rev.*, vol. 34, pp. 1048–1077, 2005.
- [2] M. H. V. Werts, "Making sense of lanthanide luminescence.," *Sci. Prog.*, vol. 34, pp. 101–131, 2005.
- [3] E. Soini and I. Hemmila, "Fluoroimmunoassay: Present status and key problems," *Clin. Chem.*, vol. 25, pp. 353–361, 1979.
- [4] J. G. SenáGupta, "Determination of scandium, yttrium and eight rare earth elements in silicate rocks and six new geological reference materials by simultaneous multi-element electrothermal atomic absorption spectrometry with Zeeman-effect background correction," *J. Anal. At. Spectrom.*, vol. 8, pp. 93–101, 1993.
- [5] J. P. Leonard, C. B. Nolan, F. Stomeo, and T. Gunnlaugsson, "Photochemistry and photophysics of coordination compounds: Lanthanides," *Top. Curr. Chem.*, vol. 281, pp. 1–43, 2007.
- [6] H. Bethe, "Zur Theorie des Zeemaneffektes an den Salzen der seltenen Erden," *Zeitschrift für Phys.*, vol. 60, pp. 218–233, 1930.
- [7] H. A. Kramers, "La rotation paramagnétique du plan de polarisation dans les cristaux uniaxes de terres rares," *Proc. K. Akad. van Wet.*, vol. 103, pp. 1176–1189, 1929.
- [8] J. Becquerel, "Einleitung in eine Theorie der magneto-optischen Erscheinungen in Kristallen," *Zeitschrift für Phys.*, vol. 58, pp. 205–216, 1929.
- [9] J. H. van Vleck, "The Puzzle of Rare-earth Spectra in Solids.," *J. Phys. Chem.*, vol. 41, pp. 67–80, 1937.
- [10] S. Cotton, "Lanthanide and Actinide Chemistry," *John Wiley Sons Ltd*, pp. 1–22, 2006.
- [11] S. Freed, S. I. Weissman, F. E. Fortess, and H. F. Jacobson, "Ions of europium distributed between different configurations in homogeneous solutions," *J. Chem. Phys.*, vol. 7, pp. 824–828, 1939.
- [12] S. I. Weissman, "Intramolecular energy transfer the fluorescence of complexes of Europium," *J. Chem. Phys.*, vol. 10, pp. 214–217, 1942.
- [13] H. and M. C. H. C. Dieke, Gerhard Heinrich, "Spectra and energy levels of rare earth ions in crystals," *John Wiley Sons, Inc.*, pp. 1901–1965, 1968.
- [14] B. R. Judd, "Optical absorption intensities of rare-earth ions," *Phys. Rev.*, vol. 127, p. 750, 1962.
- [15] G. S. Ofelt, "Intensities of crystal spectra of rare-earth ions," *J. Chem. Phys.*, vol. 37, pp. 511–520, 1962.

- [16] C. Huang and Z. Bian, "Rare Earth Coordination Chemistry 1.1 Electronic Configuration of Lanthanide Atoms in the Ground State," *John Wiley Sons Pte Ltd.*, pp. 1–39, 2010.
- [17] I. Hemmilä and V. Laitala, "Progress in lanthanides as luminescent probes," *J. Fluoresc.*, vol. 15, pp. 529–542, 2005.
- [18] C. L. Melcher, S. Friedrich, S. P. Cramer, M. A. Spurrier, P. Szupryczynski, and R. Nutt, "Cerium oxidation state in LSO:Ce scintillators," *IEEE Trans. Nucl. Sci.*, vol. 52, pp. 1809–1812, 2005.
- [19] E. G. Moore, A. P. S. Samuel, and K. N. Raymond, "From antenna to assay: lessons learned in lanthanide luminescence," *Acc. Chem. Res.*, vol. 42, pp. 542–552, 2009.
- [20] K. N. Allen and B. Imperiali, "Lanthanide-tagged proteins - an illuminating partnership," *Curr. Opin. Chem. Biol.*, vol. 14, pp. 247–254, 2010.
- [21] A. J. Kenyon, "Recent developments in rare-earthdoped materials for optoelectronics," *Prog. Quant. Elec.*, vol. 26, pp. 225–284, 2002.
- [22] J.-C. G. Bünzli, "Benefiting from the Unique Properties of Lanthanide Ions," *Acc. Chem. Res.*, vol. 39, pp. 53–61, 2006.
- [23] J.-C. G. Bünzli and S. V. Eliseeva, "Basics of lanthanide photophysics. Springer series on fluorescence; lanthanide luminescence: photophysical, analytical and biological aspects," *Springer- Verlag, Berlin*, vol. 7, pp. 1–45, 2010.
- [24] J. C. G. Bünzli, "Lanthanide luminescence for biomedical analyses and imaging," *Chem. Rev.*, vol. 110, pp. 2729–2955, 2010.
- [25] F. Gutierrez, C. Tedeschi, L. Maron, J. P. Daudey, R. Poteau, J. Azema, P. Tisnès, and C. Picard, "Quantum chemistry-based interpretations on the lowest triplet state of luminescent lanthanides complexes. Part 1. Relation between the triplet state energy of hydroxamate complexes and their luminescence properties," *J. Chem. Soc. Dalt. Trans.*, vol. 0, pp. 1334–1347, 2004.
- [26] G. Blasse and B. C. Grabmaier, "Luminescent Materials, Nonradiative Transitions," *Springer-Verlag, Berlin*, pp. 1–4, 1994.
- [27] A. Beeby, I. M. Clarkson, R. S. Dickins, S. Faulkner, D. Parker, L. Royle, A. S. De Sousa, J. A. G. Williams, and M. Woods, "Non-radiative deactivation of the excited states of europium, terbium and ytterbium complexes by proximate energy-matched OH, NH and CH oscillators: an improved luminescence method for establishing solution hydration states," *J. Chem. Soc. Perkin Trans.*, vol. 2, pp. 493–504, 1999.
- [28] K. Binnemans, "Rare-earth beta-diketonates," *Elsevier B.V.*, vol. 35, pp. 107–272, 2005.
- [29] J. C. G. Bünzli, "Lanthanide-containing luminescent molecular edifices," *J. Alloy. Compd.*, vol. 408–412, pp. 934–944, 2006.
- [30] K. Driesen, R. Van Deun, C. Görrler-Walrand, and K. Binnemans, "Near-Infrared Luminescence of Lanthanide Calcein and Lanthanide Dipicolinate Complexes Doped into a Silica-PEG Hybrid Material," *Chem. Mater.*, vol. 16, pp. 1531–1535, 2004.
- [31] S. V. Eliseeva and J. C. G. Bünzli, "Lanthanide luminescence for functional materials and bio-sciences," *Chem. Soc. Rev.*, vol. 39, pp. 189–227, 2010.
- [32] I. Hemmilä, V. M. Mukkala, and H. Takalo, "Development of luminescent lanthanide chelate

- labels for diagnostic assays," *J. Alloys Compd.*, vol. 249, pp. 158–162, 1997.
- [33] M. L. Cable, D. J. Levine, J. P. Kirby, H. B. Gray, and A. Ponce, "Luminescent lanthanide sensors. Advances in Inorganic Chemistry," *Adv. Inorg. Chem.*, vol. 63, pp. 1–45, 2011.
 - [34] C. Yang, L. M. Fu, Y. Wang, J. P. Zhang, W. T. Wong, X. C. Ai, Y. F. Qiao, B. S. Zou, and L. L. Gui, "A highly luminescent europium complex showing visible-light-sensitized red emission: Direct observation of the singlet pathway," *Angew. Chemie - Int. Ed.*, vol. 43, pp. 5010–5013, 2004.
 - [35] E. F. S. J. G.Fde Sá, O.LMalta, Cde Mello Donegá, A.MSimas, R.LLongo, P.A Santa-Cruz, "Spectroscopic properties and design of highly luminescent lanthanide coordination complexes," *Coord. Chem. Rev.*, vol. 196, pp. 165–195, 2000.
 - [36] D. L. Dexter, "A theory of sensitized luminescence in solids," *J. Chem. Phys.*, vol. 21, pp. 836–850, 1953.
 - [37] T. Förster, "Zwischenmolekulare Energiewanderung und Fluoreszenz (Intermolecular energy migration and fluorescence, Translated by Knox RS)," *Ann. Phys.*, vol. 437, pp. 55–75, 1948.
 - [38] S. Faulkner, L. S. Natrajan, W. S. Perry, and D. Sykes, "Sensitised luminescence in lanthanide containing arrays and d-f hybrids," *Dalt. Trans.*, vol. 28, pp. 3890–3899, 2009.
 - [39] G. Blasse, "The influence of charge-transfer and rydberg states on the luminescence properties of lanthanides and actinides," *Spectra Chem. Interact.*, vol. 26, pp. 43–79, 1976.
 - [40] R. S. V.F.Zolin, L.N.Puntus, V.I.Tsaryuk, V.A.Kudryashova, J.Legendziewicz, P.Gawryszewska, "Spectroscopy of europium and terbium pyridine-carboxylates," *J. Alloys Compd.*, vol. 380, pp. 279–284, 2004.
 - [41] K. Bowman-James, "Alfred Werner revisited: The coordination chemistry of anions," *Acc. Chem. Res.*, vol. 38, pp. 671–678, 2005.
 - [42] J. R. Lakowicz, "Principles of Fluorescence Spectroscopy, 3rd ed.," *Springer, New York, USA*, pp. 17–18, 2006.
 - [43] V. Balzani, P. Ceroni, and A. Juris, "Photochemistry and photophysics: concepts, research, applications.," *Wiley- VCH Verlag GmbH Co., Weinheim*, pp. 8817–8817, 2014.
 - [44] S. Lis, "Luminescence spectroscopy of lanthanide(III) ions in solution," *J. Alloys Compd.*, vol. 34, pp. 45–50, 2002.
 - [45] T. R. Martz, J. J. Carr, C. R. French, and M. D. DeGrandpre, "A submersible autonomous sensor for spectrophotometric pH measurements of natural waters," *Anal. Chem.*, vol. 75, pp. 1844–1850, 2003.
 - [46] D. R. H. Gourley, "Glass Electrodes for Hydrogen and Other Cations. Principles and Practice.," *J. Med. Chem.*, vol. 10, pp. 990–990, 1967.
 - [47] P. Atkins and J. de Paula, "Physical chemistry, 7 th edition, 2002," *Oxford Univ. Press.*, vol. 57, p. 80, 2002.
 - [48] G. Mattock and G. R. Taylor, "pH Measurement and Titration.," *Heywood Co. Ltd, London*, pp. 336–348, 1961.
 - [49] A. K. Covington, R. G. Bates, and R. A. Durst, "Definition of pH scales, standard reference values, measurement of pH and related terminology (Recommendations 1984)," *Pure Appl. Chem.*, vol. 57, pp. 531–542, 1985.

- [50] W. Nernst, "Die elektromotorische wirksamkeit der jonen," *Zeitschrift für Phys. Chemie*, vol. 4, pp. 129–181, 1889.
- [51] M. Cremer, "Über die Ursache der elektromotorischen Eigenschaften der Gewebe, zugleich ein Beitrag zur Lehre von den polyphasischen Elektrolytketten," *R. Oldenbg.*, pp. 562–608, 1906.
- [52] F. Haber and Z. Hlemensiewicz, "Über elektrische Phasengrenzkräfte," *Zeitschrift für Phys. Chemie*, vol. 67, pp. 385–431, 1909.
- [53] H. Schiller, "Über die elektromotorischen Eigenschaften der Gläser," *Ann. Phys.*, vol. 379, pp. 105–135, 1924.
- [54] J. Zim, D. Erscheinungen, and D. Vermutung, "Untersuchungen über Ionenaustausch an Gläsern," vol. 134, pp. 355–383, 1925.
- [55] D. A. MacInnes and M. Dole, "The behavior of glass electrodes of different compositions," *J. Am. Chem. Soc.*, vol. 52, pp. 29–36, 1930.
- [56] B. P. Nicolsky, "Theory of the glass electrode. I," *Zh Fis Khim*, vol. 10, pp. 495–503, 1937.
- [57] G. Haugaard, "The Mechanism of the Glass Electrode.," *J. Phys. Chem.*, vol. 45, pp. 148–157, 1941.
- [58] R. A. Durst, "Mechanism of the glass electrode response," *J. Chem. Educ.*, vol. 44, pp. 175–176, 1967.
- [59] F. G. K. Baucke, "Investigation of surface layers, formed on glass electrode membranes in aqueous solutions, by means of an ion sputtering method," *J. Non. Cryst. Solids*, vol. 14, pp. 13–31, 1974.
- [60] M. Dole, "The early history of the development of the glass electrode for pH measurements," *J. Chem. Educ.*, vol. 57, pp. 134–134, 1980.
- [61] D. Aigner, S. M. Borisov, and I. Klimant, "New fluorescent perylene bisimide indicators—a platform for broadband pH optodes," *Anal. Bioanal. Chem.*, vol. 400, pp. 2475–2485, 2011.
- [62] W. Vonau and U. Guth, "pH monitoring: a review," *J. Solid State Electrochem.*, vol. 10, pp. 746–752, 2006.
- [63] S. Carroll and R. P. Baldwin, "Self-calibrating microfabricated iridium oxide pH electrode array for remote monitoring," *Anal. Chem.*, vol. 82, pp. 878–885, 2010.
- [64] R. Ansari, M. Arvand, and L. Heydari, "The behaviour of polyaniline-coated PVC membrane based on 7, 16-didecyl-1, 4, 10, 13-tetraoxa-7, 16-diazacyclooctadecane for pH measurements in highly acidic media," *J. Chem. Sci.*, vol. 126, pp. 41–48, 2014.
- [65] H. E. K. Ertürün, A. D. Özel, S. Sayın, M. Yılmaz, and E. Kılıç, "Development of a pH sensing membrane electrode based on a new calix [4] arene derivative," *Talanta*, vol. 132, pp. 669–675, 2015.
- [66] J. Ping, Y. Wang, J. Wu, Y. Ying, and F. Ji, "A novel pH sensing membrane based on an ionic liquid-polymer composite," *Microchim. Acta*, vol. 176, pp. 229–234, 2012.
- [67] G. S. Zakharova and N. V Podval'naya, "Bifunctional potentiometric sensor based on MoO 3 nanorods," *J. Anal. Chem.*, vol. 68, pp. 50–56, 2013.

- [68] S. Erden, A. Demirel, S. Memon, M. Yılmaz, E. Canel, and E. Kılıç, "Using of hydrogen ion-selective poly (vinyl chloride) membrane electrode based on calix [4] arene as thiocyanate ion-selective electrode," *Sens. Actuat. B*, vol. 113, pp. 290–296, 2006.
- [69] B. Kim, J. Shim, and K.-C. Chung, "Study on hydrogen ion-selective solid contact electrodes based on decamethylcyclopentasiloxane," *Anal. Lett.*, vol. 44, pp. 2138–2149, 2011.
- [70] M. Jović, J. C. Hidalgo-Acosta, A. Lesch, V. C. Bassetto, E. Smirnov, F. Cortés-Salazar, and H. H. Girault, "Large-scale layer-by-layer inkjet printing of flexible iridium-oxide based pH sensors," *J. Electroanal. Chem.*, vol. 819, pp. 384–390, 2018.
- [71] X. Huang, Q. Ren, X. Yuan, W. Wen, W. Chen, and D. Zhan, "Iridium oxide based coaxial pH ultramicroelectrode," *Electrochem. commun.*, vol. 40, pp. 35–37, 2014.
- [72] I. A. Ges, B. L. Ivanov, D. K. Schaffer, E. A. Lima, A. A. Werdich, and F. J. Baudenbacher, "Thin-film IrOx pH microelectrode for microfluidic-based microsystems," *Biosens. Bioelectron.*, vol. 21, pp. 248–256, 2005.
- [73] N. Landqvist, "On the alkaline error of the glass electrode," *Acta Chem. Scand.*, vol. 9, pp. 595–612, 1955.
- [74] F. G. K. Baucke, "The modern understanding of the glass electrode response," *Fresenius. J. Anal. Chem.*, vol. 349, pp. 582–596, 1994.
- [75] F. G. K. Baucke, "Phosphate and fluoride error of pH glass electrodes. Erroneous potentials caused by a component of some membrane glasses," *J. Electroanal. Chem.*, vol. 367, pp. 131–139, 1994.
- [76] D. C. Harris, "Quantitative Chemical Analysis, 7th ed.," *W. H. Free. Company, New York.*, p. 311, 2007.
- [77] O. S. Wolfbeis, "Fiber optic chemical sensors and biosensors.," *CRC Press. Boca Raton, Florida.*, vol. 1, p. 413, 1991.
- [78] C. Dafu, C. Qiang, H. Jinghong, C. Jinge, L. Yating, and Z. Zemin, "Optical-fibre pH sensor," *Sens. Actuat. B*, vol. 12, pp. 29–32, 1993.
- [79] F. J. A. Andrea Cusano Michele Giordano, Antonello Cutolo, "Optochemical Nanosensors," *Boca Raton, USA*, pp. 35–50, 2013.
- [80] D. Wencel, T. Abel, and C. McDonagh, "Optical chemical pH sensors," *Anal. Chem.*, vol. 86, pp. 15–29, 2013.
- [81] O. S. Wolfbeis, "Fiber Optic Chemical Sensors and Biosensors, Ch.19," *CRC Press. Inc, USA.*, vol. 2, pp. 267–300, 1991.
- [82] X. D. Wang and O. S. Wolfbeis, "Fiber-optic chemical sensors and biosensors (2008-2012)," *Anal. Chem.*, vol. 85, pp. 487–508, 2013.
- [83] J. Lin, "Recent development and applications of optical and fiber-optic pH sensors," *Trends Anal. Chem.*, vol. 19, pp. 541–552, 2000.
- [84] L. Bilro, N. Alberto, J. L. Pinto, and R. Nogueira, "Optical sensors based on plastic fibers," *Sensors*, vol. 12, pp. 12184–12207, 2012.
- [85] O. S. Wolfbeis, "Fiber optic chemical sensors and biosensors," *Anal. Chem.*, vol. 74, pp. 2663–2678, 2002.

- [86] W. R. Seitz and M. J. Sepaniak, "Chemical sensors based on immobilized indicators and fiber optics," *CRC Crit. Rev. Anal. Chem.*, vol. 19, pp. 135–173, 1988.
- [87] J. Janata, "Do optical sensors really measure pH?," *Anal. Chem.*, vol. 59, pp. 1351–1356, 1987.
- [88] Z. Liu, F. Luo, and T. Chen, "Phenolphthalein immobilized membrane for an optical pH sensor," *Anal. Chim. Acta*, vol. 510, pp. 189–194, 2004.
- [89] O. S. Wolfbeis, "Fiber-optic chemical sensors and biosensors," *Anal. Chem.*, vol. 78, pp. 3859–3873, 2006.
- [90] J. I. Peterson, S. R. Goldstein, R. V Fitzgerald, and D. K. Buckhold, "Fiber optic pH probe for physiological use," *Anal. Chem.*, vol. 52, pp. 864–869, 1980.
- [91] N. Chamkouri, "Development of long-term optical pH sensor using phenol red based on triacetylcellulose membranes," *Int. J. Pharm. Technol.*, vol. 7, pp. 9096–9104, 2015.
- [92] G. F. Kirkbright, R. Narayanaswamy, and N. A. Welti, "Fibre-optic pH probe based on the use of an immobilised colorimetric indicator," *Analyst*, vol. 109, pp. 1025–1028, 1984.
- [93] T. E. Edmonds and I. D. Ross, "Low-cost fibre optic chemical sensors," *Anal. Proceed*, vol. 22, pp. 206–207, 1985.
- [94] M. Bacci, F. Baldini, and A. M. Scheggi, "Spectrophotometric investigations on immobilized acid-base indicators," *Anal. Chim. Acta*, vol. 207, pp. 343–348, 1988.
- [95] G. J. Mohr and O. S. Wolfbeis, "Optical sensors for a wide pH range based on azo dyes immobilized on a novel support," *Anal. Chim. Acta*, vol. 292, pp. 41–48, 1994.
- [96] A. B. Ganesh and T. K. Radhakrishnan, "Fiber-optic pH sensor," *Fiber Integr. Opt.*, vol. 25, pp. 403–409, 2006.
- [97] Z. Yan, X. Zhang, C. Bao, H. Tang, Q. Zhao, L. Hu, and J. You, "A novel luminol derivative and its functionalized filter-paper for reversible double-wavelength colorimetric pH detection in fruit juice," *Sens. Actuat. B*, vol. 262, pp. 869–875, 2018.
- [98] S. Rastegarzadeh and Z. Moradpour, "Optical pH sensor based on Calcon immobilization membrane," *J. Iran. Chem. Soc.*, vol. 6, pp. 858–862, 2009.
- [99] P. Hashemi and R. A. Zarjani, "A wide range pH optical sensor with mixture of Neutral Red and Thionin immobilized on an agarose film coated glass slide," *Sens. Actuat. B*, vol. 135, pp. 112–115, 2008.
- [100] I. M. P. de Vargas Sansalvador, C. D. Fay, J. Cleary, A. M. Nightingale, M. C. Mowlem, and D. Diamond, "Autonomous reagent-based microfluidic pH sensor platform," *Sens. Actuat. B.*, vol. 225, pp. 369–376, 2016.
- [101] E. J. Netto, J. I. Peterson, M. McShane, and V. Hampshire, "A fiber-optic broad-range pH sensor system for gastric measurements," *Sens. Actuat. B*, vol. 29, pp. 157–163, 1995.
- [102] X. Chen and Z. Gu, "Absorption-type optical pH sensitive film based on immobilized purple cabbage pigment," *Sens. Actuat. B*, vol. 178, pp. 207–211, 2013.
- [103] M. M. Abolghasemi, M. Sobhi, and M. Piryaee, "Preparation of a novel green optical pH sensor based on immobilization of red grape extract on bioorganic agarose membrane," *Sens. Actuat. B*, vol. 224, pp. 391–395, 2016.

- [104] A. Yari and M. Dinarvand, "Sol-gel film doped with bromopyrogallol red as a highly sensitive sensing element for a new pH optical sensor," *J. Iran. Chem. Soc.*, vol. 8, pp. 1091–1097, 2011.
- [105] M. Noroozifar, M. K. Motlagh, S. Bahmanzadeh, and S. Boroon, "A novel optical membrane with extended detection range of pH," *Turkish J. Chem.*, vol. 34, pp. 719–730, 2010.
- [106] S. Khodadoust, N. C. Kouri, M. S. Talebiyanpoor, J. Deris, and A. A. Pebdani, "Design of an optically stable pH sensor based on immobilization of Giemsa on triacetylcellulose membrane," *Mater. Sci. Eng. C*, vol. 57, pp. 304–308, 2015.
- [107] M. Shamsipur, F. Abbasitabar, V. Zare-Shahabadi, Shahabadi, and M. Akhond, "Broad-range optical pH sensor based on binary mixed-indicator doped sol-gel film and application of artificial neural network," *Anal. Lett.*, vol. 41, pp. 3113–3123, 2008.
- [108] D. Jeon, W. J. Yoo, J. K. Seo, S. H. Shin, K.-T. Han, S. G. Kim, J.-Y. Park, and B. Lee, "Fiber-optic pH sensor based on sol-gel film immobilized with neutral red," *Opt. Rev.*, vol. 20, pp. 209–213, 2013.
- [109] M. Schäferling and A. Duerkop, "Intrinsically referenced fluorimetric sensing and detection schemes: methods, advantages and applications. , Techniques (Springer Series on Fluorescence), U. Resch-Genger ed.," *Stand. Qual. Assur. Fluoresc. Meas. I*, vol. 5, pp. 373–414, 2008.
- [110] H. Shinohara, "Optical PH sensors using a polyaniline thin film," *Proc. 3rd. Int. Meet. Chem. Sensors*, p. 326, 1990.
- [111] E. Pringsheim, E. Terpetschnig, and O. S. Wolfbeis, "Optical sensing of pH using thin films of substituted polyanilines," *Anal. Chim. Acta*, vol. 357, pp. 247–252, 1997.
- [112] N. Abu-Thabit, Y. Umar, E. Ratemi, A. Ahmad, and F. Ahmad Abuilaiwi, "A flexible optical pH sensor based on polysulfone membranes coated with pH-responsive polyaniline nanofibers," *Sensors*, vol. 16, p. 986, 2016.
- [113] C. Florea, Larisa Fay, T. Lahiff, Emer Phelan, and O'Connor, "Dynamic pH mapping in microfluidic devices by integrating adaptive coatings based on polyaniline with colorimetric imaging techniques," *Lab Chip*, vol. 13, pp. 1079–1085, 2013.
- [114] A. Martinez-Olmos, S. Capel-Cuevas, N. López-Ruiz, A. J. Palma, I. De Orbe, and L. F. Capitán-Vallvey, "Sensor array-based optical portable instrument for determination of pH," *Sens. Actuat. B*, vol. 156, pp. 840–848, 2011.
- [115] A. Palma, A. Lapresta-Fernandez, J. M. Ortigosa-Moreno, M. D. Fernandez-Ramos, M. A. Carvajal, and L. F. Capitán-Vallvey, "A simplified measurement procedure and portable electronic photometer for disposable sensors based on ionophore-chromoionophore chemistry for potassium determination," *Anal. Bioanal. Chem.*, vol. 386, pp. 1215–1224, 2006.
- [116] M. D. Fernández-Ramos, M. Greluk, A. J. Palma, E. Arroyo-Guerrero, J. Gómez-Sánchez, and L. F. Capitán-Vallvey, "The use of one-shot sensors with a dedicated portable electronic radiometer for nitrate measurements in aqueous solutions," *Meas. Sci. Technol.*, vol. 19, p. 95204 (7pp), 2008.
- [117] S. Capel-Cuevas, M. P. Cuéllar, I. de Orbe-Payá, M. C. Pegalajar, and L. F. Capitán-Vallvey, "Full-range optical pH sensor based on imaging techniques," *Anal. Chim. Acta*, vol. 681, pp. 71–81, 2010.
- [118] Y. Egawa, R. Hayashida, and J. Anzai, "Multilayered assemblies composed of brilliant yellow

- and poly (allylamine) for an optical pH sensor," *Anal. Sci.*, vol. 22, pp. 1117–1119, 2006.
- [119] N. Raoufi, F. Surre, T. Sun, M. Rajarajan, and K. T. V Grattan, "Wavelength dependent pH optical sensor using the layer-by-layer technique," *Sens. Actuat. B*, vol. 169, pp. 374–381, 2012.
 - [120] F. J. Arregui, M. Otano, C. Fernandez-Valdivielso, and I. R. Matias, "An experimental study about the utilization of Liquicoat® solutions for the fabrication of pH optical fiber sensors," *Sens. Actuat. B*, vol. 87, pp. 289–295, 2002.
 - [121] W. Li, H. Cheng, M. Xia, and K. Yang, "An experimental study of pH optical sensor using a section of no-core fiber," *Sens. Actuat. A*, vol. 199, pp. 260–264, 2013.
 - [122] A. K. Pathak and V. K. Singh, "A wide range and highly sensitive optical fiber pH sensor using polyacrylamide hydrogel," *Opt. Fiber Technol.*, vol. 39, pp. 43–48, 2017.
 - [123] B. Gu, M.-J. Yin, A. P. Zhang, J.-W. Qian, and S. He, "Low-cost high-performance fiber-optic pH sensor based on thin-core fiber modal interferometer," *Opt. Express*, vol. 17, pp. 22296–22302, 2009.
 - [124] V. Bhardwaj, A. K. Pathak, and V. K. Singh, "No-core fiber-based highly sensitive optical fiber pH sensor," *J. Biomed. Opt.*, vol. 22, pp. 057001-1-057001-8, 2017.
 - [125] A. K. Pathak, V. Bhardwaj, R. K. Gangwar, M. De, and V. K. Singh, "Fabrication and characterization of TiO₂ coated cone shaped nano-fiber pH sensor," *Opt. Commun.*, vol. 386, pp. 43–48, 2017.
 - [126] S. K. Mishra, B. Zou, and K. S. Chiang, "Wide-range pH sensor based on a smart-hydrogel-coated long-period fiber grating," *IEEE J. Sel. Top. Quantum Electron.*, vol. 23, p. 5601405, 2017.
 - [127] S. Dong, M. Luo, G. Peng, and W. Cheng, "Broad range pH sensor based on sol–gel entrapped indicators on fibre optic," *Sens. Actuat. B*, vol. 129, pp. 94–98, 2008.
 - [128] X. Yang, Y. Gao, Z. Huang, X. Chen, Z. Ke, P. Zhao, Y. Yan, R. Liu, and J. Qu, "Fluorescent probe based on heteroatom containing styrylcyanine: pH-sensitive properties and bioimaging in vivo," *Mater. Sci. Eng. C*, vol. 52, pp. 97–102, 2015.
 - [129] H. Offenbacher, O. S. Wolfbeis, and E. Förlinger, "Fluorescence optical sensors for continuous determination of near-neutral pH values," *Sens. Actuat.*, vol. 9, pp. 73–84, 1986.
 - [130] D. Wencel, B. D. MacCraith, and C. McDonagh, "High performance optical ratiometric sol–gel-based pH sensor," *Sens. Actuat. B*, vol. 139, pp. 208–213, 2009.
 - [131] C.-G. Niu, X.-Q. Gui, G.-M. Zeng, A.-L. Guan, P.-F. Gao, and P.-Z. Qin, "Fluorescence ratiometric pH sensor prepared from covalently immobilized porphyrin and benzothioxanthene," *Anal. Bioanal. Chem.*, vol. 383, pp. 349–357, 2005.
 - [132] F. J. F. Martín, J. C. C. Rodríguez, J. C. A. Anton, J. C. V. Perez, I. Sánchez-Barragán, J. M. Costa-Fernández, and A. Sanz-Medel, "Design of a low-cost optical instrument for pH fluorescence measurements," *IEEE Trans. Instrum. Meas.*, vol. 55, pp. 1215–1221, 2006.
 - [133] I. Sánchez-Barragán, J. M. Costa-Fernández, A. Sanz-Medel, M. Valledor, F. J. Ferrero, and J. C. Campo, "A ratiometric approach for pH optosensing with a single fluorophore indicator," *Anal. Chim. Acta*, vol. 562, pp. 197–203, 2006.

- [134] C.-Y. Li, X.-B. Zhang, Z.-X. Han, B. Åkermark, L. Sun, G.-L. Shen, and R.-Q. Yu, "A wide pH range optical sensing system based on a sol-gel encapsulated amino-functionalised corrole," *Analyst*, vol. 131, pp. 388–393, 2006.
- [135] S. Trupp, P. Hoffmann, T. Henkel, and G. J. Mohr, "Novel pH indicator dyes for array preparation via NHS ester activation or solid-phase organic synthesis," *Org. Biomol. Chem.*, vol. 6, pp. 4319–4322, 2008.
- [136] Y. Hiruta, N. Yoshizawa, D. Citterio, and K. Suzuki, "Highly durable double sol-gel layer ratiometric fluorescent pH optode based on the combination of two types of quantum dots and absorbing pH indicators," *Anal. Chem.*, vol. 84, pp. 10650–10656, 2012.
- [137] M. Fritzsche, C. G. Barreiro, B. Hitzmann, and T. Scheper, "Optical pH sensing using spectral analysis," *Sens. Actuat. B*, vol. 128, pp. 133–137, 2007.
- [138] A. S. Vasylevska, A. A. Karasyov, S. M. Borisov, and C. Krause, "Novel coumarin-based fluorescent pH indicators, probes and membranes covering a broad pH range," *Anal. Bioanal. Chem.*, vol. 387, pp. 2131–2141, 2007.
- [139] F. Yuan, L. Ding, Y. Li, X. Li, L. Fan, S. Zhou, D. Fang, and S. Yang, "Multicolor fluorescent graphene quantum dots colorimetrically responsive to all-pH and a wide temperature range," *Nanoscale*, vol. 7, pp. 11727–11733, 2015.
- [140] C.-S. Chu and C.-J. Su, "Fluorescence ratiometric optical broad range pH sensor based on CdSe/ZnS quantum dots and O170 embedded in ethyl cellulose matrix," *J. Light. Technol.*, vol. 36, pp. 857–862, 2018.
- [141] Z. Qian, J. Ma, X. Shan, H. Feng, L. Shao, and J. Chen, "Highly Luminescent N-Doped Carbon Quantum Dots as an Effective Multifunctional Fluorescence Sensing Platform," *Chem. Eur. J.*, vol. 20, pp. 2254–2263, 2014.
- [142] S. Derinkuyu, K. Ertekin, O. Oter, S. Denizalti, and E. Cetinkaya, "Fiber optic pH sensing with long wavelength excitable Schiff bases in the pH range of 7.0–12.0," *Anal. Chim. Acta*, vol. 588, pp. 42–49, 2007.
- [143] W. W. Al-Qaysi and A. Duerkop, "Luminescent europium complex for wide-range pH sensor and sensor microtiterplate," *Analyst*, vol. 143, pp. 3176–3183, 2018.
- [144] A. Dürkop, F. Lehmann, and O. S. Wolfbeis, "Polarization immunoassays using reactive ruthenium metal-ligand complexes as luminescent labels," *Anal. Bioanal. Chem.*, vol. 372, pp. 688–694, 2002.
- [145] H.-J. Kim, Y.-C. Jeong, J. Heo, J. Il Rhee, and K.-J. Hwang, "A wide-range luminescent pH sensor based on ruthenium (II) complex," *Bull. Korean Chem. Soc.*, vol. 30, pp. 539–540, 2009.
- [146] A. Lobnik, N. Majcen, K. Niederreiter, and G. Uray, "Optical pH sensor based on the absorption of antenna generated europium luminescence by bromothymolblue in a sol-gel membrane," *Sens. Actuat. B*, vol. 74, pp. 200–206, 2001.
- [147] D. Aigner, S. M. Borisov, F. J. O. Fernández, J. F. F. Sánchez, R. Saf, and I. Klimant, "New fluorescent pH sensors based on covalently linkable PET rhodamines," *Talanta*, vol. 99, no. 15, pp. 194–201, 2012.
- [148] T. Jokic, S. M. Borisov, R. Saf, D. A. Nielsen, M. Kühl, and I. Klimant, "Highly photostable near-infrared fluorescent pH indicators and sensors based on BF₂-chelated tetraarylazadipyrrromethene dyes," *Anal. Chem.*, vol. 84, pp. 6723–6730, 2012.

- [149] H. Cui, Y. Chen, L. Li, Y. Wu, Z. Tang, H. Fu, and Z. Tian, "Hybrid fluorescent nanoparticles fabricated from pyridine-functionalized polyfluorene-based conjugated polymer as reversible pH probes over a broad range of acidity-alkalinity," *Microchim. Acta*, vol. 181, pp. 1529–1539, 2014.
- [150] J. Qi, D. Liu, X. Liu, S. Guan, F. Shi, H. Chang, H. He, and G. Yang, "Fluorescent pH sensors for broad-range pH measurement based on a single fluorophore," *Anal. Chem.*, vol. 87, pp. 5897–5904, 2015.
- [151] M. Strobl, T. Rappitsch, S. M. Borisov, T. Mayr, and I. Klimant, "NIR-emitting aza-BODIPY dyes—new building blocks for broad-range optical pH sensors," *Analyst*, vol. 140, pp. 7150–7153, 2015.
- [152] R. Gotor, P. Ashokkumar, M. Hecht, K. Keil, and K. Rurack, "Optical pH sensor covering the range from pH 0–14 compatible with mobile-device readout and based on a set of rationally designed indicator dyes," *Anal. Chem.*, vol. 89, pp. 8437–8444, 2017.
- [153] S. Chen, J. Liu, Y. Liu, H. Su, Y. Hong, C. K. W. Jim, R. T. K. Kwok, N. Zhao, W. Qin, and J. W. Y. Lam, "An AIE-active hemicyanine fluorogen with stimuli-responsive red/blue emission: extending the pH sensing range by 'switch+ knob' effect," *Chem. Sci.*, vol. 3, pp. 1804–1809, 2012.
- [154] D. Aigner, B. Ungerböck, T. Mayr, R. Saf, I. Klimant, and S. M. Borisov, "Fluorescent materials for pH sensing and imaging based on novel 1,4-diketopyrrolo-[3,4-c]pyrrole dyes," *J. Mater. Chem. C*, vol. 1, pp. 5685–5693, 2013.
- [155] C. J. Tsou, C. Y. Chu, Y. Hung, and C. Y. Mou, "A broad range fluorescent pH sensor based on hollow mesoporous silica nanoparticles, utilising the surface curvature effect," *J. Mater. Chem. B*, vol. 1, pp. 5557–5563, 2013.
- [156] C.-J. Tsou, Y. Hung, and C.-Y. Mou, "Hollow mesoporous silica nanoparticles with tunable shell thickness and pore size distribution for application as broad-ranging pH nanosensor," *Microporous Mesoporous Mater.*, vol. 190, pp. 181–188, 2014.
- [157] P. Kumar EK, L. N. Feldborg, K. Almdal, and T. L. Andresen, "Synthesis and characterization of a micelle-based pH nanosensor with an unprecedented broad measurement range," *Chem. Mater.*, vol. 25, pp. 1496–1501, 2013.
- [158] J. Aguilera-Sigalat and D. Bradshaw, "A colloidal water-stable MOF as a broad-range fluorescent pH sensor via post-synthetic modification," *Chem. Commun.*, vol. 50, pp. 4711–4713, 2014.
- [159] X. Zhang, K. Jiang, H. He, D. Yue, D. Zhao, Y. Cui, Y. Yang, and G. Qian, "A stable lanthanide-functionalized nanoscale metal-organic framework as a fluorescent probe for pH," *Sens. Actuat. B*, vol. 254, pp. 1069–1077, 2018.
- [160] P. Chen, Z. Wang, S. Zong, H. Chen, D. Zhu, Y. Zhong, and Y. Cui, "A wide range optical pH sensor for living cells using Au@ Ag nanoparticles functionalized carbon nanotubes based on SERS signals," *Anal. Bioanal. Chem.*, vol. 406, pp. 6337–6346, 2014.
- [161] G. Li, S. Zhang, N. Wu, Y. Cheng, and J. You, "Spontaneous Counterion-Induced Vesicle Formation: Multivalent Binding to Europium (III) for a Wide-Range Optical pH Sensor," *Adv. Funct. Mater.*, vol. 24, pp. 6204–6209, 2014.
- [162] M. Zhang, R. V. Søndergaard, E. K. P. Kumar, J. R. Henriksen, D. Cui, P. Hammershøj, M. H. Clausen, and T. L. Andresen, "A hydrogel based nanosensor with an unprecedented broad

- sensitivity range for pH measurements in cellular compartments,” *Analyst*, vol. 140, pp. 7246–7253, 2015.
- [163] R. V Benjaminsen, H. Sun, J. R. Henriksen, N. M. Christensen, K. Almdal, and T. L. Andresen, “Evaluating nanoparticle sensor design for intracellular pH measurements,” *ACS Nano*, vol. 5, pp. 5864–5873, 2011.
 - [164] B. Chu, H. Wang, B. Song, F. Peng, Y. Su, and Y. He, “Fluorescent and photostable silicon nanoparticles sensors for real-time and long-term intracellular pH measurement in live cells,” *Anal. Chem.*, vol. 88, pp. 9235–9242, 2016.
 - [165] R. J. Meier, J. M. B. Simbürger, T. Soukka, and M. Schäferling, “A FRET based pH probe with a broad working range applicable to referenced ratiometric dual wavelength and luminescence lifetime read out,” *Chem. Commun.*, vol. 51, pp. 6145–6148, 2015.
 - [166] B. Shi, Y. Su, L. Zhang, R. Liu, M. Huang, and S. Zhao, “Nitrogen-rich functional groups carbon nanoparticles based fluorescent pH sensor with broad-range responding for environmental and live cells applications,” *Biosens. Bioelectron.*, vol. 82, pp. 233–239, 2016.
 - [167] P. Gruber, M. P. C. Marques, P. Sulzer, R. Wohlgemuth, T. Mayr, F. Baganz, and N. Szita, “Real-time pH monitoring of industrially relevant enzymatic reactions in a microfluidic side-entry reactor (μ SER) shows potential for pH control,” *Biotechnol. J.*, vol. 12, p. 1600475, 2017.
 - [168] J. Wang, S. Xia, J. Bi, M. Fang, W. Mazi, Y. Zhang, N. Conner, F.-T. Luo, H. P. Lu, and H. Liu, “Ratiometric Near-Infrared Fluorescent Probes Based On Through-Bond Energy Transfer and π -Conjugation Modulation between Tetraphenylethene and Hemicyanine Moieties for Sensitive Detection of pH Changes in Live Cells,” *Bioconjug. Chem.*, vol. 29, pp. 1406–1418, 2018.
 - [169] H. Lu, Y. Jin, Y. Tian, W. Zhang, M. R. Holl, and D. R. Meldrum, “New ratiometric optical oxygen and pH dual sensors with three emission colors for measuring photosynthetic activity in cyanobacteria,” *J. Mater. Chem.*, vol. 21, pp. 19293–19301, 2011.
 - [170] Y. Tian, E. Fuller, S. Klug, F. Lee, F. Su, L. Zhang, S. Chao, and D. R. Meldrum, “A fluorescent colorimetric pH sensor and the influences of matrices on sensing performances,” *Sens. Actuat. B*, vol. 188, pp. 1–10, 2013.
 - [171] X. Wang, R. J. Meier, and O. S. Wolfbeis, “Fluorescent pH-Sensitive Nanoparticles in an Agarose Matrix for Imaging of Bacterial Growth and Metabolism,” *Angew. Chemie*, vol. 125, pp. 424–427, 2013.
 - [172] S. H. Lim, L. Feng, J. W. Kemling, C. J. Musto, and K. S. Suslick, “An optoelectronic nose for the detection of toxic gases,” *Nat. Chem.*, vol. 1, pp. 562–567, 2009.
 - [173] S. A. Brittle, T. H. Richardson, A. D. F. Dunbar, S. M. Turega, and C. A. Hunter, “Tuning free base tetraphenylporphyrins as optical sensing elements for volatile organic analytes,” *J. Mater. Chem.*, vol. 21, pp. 4882–4887, 2011.
 - [174] V. M. C. Rérolle, C. F. A. Floquet, A. J. K. Harris, M. C. Mowlem, R. R. G. J. Bellerby, and E. P. Achterberg, “Development of a colorimetric microfluidic pH sensor for autonomous seawater measurements,” *Anal. Chim. Acta*, vol. 786, pp. 124–131, 2013.
 - [175] L. Ferrari, L. Rovati, P. Fabbri, and F. Pilati, “Disposable fluorescence optical pH sensor for near neutral solutions,” *Sens.*, vol. 13, pp. 484–499, 2012.
 - [176] T. P. Jones and M. D. Porter, “Optical pH sensor based on the chemical modification of a

porous polymer film," *Anal. Chem.*, vol. 60, pp. 404–406, 1988.

- [177] O. S. Wolfbeis and H. Offenbacher, "Fluorescence sensor for monitoring ionic strength and physiological pH values," *Sens. Actuat.*, vol. 9, pp. 85–91, 1986.

Parts of this chapter has been submitted.to Analytical and Bioanalytical Chemistry.

Wafaa Waleed Al-Qaysi and Axel Duerkop

Author contributions

WW collect the all references and wrote the manuscript. AD revised the manuscript

2. A luminescent europium complex for wide-range pH sensors and sensor microtiterplates

2.1 Introduction

pH is an important chemical parameter to be controlled in various fields like in medical, environmental and life sciences, for monitoring the availability of inorganic compounds for aquatic organisms and in industrial applications [1],[2]. Moreover, pH governs processes in the biotechnological or chemical industry, [3],[4] or physiological processes inside (intracellular pH) and outside (extracellular pH) tumours [5],[6]. pH further has an impact on global ecology and physiological biochemistry [7],[8]. Many chemical and biological processes occurring in seawater, freshwater, and marine systems are associated with strong changes of pH [9],[10]. There is a further need to control pH in biotechnological processes (such as production of bacteria), lactic acid growth, and fermentation of yogurt [11],[12]. Acidic pH is often important to be monitored in organelles such as lysosomes and endosomes, [13] in soils [14] or even in the human stomach [15], [16]. A well-balanced intracellular pH is important for cell vitality, function, and metabolism [17] because diseases like cancer [18] and Alzheimer's [19] have been shown to be associated with abnormal cellular pH.

Mostly, pH is determined by electrochemical or optical sensors and pH test paper strips. Although pH test strips are inexpensive, can cover a wide range and can be used by nonscientific staff, they frequently do not offer high resolution.

The pH glass electrode is the most frequently used sensor for pH measurement. Despite its capability for wide-range measurement, its use is limited at the extremes of the pH scale (especially at highly alkaline pH). As glass electrodes are bulky, they often do not offer high local (μm) resolution and may represent a source of electric shock during an *in vivo* measurement [20]. In addition, glass electrodes suffer from interference by ionic strength, certain organic matter and electromagnetic radiation. Optical sensors, however, can avoid many of these shortcomings because

such sensors can be easily produced in various shapes and may read changes of absorption, fluorescence, or reflectivity upon variation of pH. Ideally, the optical properties of an indicator are transformed continuously and reversibly with the change of proton concentration [21]. Optical sensors offer some advantages, like being insensitive to electrical interference and being electrically safe (in a living environment), and they can be fabricated easily and inexpensively, provide good selectivity and high sensitivity and can be disposable. Optical pH sensors can offer a better resolution compared to glass electrodes and once the indicators are immobilized in a thin layer of a suitable polymer, they can be used in various environments like in continuous flow-through sensing but also in microtiterplates for high-throughput [22],[23]. While also being capable of miniaturization for high local resolution, pH sensors are suitable for imaging experiments [24]. Leaching of a pH indicator off the sensor membrane into the analyte solution should be avoided, because most indicators are hydrophilic and charged, and the matrix used is always permeable to ions. Improved sensors therefore contain indicators that are embedded into sol-gels [25] or coupled covalently to the polymer matrix [26].

Also fluorescent pH sensors have several shortcomings. Their signal can be dependent on the ionic strength (IS) of the sample solution. Unlike the glass electrode, optical sensors relying on the transition between two species of one indicator allow a very precise measurement of pH. However, this is achieved in a narrow range within 3–4 pH units only, [27] which often is not acceptable for certain applications. In order to determine the pH in a broader range [28] either a mixture of absorption-based pH indicators or a single indicator with multiple dissociation steps was used [29]. A fluorescent pH indicator was reported using new simple polyamines for a wide pH coverage, [30] or longwave (LED-) excitable iminocoumarin derivatives which were used in optical pH sensors for wide-range measurement providing high brightness and excellent photostability [16]. Optical pH sensors require changes in the protonation state of the indicator induced by pH to be transduced into changes such as absorption, [31] reflectance, [21] and luminescence [25]. Among these techniques, a luminescent pH sensor [32], [33] is the preferred setup due to its high sensitivity and applicability

to real samples without frequent recalibration. If embedded into a sensor membrane, a luminescent pH indicator should provide large Stokes shifts, a high quantum yield and excellent photostability. The literature shows that luminescent lanthanide (Ln) complexes can fulfil these requirements quite nicely [34] and exhibit sharp emission peaks compared to organic dyes, and a long excited-state lifetime ranging from μs to ms (Eu^{3+} , Tb^{3+}). These properties made lanthanide complexes important in various areas such as luminescent labels, probes, and phosphors, and for applications in environmental, biological, and clinical analyses [35]. Up to now, only one recent paper has shown the potential of lanthanide complexes for wide range sensing of pH [36] but only one single ligand was employed. However, the possibility of binding different ligands with various pK_{a} s to a lanthanide ion to cover a wider pH range has not been published so far.

Therefore, we developed a new strategy and complexed a mixture of ligands (some of which have multiple pK_{a} s that cover a wide range) to europium ions so to form a europium complex that acts as a wide range pH indicator. Hence, we employed pyridine-2,6-dicarboxylic acid (PDA) as a bidentate ligand that can strongly coordinate to Eu^{3+} and retain a deprotonable group after complexation with a pK_{a} of about 3. Gallic acid (Gall) acts as a ligand that also coordinates via its carboxylic acid group and then has two OH groups with $\text{pK}_{\text{a}1} = 4.5$ and $\text{pK}_{\text{a}2} = 10$. The weak absorbance and emission intensity of the bare europium ion is overcome through coordinating 2-thenoyl trifluoroacetone (TTA) which works as an efficient sensitizer. Complexes of these ligands with Eu^{3+} were formed in a 1 : 3 : 1 : 1 stoichiometry. This indicator shows a wide-range luminescence response from pH 2–10. The Eu–TTA–PDA–Gall complex was then embedded into a suitable polymeric membrane made of cellulose acetate (CA) coated on a Mylar support. The membrane enabled reversible pH sensing over time from pH 2–7 which is much wider than with conventional luminescent pH indicators. Sensor microtiterplates having a layer of Eu–TTA–PDA–Gall indicator in CA on the bottom of each well were developed to demonstrate high-throughput sensing capabilities over a wide pH range.

2.2 Results and discussion

2.2.1 Tested Eu/Tb - complexes with different ligands as a potential wide-range pH indicator.

In the beginning, we screened Eu/Tb- complexes as potential wide-range pH-indicators with various ligands and various molar ratios. We recorded spectra for absorption, excitation and luminescence in every molar ratio at various pH. Eu/Tb- complexes were used because they commonly show higher quantum yields which would make them more suitable for sensing. We show the overview of the results in the table 3 below and the comments indicate, why the complexes were chosen for further evaluation or not.

Table 4 Spectroscopy properties of tested Eu/Tb- complexes.

Complex	Ligand	M ³⁺ : Lig ratio	Abs. Spectrum	E _{xe.} Spectrum	E _{mi.} Spectrum	Comment
Eu ³⁺ / Tb ³⁺ - Acid Blue 45	Acid Blue 45	1:1 → 1:7	√	×	×	no luminescence
Eu ³⁺ / Tb ³⁺ - Curcumin	Curcumin	1:1 → 1:7	√	×	×	no luminescence
Eu ³⁺ / Tb ³⁺ - Carminic acid	Carminic acid	1:1 → 1:7	√	×	×	no luminescence
Eu ³⁺ / Tb ³⁺ - Purpurin	Purpurin	1:1 → 1:7	√	×	×	no luminescence
Eu ³⁺ / Tb ³⁺ - Alizarin red S	Alizarin red S	1:1 → 1:7	√	×	×	no luminescence
Eu ³⁺ / Tb ³⁺ - Alizarin Yellow R	Alizarin Yellow R	1:1 → 1:7	√	×	×	no luminescence
Eu ³⁺ / Tb ³⁺ - Alizarin Complexone dihydrate	Alizarin Complexone dihydrate	1:1 → 1:7	√	×	×	no luminescence
Eu ³⁺ / Tb ³⁺ - chromotropic acid	Chromotropic acid	1:3 and 1:4	√	×	×	no luminescence
Eu ³⁺ / Tb ³⁺ - Chromotropic acid- Nicotinic acid	Chromotropic acid and Nicotinic acid	1:1:3	√	×	×	no luminescence
Eu ³⁺ / Tb ³⁺ - Chromotropic acid- Salicylic acid	Chromotropic acid and Salicylic acid	1:1:3	√	×	×	no luminescence
Eu ³⁺ - Gallic acid	Gallic acid	1:1 → 1:4	√	×	×	no luminescence
Eu ³⁺ / Tb ³⁺ - Dithranol	Dithranol	1:3 and 1:4	√	×	×	no luminescence
Eu ³⁺ - TTA -Gall	TTA and Gall	1:3:1	√	√	√	emission drop at high pH
Eu ³⁺ - TTA -Gall - PDA	TTA -Gall - PDA	1:3:1:1	√	√	√	Strong emission over 5 pH-units
Tb ³⁺ - Gallic acid	Gallic acid	1:1 → 1:4	√	×	√	Very low emission band

Tb ³⁺ - TTA -Gall	TTA and Gall	1:3:1	√	×	×	no luminescence
Tb ³⁺ - PDA	PDA	1:1 → 1:4	√	√	√	emission drop at high pH
Tb ³⁺ -TTA-PDA-Gall	TTA & PDA & Gall	1:3:1:1	×	√	√	emission drop at high pH
Tb ³⁺ -PDA-TTA	PDA & TTA	1:1:1 & 1:2:1	×	√	√	emission drop at high pH
Tb ³⁺ -Xyla	Xyla	1:1-1:4	×	√	√	emission drop at high pH
Tb ³⁺ -PDA-Xyla	PDA & Xyla	1:4:0,25	×	√	√	emission drop at high pH
Tb ³⁺ - PDA-TTA-Xyla	PDA & TTA & Xyla	1:2:2:0,25	×	√	√	emission drop at high pH
Tb ³⁺ - PDA-Gall-Xyla	PDA & Gall & Xyla	1:2:2:0,25	×	√	√	emission drop at high pH
Tb ³⁺ - Diff-Tiron	Diff & Tiron	1:2:2 & 1:2:3 & 1:2:4	√	√	√	emission drop at high pH
Tb ³⁺ - PDA-Tiron	PDA & Tiron	1:2:2 & 1:3:2 & 1:2:3	×	√	√	emission drop at high pH
Tb ³⁺ - Diff- PDA	PDA & Diff	1:2:2 & 1:2:3 & 1:2:4 & 1:3:1 & 1:3:2	√	√	√	emission drop at high pH
Tb ³⁺ - PDA-ASA	PDA & ASA	1:3:1 & 1:1:3 & 1:1:4	√	√	√	emission drop at high pH
Tb ³⁺ - PDA-Isatin	PDA & Isatin	1:1:3 & 1:2:2 & 1:3:1 & 1:3:2	√	√	√	emission drop at high pH
Tb ³⁺ - PDA-Gall	PDA & Gall	1:3:1 & 1:3:2	×	√	√	emission drop at high pH
Tb ³⁺ - PDA-Kynurenic acid	PDA & Kynur	1:3:1 & 1:3:2	√	√	√	emission drop at high pH
Tb ³⁺ - PDA-Xanthurenic acid	PDA & Xanth	1:3:1 & 1:3:2	√	√	√	emission drop at high pH

First of all, we tested Eu³⁺ with various ligands such as Acid Blue 45. From fig. 22 we can see that a new absorption band at 625 nm appeared for the complex. With variation of the molar ratios at pH=9 the absorbance increased from 0.06 to 0.13 with increasing molar ratio while for the ligand Acid Blue 45 alone only an absorbance band appeared at 590 nm and no band at 625 nm. No excitation and emission bands were found for of Eu³⁺ : Acid Blue 45 complexes. Similar results were obtained for the ligands Curamine, and Carminic acid.

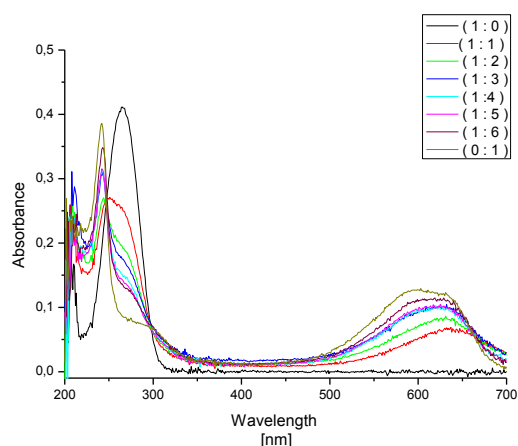


Figure 22 Absorption spectra of Eu^{3+} : Acid Blue 45, in various molar ratio, $n=100$ nmol, at $\text{pH}=9$, MOPS buffer (10 mmol L^{-1}).

Then we tested Eu^{3+} with Alizarin dihydrate (Ali). From fig. 23 we can see that a new absorption band at 535 nm appeared for the complex. With variation of pH at $\text{pH}=4-10$ this absorbance. With variation of pH at $\text{pH}=4-10$ this absorbance increases from 0,07 - to 0,30. For the ligand Ali alone this absorbance band appears at 425 nm and no band at 535 exists. Again, no excitation and emission band is found for of Eu^{3+} : Ali complexes.

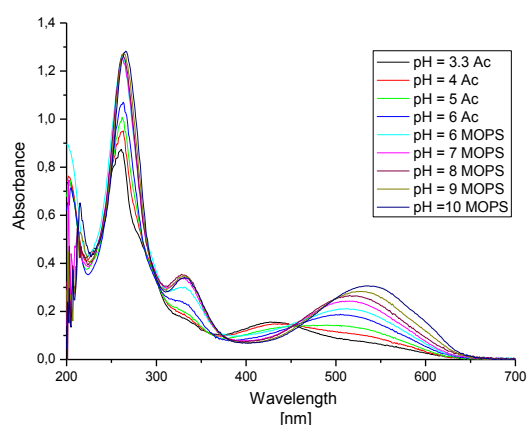


Figure 23 Absorption spectra of Eu^{3+} : Ali, in molar ratio 1:3, $n=100$ nmol, Ac or MOPS buffer (10 mmol L^{-1}), variation of color upon variation of pH.

We also tested with Tb- complexes as potential wide-range pH-indicators with various ligands and molar ratios, and recorded spectra for absorption, excitation and luminescence. Due to the huge amount of data (up to 10 spectra, each, for absorption, excitation and luminescence at every molar

ratio at various pH) we show the major part of the results in the table above. We first used Tb^{3+} with Ali. In fig. 24 we can see that a new absorption band at 524 nm emerged for the complex with variation of pH, at pH= 4-10. For the ligand Ali, however the absorbance band appears at 425 nm and not at 522 nm. No excitation and emission bands appeared for of Tb^{3+} : Ali complexes. Similar results were obtained when we tested Eu^{3+} / Tb^{3+} with other ligands like Purpurin, Alizarin Red S (ARS) and Alizarin Yellow R.

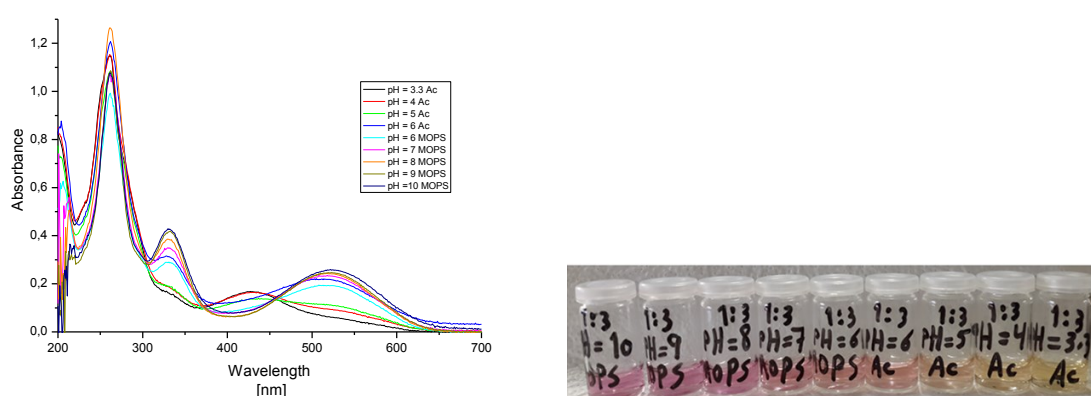


Figure 24 Absorption spectra of Tb^{3+} : Ali, in molar ratio 1:3, $n=100$ nmol, Ac or MOPS buffer (10 mmol L^{-1}), variation of color upon variation of pH.

We also tested the Tb :PDA:Gall complex. The excitation and emission spectra of the Tb :PDA:Gall complex in molar ratio 1:3:2 are pH-dependent in aqueous solution from pH 2-8 and this increase is suitable because it spans over 6 pH units. Fig. 25, shows the absorption spectra of Tb :PDA:Gall in a molar ratio of 1:3:2. No appear change of absorbance with variation of pH is visible.

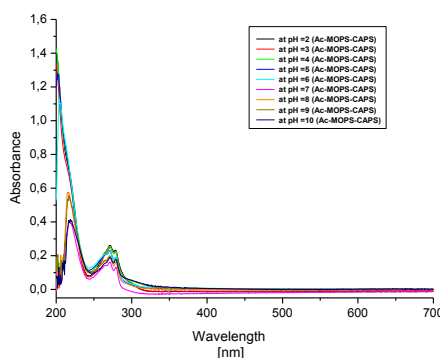


Figure 25 Absorption spectra of Tb^{3+} : PDA:Gall in molar ratio 1:3:2, $c=10 \mu \text{ mol L}^{-1}$ related to $c(\text{Tb}^{3+})$, Ac-MOPS-CAPS buffer (10 mmol L^{-1}).

Fig. 26 shows the excitation spectra of Tb:PDA:Gall in molar ratio 1:3:2 which is located at 280 nm if emission is recorded at 544 nm. The excitation is pH dependent over a wide range from pH 2-8, but drops at pH>8.

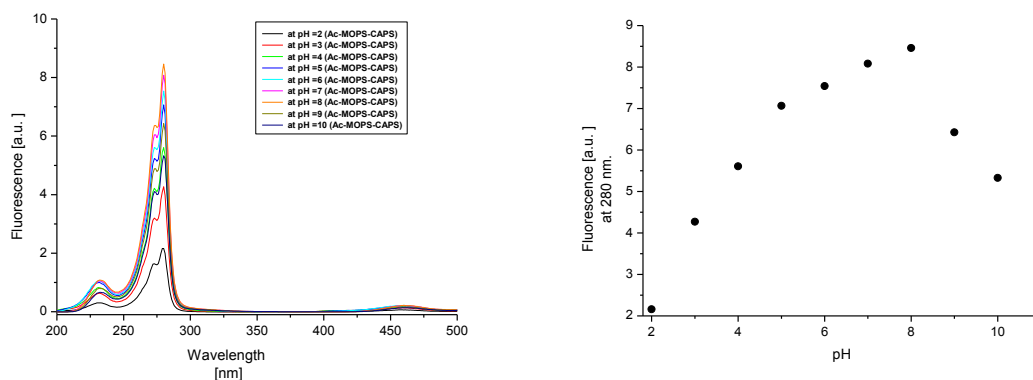


Figure 26 Excitation spectra of Tb:PDA:Gall in molar ratio 1:3:2, $c=10 \mu \text{ mol L}^{-1}$ related to $c(\text{Tb}^{3+})$, Ac-MOPS-CAPS buffer (10 mmol L^{-1}), $\lambda_{\text{em}}=544 \text{ nm}$.

Fig. 27 shows the emission spectra of Tb:PDA:Gall in molar ratio 1:3:2. The typical bands of a Tb^{3+} emission at 493 nm, 544 nm, and at 583 nm, respectively are seen. An increase of the fluorescence intensity at 545 nm ($\lambda_{\text{exc}}=280 \text{ nm}$) with variation of pH is clearly visible. The emission is pH-dependent over a wide range from pH 2-8 in an aqueous wide-range buffer (Ac-MOPS-CAPS buffer). This increase is a suitable because it spans over 6 pH units, but the results show that the emission drops at pH>8. For this the reason we could not chose this complex for sensor fabrication.

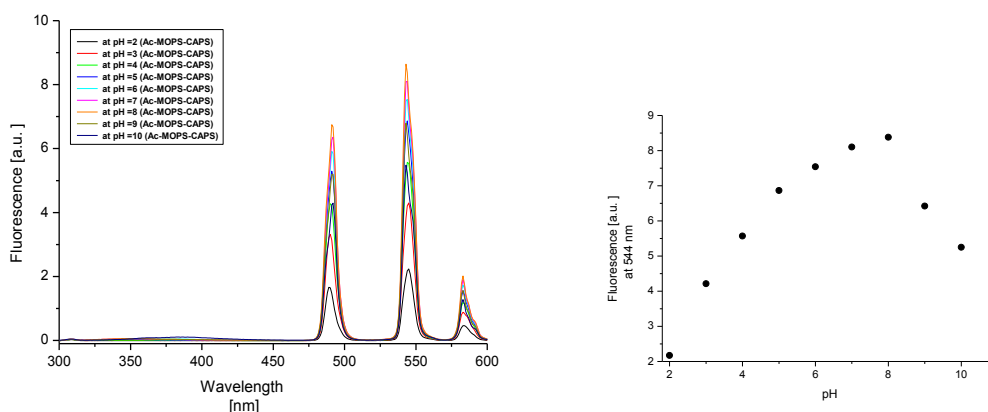


Figure 27 Emission Spectra of Tb:PDA:Gall in molar ratio 1:3:2, $c=10 \mu \text{ mol L}^{-1}$ related to $c(\text{Tb}^{3+})$, Ac-MOPS-CAPS buffer (10 mmol L^{-1}), $\lambda_{\text{exc}}=280 \text{ nm}$.

2.2.2 Choice of ligands and conceptual remarks

Ln complexes can exhibit favourable luminescence properties like sharp emission peaks, a large Stokes shift, insensitivity to oxygen, and a long excited state lifetime ranging from μs to ms (Eu^{3+} , Tb^{3+}). In the complex, the excitation light absorbed by the ligands is transferred to the ligand triplet state by intersystem crossing, and then intramolecularly transferred to the Eu^{3+} ion. However, the absorbance and emission intensities of the lanthanide ions in aqueous solution are weak due to low quantum yields and low absorption coefficients or low yields of the optical transitions following absorption. Hence, the ligands to be employed for this work had to fulfil three requirements. (1) They should efficiently sensitize lanthanide luminescence [37] and (2) contain bidentate moieties to strongly coordinate to the lanthanide ion and (3) contain deprotonable groups when coordinated. Pyridine-2,6-dicarboxylic acid (PDA) is a water-soluble ligand that can strongly coordinate to Eu^{3+} ions via one carboxylic acid group with a $\text{pK}_{\text{a}1} = 2.16$. The other one is used as a deprotonable group with a $\text{pK}_{\text{a}2} = 2.8$ [38], [39], [40] in the latter complex. Gallic acid (Gall) is a trihydroxybenzoic acid and a water-soluble ligand that can strongly coordinate to Eu^{3+} ions via the carboxylic acid group. The hydroxyl groups that remain after complexation have $\text{pK}_{\text{a}1} = 4.5$ and $\text{pK}_{\text{a}2} = 10$, [41], [42] respectively. Additionally, 2-thenoyl trifluoroacetone was employed because it is a well-known antenna ligand [43] for enhancing the lanthanide luminescence. TTA has a $\text{pK}_{\text{a}} = 6.38$ and its antenna effect can be modulated depending on the protonation in the complexed state. [44], [45] Once a Eu^{3+} -TTA-PDA-Gall complex is formed, the degree of protonation of one carboxylic group, one β -diketonate group and two phenolic OH groups impacts the luminescence behaviour of the complex with pH. As the pK_{a} s cover a range between 3 and 10 we hypothesized that such a complex could be a valuable model to be used as a wide-range pH indicator and as a probe in various optical pH sensor regimes.

Hence, we choose a Eu-TTA-PDA-Gall stoichiometry of 1 : 3 : 1 : 1. We are well aware of the fact that at this stoichiometry these ligands can occupy more coordination sites than Eu^{3+} has (usually 8–

9), but our experiments showed a better response to pH, less leaching off sensor membranes and a brighter emission if we choose a Eu–TTA–PDA–Gall stoichiometry of 1 : 3 : 1 : 1 instead of 1 : 2 : 1 : 1. As we cannot confirm that the response to pH is due to the presence of only one complex species but receive the best response to pH (especially in the latter sensor membrane) by Eu–TTA–PDA–Gall in a stoichiometry of 1 : 3 : 1 : 1, we refer to Eu–TTA–PDA–Gall in a feed ratio of 1 : 3 : 1 : 1 as the indicator in the ongoing text. Complexation constants of the ligands for Eu–PDA complexes in a 1 : 1 molar ratio, [46] for Eu–Gall (1 : 1 molar ratio), [47] and of TTA [48] (1 : 3) in aqueous solutions from literature data are similar. An Ac-MOPS-CAPS buffer (10 mmol L⁻¹) was chosen because its buffer range nicely matches with our desired pH range. Importantly, a Britton–Robinson buffer could not be chosen because its high content of phosphate can lead to precipitation of insoluble EuPO₄.

In preliminary experiments we wanted to determine if we could achieve a complex stoichiometry with respect to an optimized response of the indicator to be used inside the sensor membrane. For this purpose, we determined the absorption and emission spectra of Eu–Gall, Eu–TTA–Gall, Eu–PDA and Eu–TTA–PDA–Gall in acetate and MOPS buffer, respectively. It is important to note that in these earlier experiments the mixed Ac-MOPS-CAPS buffer was not used but the spectra were detected in acetate and MOPS buffer, separately. Therefore, two data points always appear at pH 6 (one from the spectrum in acetate and one from the spectrum in MOPS buffer) where the buffer ranges of acetate and MOPS overlap.

2.2.3 Absorption spectra

2.2.3.1 Absorption spectra of Eu-Gall & Eu-PDA & Eu-TTA -Gall

Fig. 28 shows the absorption spectra of Eu-Gall in molar ratio 1:1. The absorption at 280 nm is modestly dependent on pH.

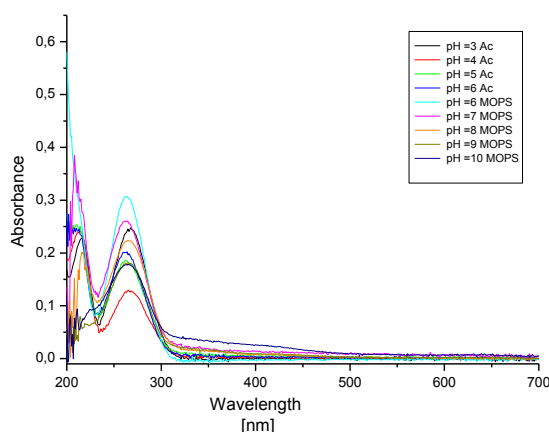


Figure 28 Absorption Spectra of Eu-Gall in molar ratio 1:1, $c=10 \mu\text{mol L}^{-1}$ related to $c(\text{Eu}^{3+})$, Ac or MOPS buffer (10 mmol L^{-1}).

The absorption spectra of Eu-PDA in Fig. 29 show pH dependence between pH 2 and pH 5, as well.

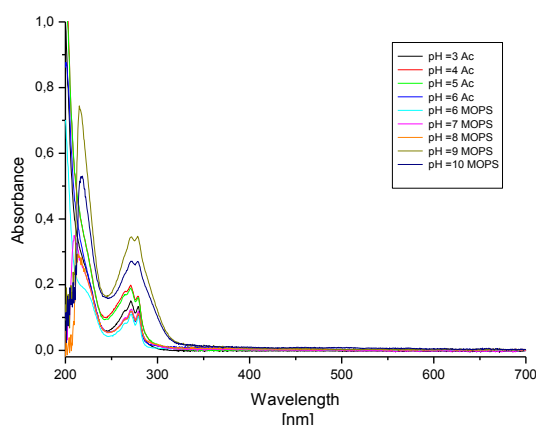


Figure 29 Absorbance Spectra of Eu-PDA in molar ratio (1:1), $c=10 \mu\text{mol L}^{-1}$ related to $c(\text{Eu}^{3+})$, Ac or MOPS buffer (10 mmol L^{-1}).

Hence, we decided to employ TTA as a well-known antenna ligand to enhance the emission of Eu^{3+} and to introduce the pH-dependence mainly via the Gall and PDA ligands. The absorption spectra of Eu-TTA-Gall (in molar ratio 1:3:1) in acetate and MOPS buffer were recorded, as well as the absorption spectra of all ligands alone. Fig. 30 shows a pH dependence of the luminescence of the complex between pH 4 and pH 8. This is close to the $\text{pK}_{\text{a}1} = 4.5$ of Gall [41], [42] but obviously the pK_{a} of Gall is a bit shifted to neutral pH upon complexation.

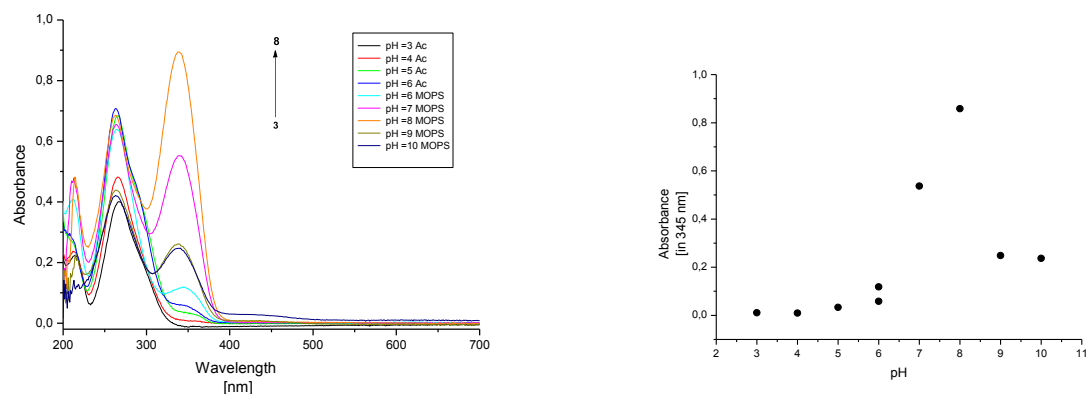


Figure 30 Absorbance Spectra of Eu-TTA-Gall in molar ratio (1:3:1), $C = 10 \mu\text{mol L}^{-1}$, Ac or MOPS buffer (10 mmol L⁻¹), and titration plot derived from the absorption spectra of Eu-TTA-Gall in 1:3:1 molar ratio at 340 nm.

2.2.3.2 Absorption spectra of Eu-TTA-PDA-Gall indicator

We acquired the absorption spectra of Eu³⁺-TTA-PDA-Gall (in molar ratio 1:3:1:1) in Ac-MOPS-CAPS buffer. As shown in Fig. 31, the complex shows two absorption maxima. The first one is located at 264 nm and shows higher absorbance ($\epsilon = 7.0 \times 10^4 \text{ L (mol cm)}^{-1}$ at pH 9) and is hardly dependent on pH. The more longwave absorption band shows a maximum at 340 nm ($\epsilon = 4.8 \times 10^4 \text{ L (mol cm)}^{-1}$ at pH 9) and a pronounced increase of the maximum absorption from pH 2–9. The new absorption band of Eu³⁺-TTA-PDA-Gall (1 : 3 : 1 : 1) at 340 nm proved the formation of the complex because it is absent in the absorption spectra of the pure ligands over the respective pH range. This indicates that a change of the luminescence spectra over a wide range could be expected.

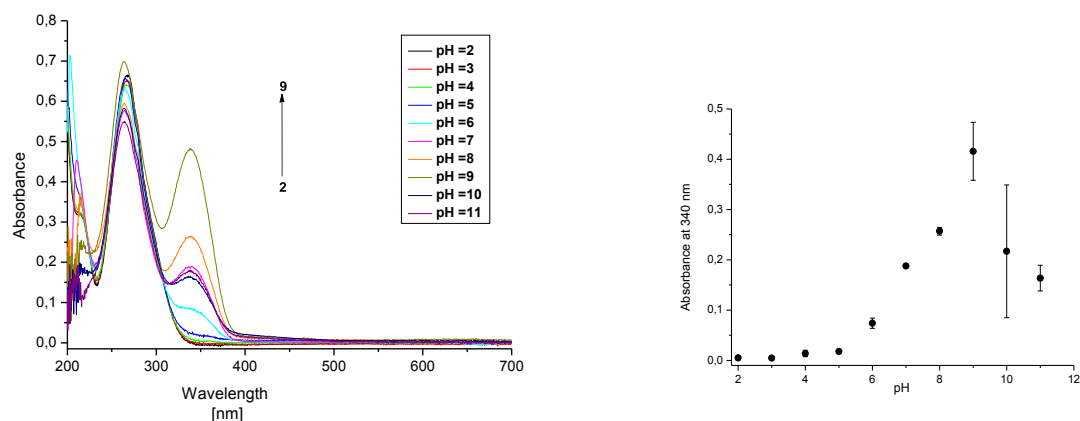


Figure 31 Absorption Spectra of Eu³⁺-TTA-PDA-Gall ($c=10 \mu\text{mol L}^{-1}$ related to $c(\text{Eu}^{3+})$, Ac-MOPS- CAPS buffer (10 mmol L^{-1} $n=3$).

2.2.4 Excitation spectra

2.2.4.1 Excitation spectra of Eu-Gall & Eu-TTA & Eu-TTA -Gall

Fig. 32 shows the excitation spectra of Eu-Gall in molar ratio 1:1. No emission is seen, just second order stray light.

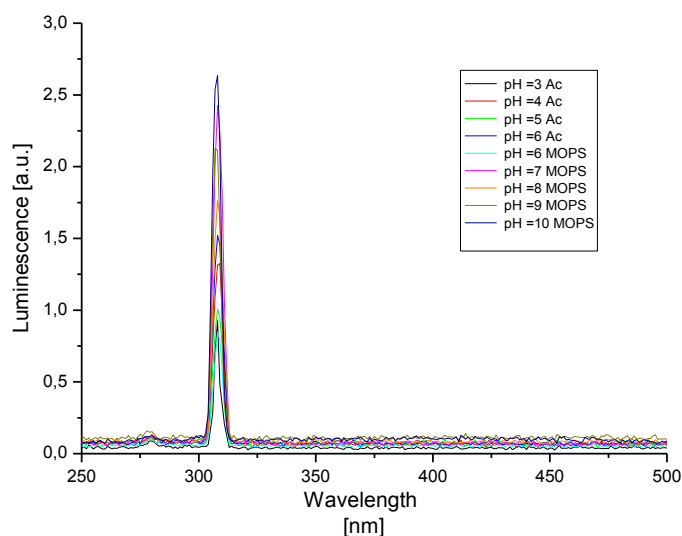


Figure 32 Excitation Spectra of Eu³⁺-Gall in molar ratio 1:1, ($c=10 \mu\text{mol L}^{-1}$ related to $c(\text{Eu}^{3+})$, Ac or MOPS buffer (10 mmol L^{-1}), $\lambda_{\text{em}}=615 \text{ nm}$).

The excitation spectra of Eu-TTA in Fig. 33 shows that there is no pH-dependent emission from Eu³⁺-TTA at $\lambda_{\text{exc}} > 300 \text{ nm}$, as well, except second order stray light.

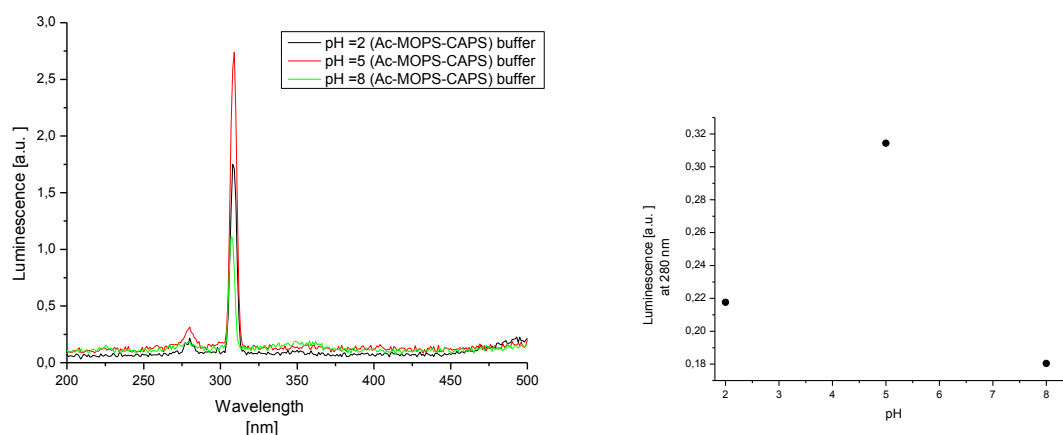


Figure 33 Excitation Spectra of Eu^{3+} -TTA in molar ratio 1:3, ($c=10 \mu\text{mol L}^{-1}$ related to $c(\text{Eu}^{3+})$, Ac-MOPS-CAPS buffer (10 mmol L^{-1}), $\lambda_{\text{em}}=615 \text{ nm}$.

The excitation maximum of Eu^{3+} -TTA-Gal in molar ratio 1:3:1 in acetate and MOPS buffer is at 345 nm. Fig. 34 shows pH-dependence over a range from pH 3 to pH 7, while for the ligand Gall the luminescence intensity is much lower at the same wavelength.

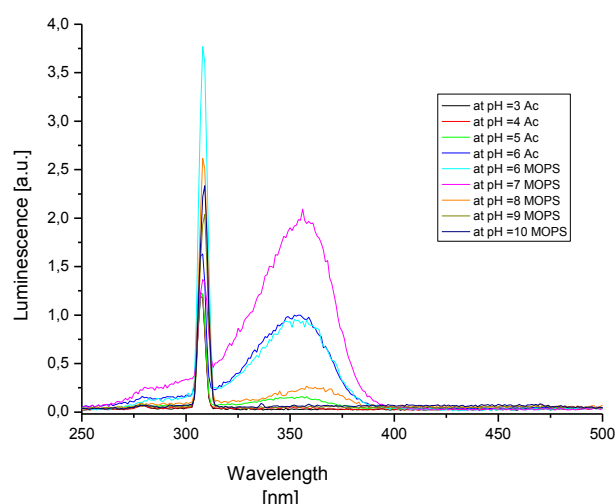


Figure 34 Excitation Spectra of Eu^{3+} -TTA-Gall ($c=10 \mu\text{mol L}^{-1}$ related to $c(\text{Eu}^{3+})$, Ac or MOPS buffer (10 mmol L^{-1}), $\lambda_{\text{em}}=615 \text{ nm}$).

2.2.4.2 Excitation spectra of Eu-TTA-PDA-Gall indicator

The excitation spectra of Eu^{3+} -TTA-PDA-Gall (molar ratio 1:3:1:1) in (Ac-MOPS-CAPS) buffer show three bands of the main $^5\text{D}_0 \rightarrow ^7\text{F}_2$ luminescence transition of Eu^{3+} ($\lambda_{\text{em}}=615 \text{ nm}$) that is used for detection (Fig. 35). Unlike in the absorption spectra (fig. 31), the shortwave excitation band (located at 280 nm) is strongly pH-dependent over a wide range from pH 2-10,

while the second band (at 350 nm) only slightly changed until pH 7. The reason for this is that the antenna effect of TTA on PDA is much higher than on Gall (compare intensity at 280 nm in fig. 35 with the one at 350 nm in fig. 35.) The small peak at 308 nm is second order diffraction.

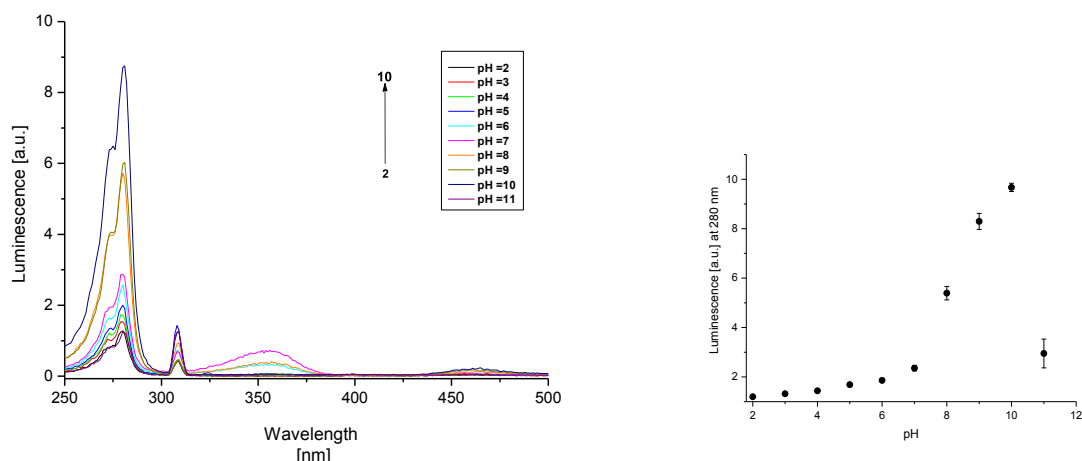


Figure 35 Excitation Spectra of Eu³⁺-TTA-PDA-Gall ($c=10 \mu\text{mol L}^{-1}$ related to $c(\text{Eu}^{3+})$, Ac-MOPS-CAPS buffer. (10 mmol L^{-1}), $\lambda_{\text{em}}=615 \text{ nm}$, $n=3$).

2.2.5 Emission spectra

2.2.5.1 Emission spectra of Eu-Gall & Eu-TTA & Eu-TTA -Gall

Fig. 36 shows the luminescence spectra of Eu³⁺-Gall (molar ratio 1:1) in acetate or MOPS buffer, respectively upon using 300 nm excitation. No emission is seen except from second order stray light at 600 nm.

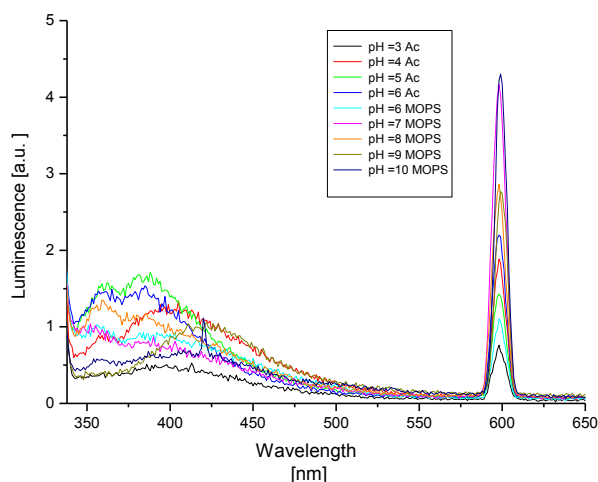


Figure 36 Emission spectra of Eu-Gall in 1:1 molar ratio ($c = 10 \mu\text{mol L}^{-1}$ related to $c(\text{Eu}^{3+})$, Ac or MOPS buffer 10 mmol L^{-1}), $\lambda_{\text{exc}}=300 \text{ nm}$.

The emission spectra of Eu–TTA are shown in Fig. 37 (molar ratio 1:3) in acetate or MOPS buffer, respectively, upon using 280 nm excitation. No emission is seen except from second order stray light at 560 nm.

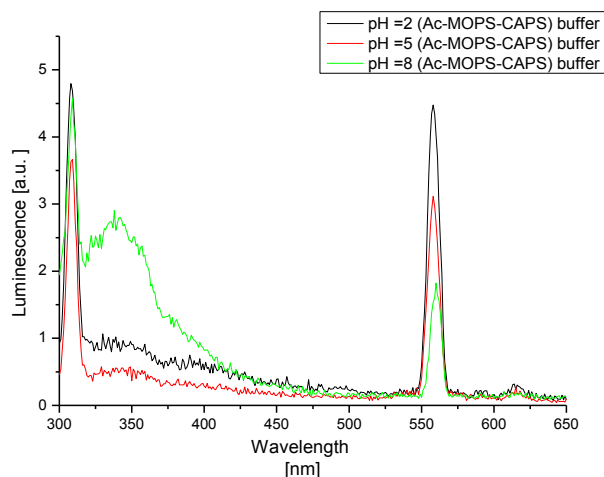


Figure 37 Emission spectra of Eu-TTA in 1:3 molar ratio ($c = 10 \mu\text{mol L}^{-1}$ related to $c(\text{Eu}^{3+})$, Ac–MOPS- CAPS buffer 10 mmol L^{-1}), $\lambda_{\text{exc}} = 280 \text{ nm}$.

Fig. 38 shows the luminescence spectra of Eu^{3+} –TTA–Gall (molar ratio 1 : 3 : 1) in acetate and MOPS buffer, respectively, upon using 345 nm excitation. They display the typical pattern of Eu^{3+} emission bands at 580 nm, 594 nm, and 615 nm, respectively. pH-dependent luminescence at 615 nm is found over a range from pH 5 - pH 7. An increase of the fluorescence intensity at 615 nm with variation of pH is clearly visible. However, the pH range is too small to use this complex in sensors.

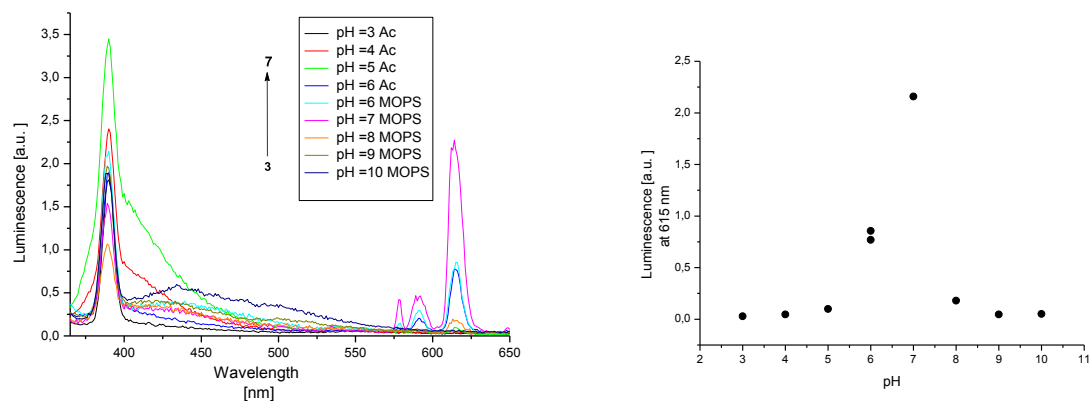


Figure 38 Emission spectra of Eu-TTA-Gall in 1:3:1 molar ratio ($c = 10 \mu\text{mol L}^{-1}$ related to $c(\text{Eu}^{3+})$, Ac or MOPS buffer 10 mmol L^{-1}), $\lambda_{\text{exc}} = 345 \text{ nm}$ and titration plot derived from the emission spectra of Eu-TTA-Gall in 1:3:1 molar ratio at 615 nm .

In Fig. 39 we show a wider response of the indicator complex Eu-PDA. This was expected by employing PDA as a ligand at Eu^{3+} with its $\text{pK}_{\text{a}1} = 2.16$ and $\text{pK}_{\text{a}2} = 2.8$ [38], [39], [40]. Eu-PDA gives a wider response in the range between pH 3-8 at 615 nm . This suggested the use of Eu-PDA inside pH sensor membranes. However, experiments to embed Eu-PDA in various sensor membrane materials failed because a high degree of leaching of the complex was found. This is presumably due to its high polarity.

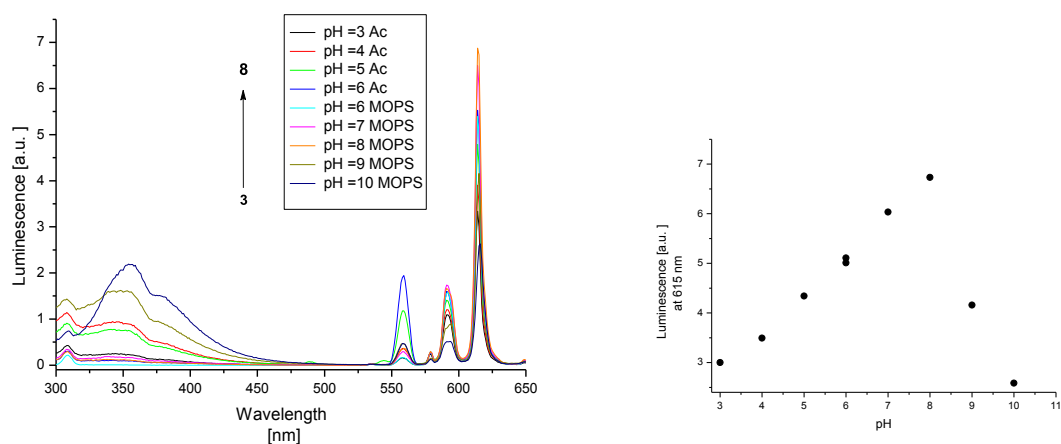


Figure 39 Emission spectra of Eu-PDA in 1:1 molar ratio; ($c = 10 \mu\text{mol L}^{-1}$ related to $c(\text{Eu}^{3+})$, Ac or MOPS buffer 10 mmol L^{-1}), $\lambda_{\text{exc}} = 345 \text{ nm}$ and titration plot derived from the emission spectra of Eu-PDA in 1:3:1 molar ratio at 615 nm .

By choosing PDA and Gall as pH-dependent ligands to be coordinated to Eu^{3+} we aimed at decreasing the overall polarity of the complex. The TTA antenna ligands further decrease complex

polarity so that leaching could be reduced to a negligible extent (see section on response time and reversibility).

Hence, we choose a Eu-TTA-PDA-Gall stoichiometry of 1:3:1:1. We are well aware of the fact that these ligands can occupy more coordination sites than Eu^{3+} has (usually 8-9), but our experiments showed a better response to pH, less leaching off sensor membranes and a brighter emission if we choose a Eu-TTA-PDA-Gall stoichiometry of 1:3:1:1 instead of 1:2:1:1. As we cannot confirm that the response to pH is due to the presence of only one complex species but receive the best response to pH (especially in the later sensor membrane) by Eu-TTA-PDA-Gall in a stoichiometry of 1:3:1:1. We refer to Eu-TTA-PDA-Gall in a feed ratio of 1 : 3 : 1 : 1 as the indicator in the ongoing text. Complexation constants of the ligands for Eu-PDA complexes in a 1 : 1 molar ratio, [46] for Eu-Gall (1 : 1 molar ratio), [47] and of TTA [48] (1 : 3) in aqueous solutions from literature data are similar. An Ac-MOPS-CAPS buffer (10 mmol L⁻¹) was chosen because its buffer range nicely matches with our desired pH range. Importantly, a Britton–Robinson buffer could not be chosen because its high content of phosphate can lead to precipitation of insoluble EuPO_4 .

2.2.5.2 Emission spectra of Eu-TTA-PDA-Gall indicator

We used 345 nm excitation, and measured the luminescence spectra of Eu^{3+} -TTA-PDA-Gall (molar ratio 1 : 3 : 1 : 1) in Ac or MOPS buffer. The typical pattern of Eu^{3+} emission bands appear at 580 nm, 594 nm, and 615 nm, respectively, for all pH values, but pH-dependence is weak.

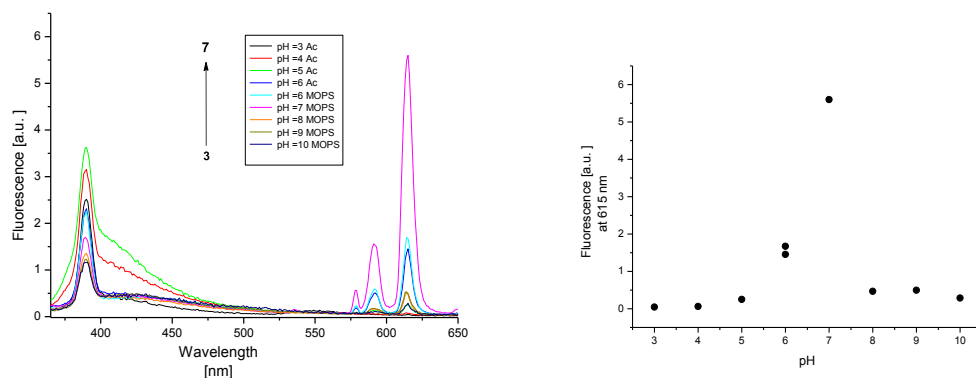


Figure 40 Emission Spectra of Eu^{3+} -TTA-PDA-Gall ; $c(\text{Eu}^{3+})$, Ac or MOPS buffer 10 mmol L⁻¹, $\lambda_{\text{exc}} = 345$ nm

Then we changed to 280 nm excitation. Fig. 41 shows the luminescence spectra enhancement of Eu^{3+} -TTA-PDA-Gall (molar ratio 1 : 3 : 1 : 1) in Ac or MOPS buffer over pH. Again, the typical pattern of Eu^{3+} emission bands at 580 nm, 594 nm, and 615 nm, respectively, are found for all pH values.

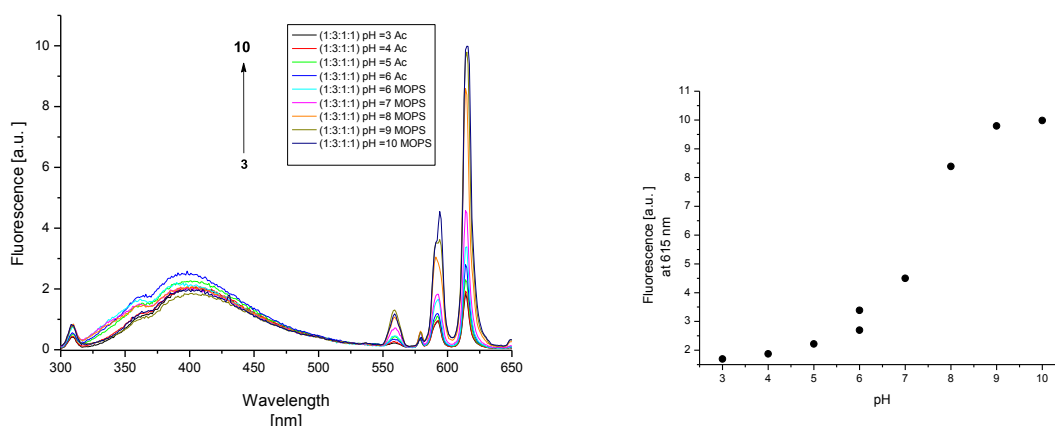


Figure 41 Emission Spectra of Eu^{3+} -TTA-PDA-Gall ($c = 10 \mu\text{mol L}^{-1}$ related to $c(\text{Eu}^{3+})$, Ac or MOPS buffer 10 mmol L^{-1}), $\lambda_{\text{exc}} = 280 \text{ nm}$.

Finally, Fig. 42 shows the luminescence spectra of Eu^{3+} -TTA-PDA-Gall (molar ratio 1 : 3 : 1 : 1) in a joint Ac-MOPS- CAPS buffer mixture upon using 280 nm excitation. The typical pattern of Eu^{3+} emission bands at 580 nm, 594 nm, and 615 nm, respectively, are found for all pH values. These bands correspond to the $^5\text{D}_0 \rightarrow ^7\text{F}_0$, $^5\text{D}_0 \rightarrow ^7\text{F}_1$ and $^5\text{D}_0 \rightarrow ^7\text{F}_2$ transitions of Eu^{3+} . An increase of the fluorescence intensity at 615 nm with variation of pH is clearly visible. This was expected with regard to the pK_{a} s of the ligands and is similar to the behaviour of Tb complexes with PDA derivatives. [37] The change of luminescence spans over 8 pH units (from pH 2–10). To our knowledge, this is the widest range covered by an optical pH-indicator based on lanthanide complexes. The only indicator system employing a FRET system from a europium chelate donor to a naphthofluorescein pH indicator yields a narrower pH response (6 pH units) in solution than our Ln complex (8 pH units) but has not been shown to work in a sensor membrane or a sensor microtiterplate. [49] Furthermore, this is a much wider pH range as the one that can be covered by the transition between two luminescent species of a single indicator. So far, the lanthanide

complexes are advantageous pH-indicators because their high coordination number of 8–9 permits the use of various ligands with various pK_a s in one molecule to spread the detection range of the luminescence indicator. According to the various pK_a s of the ligands, the luminescence of the complex can respond over a much wider range to changes of pH. The drop of emission at pH = 11 was probably due to the formation of traces of insoluble $\text{Eu}(\text{OH})_3$.

A detection range of about 8 pH units with luminescence is promising with respect to the fabrication sensor membranes which then could be used for continuous detection over time in a flow cell or in a high throughput regime in a sensor microtiterplate.

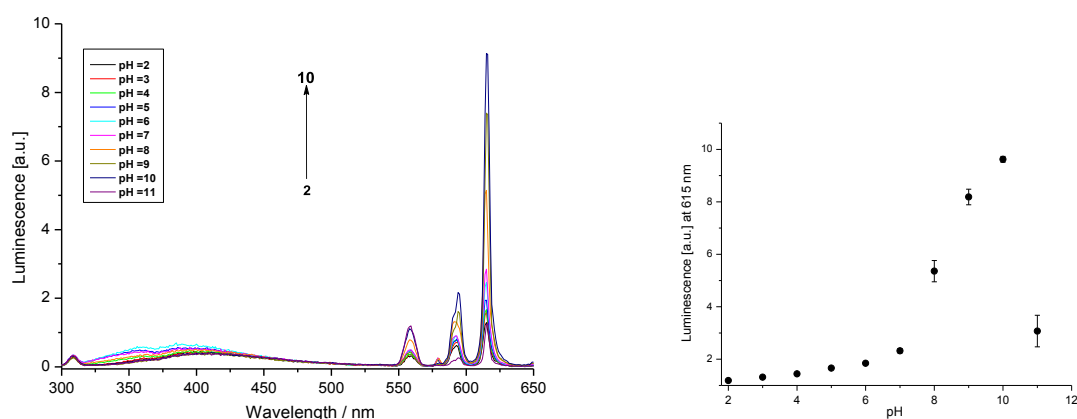


Figure 42 Emission Spectra of Eu^{3+} -TTA-PDA-Gall, ($c = 10 \mu\text{mol L}^{-1}$ related to $c(\text{Eu}^{3+})$, Ac-MOPS-CAPS buffer (10 mmol L^{-1}), $\lambda_{\text{exc}} = 280 \text{ nm}$, $n=3$).

2.2.6 Excitation spectra of pH-sensor membrane

The Eu -TTA-PDA-Gall complex was embedded into a suitable polymeric membrane made of cellulose acetate (CA). CA bears OH-groups and ester groups that make it rather hydrophilic and allow easy permeation of protons. CA is stable over a wide range of pH and a cocktail can be made in DMF to which the Eu^{3+} indicator is added in DMF solution. After two days of stirring at elevated temperature, the cocktail is knife-coated onto a mylar support ($125 \mu\text{m}$ thick) and dried overnight. As a result, strong luminescence of the complex in the membrane was visible upon irradiation with a UV-lamp at 366 nm (taken with a digital camera; see Figure 43).

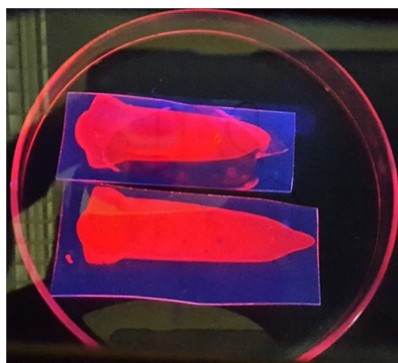


Figure 43 pH sensor foil containing Eu^{3+} -TTA- PDA-Gall (1:3:1:1) upon illumination with a UV lamp.(366 nm.).

In Figure 44, we show the excitation spectra of a sensor foil containing Eu^{3+} -TTA- PDA-Gall (molar ratio 1:3:1:1) by using the luminescence band of Eu^{3+} ($\lambda_{\text{em}} = 615 \text{ nm}$) at various pH. Aside from second order diffraction (at 308 nm), we found pH dependent excitation of Eu^{3+} -TTA-PDA-Gall to be located at 350 nm which is 70 nm more longwave than in aqueous solution. This can be a result of embedding the complex in the CA sensor membrane due to a change of the polarity of the microenvironment around the Eu^{3+} indicator inside the polymer. The more longwave excitation is a further advantage with respect to sensing because it induces less co-excitation of luminescence background in real samples. The pH-dependence spans from pH 2 to 7 over a wide range of 5 pH units.

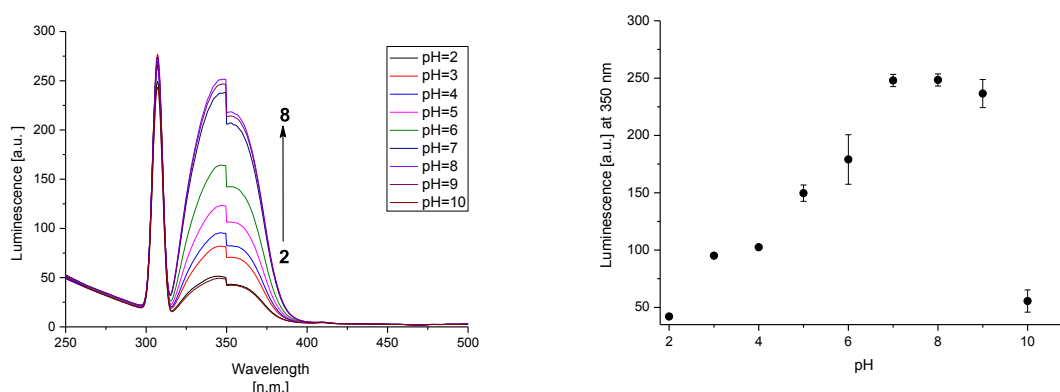


Figure 44 Excitation spectra of sensor membrane containing Eu^{3+} -TTA-PDA-Gall in molar ratio 1:3:1:1, ($c = 10 \text{ mmol L}^{-1}$ related to Eu^{3+} , Ac-MOPS-CAPS buffer (10 mmol L^{-1}), $\lambda_{\text{em}} = 615 \text{ nm}$, $n = 4$). The sudden drops of the emission at 352 nm in the spectra are an instrumental artifact.

2.2.7 Emission spectra of pH-sensor membrane

The pH-dependent luminescence spectra of the sensor membrane containing Eu^{3+} -TTA-PDA-Gall (molar ratio 1:3:1:1) are shown upon using 350 nm as excitation wavelength. Again, the typical bands of Eu^{3+} emission at 580 nm, 594 nm, and at 615 nm, respectively, are found (Fig. 45), similar to the spectra in aqueous buffer (Fig. 42). This points to a very hydrophilic environment around the indicator which is required for pH measurements. The pH dependence has a range from pH 2-7, as could be expected from the excitation spectra. Notably, the errors are smaller than in Fig. 42 and hence, a better reproducibility was achieved. The longwave pink colored emission of the complex (at 616 nm) is very longwave and thus little affected by potential co-fluorescent interferents which mostly emit in the more shortwave range of the visible spectrum, i.e. in the blue or green range. Hence, the large Stokes' shift of >260 nm of our pH probe can make measurements less prone to a potential interference of luminescent contaminants in real samples. The smaller dynamic range of the sensor membrane can be attributed to the fact that the membrane represents a diffusion barrier as compared to the situation when the complex is free in solution. Hence, at higher pH (which equals a lower concentration of the proton as the analyte) we are earlier approaching a point where one cannot discriminate the minute change of luminescence induced by the change of proton concentration inside the membrane. As diffusion is more limited inside the membrane than in solution, we find a reduced dynamic range of the indicator inside the membrane at higher pHs as compared to when the complex can exchange protons free in solution (Fig. 42). The pH response of the sensor membrane from 2-7 can be fitted with $y = 53.2 \cdot \text{pH} - 62.9$ ($r^2=0.98$) which gives the sensor a very good resolution.

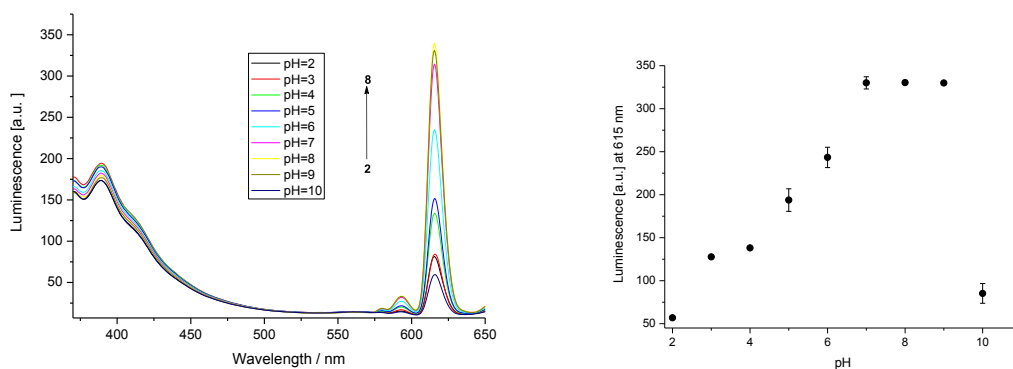


Figure 45 Emission spectra of pH sensor membrane containing Eu^{3+} -TTA-PDA-Gall (Ac – MOPS-CAPS buffer (10 mmol L^{-1}), $\lambda_{\text{exc}} = 350 \text{ nm}$, $n=4$).

2.2.8 Response time and reversibility of pH-sensor membrane

Fig. 46 shows that pH sensing over time is possible on-line over a time period of $>2.5 \text{ h}$ with only minor leaching (2.6% loss of luminescence intensity at $t = 9000 \text{ s}$ compared to the luminescence intensity at $t = 500 \text{ s}$) of the complex off the sensor membrane. The measurement range again spans over 5 pH units and is highly reversible. The forward response time t_{90} per pH unit is on average at 12.8 min from which 4.5 min are required for the exchange of the sample medium in the flow cell. Therefore, one could deduce an even more rapid response as low as 480 s which is more rapid or similar to what was found earlier. [25], [32], [33] Other authors found a slightly lower t_{90} value (120 s (pH 8.5 \rightarrow 7.5)/230 s (pH 7.5 \rightarrow 8.5)) [9] or a t_{95} of about 60 s when going from pH 2 pH 12. [16] A further reduction of the response time of our sensor can be achieved by reducing the thickness of the membrane to $30 \mu\text{m}$ (see fig. 47 and 48). Qi et al. reported on similar response times of a sensor membrane containing various immobilized photoinduced electron transfer (PET) probes to cover a wide pH range. [50] However, these more rapid responding sensors required covalent conjugation of the indicators to the polymer[25], [50] and the presence of more than one indicator [50] making sensor fabrication more complex than in our case with just one indicator being mixed with the polymer. However, this sensor has a Stokes shift of only 70 nm and an emission maximum at 550 nm whereas our concept provides $>200 \text{ nm}$ and more longwave 615 nm emission which both are a benefit for measurements in strongly scattering media.

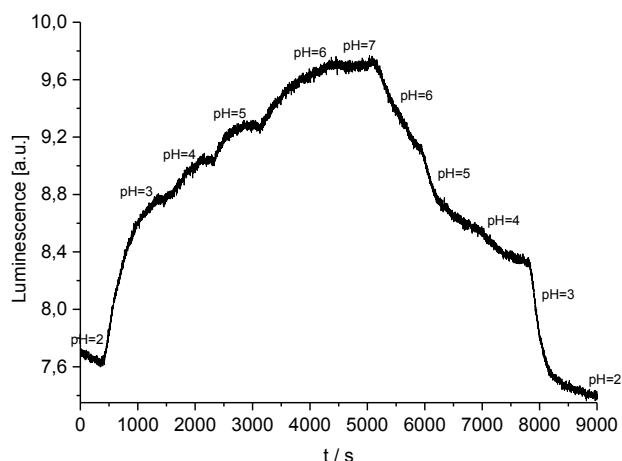


Figure 46 Reversibility of a 60 µm pH sensor membrane in Ac-MOPS-CAPS buffer (10 mmol L⁻¹) over time at variation pH.

Fig. 47 and 48 show again that pH sensing over a longer time is possible on-line with only minute leaching (1–2%) of the complex off the sensor membrane. Again, the measurement range spans over 5 pH units and is highly reversible. The thinner foil (Fig. 48; 30 µm thick) contributes to a more rapid response here at the cost of a slightly reduced reversibility. In agreement with the previous experiment with continuously increasing/decreasing pH, the back response time of the membrane is considerably shorter when switching from neutral to acidic pH. This can be an additional advantage if samples are monitored that show high and distinct changes of pH.

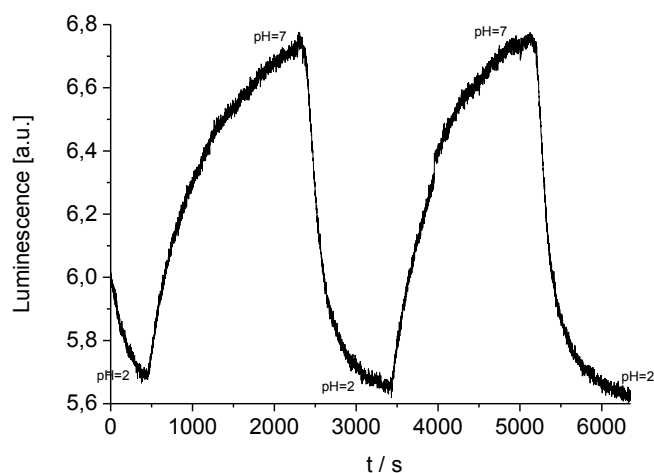


Figure 47 Reversibility of pH sensor membrane (60 µm) when switching from pH 2-7.

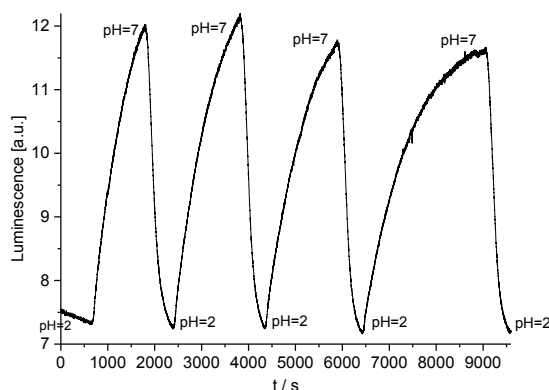


Figure 48 Reversibility of pH sensor membrane (thickness 30 μm) when switching from pH 2-7.

2.2.9 pH sensor microtiterplate

In CA, a strong luminescence of the complex of the cocktail is visible (Fig. 49) once it is deposited in a microtiterplate. The drying procedure and the cocktail had to be modified (see the experimental section) to avoid cracks in the membrane and the microtiterplate upon drying. Unlike the mylar used as the supporting material for the sensor membranes, the polystyrene the microtiterplate is made of is more sensitive to the DMF solvent of the sensor cocktail.

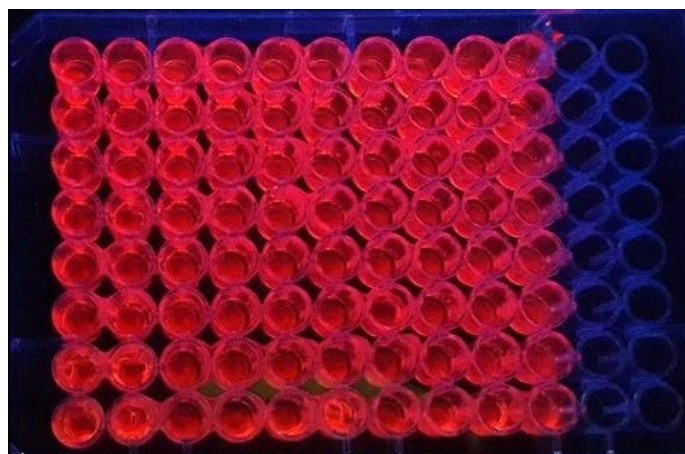


Figure 49 pH sensor microtiterplate with Eu^{3+} -TTA-PDA-Gall (1:3:1:1) upon illumination with UV lamp (366 nm.).

In Fig. 50 we show the plot of the luminescence at 615 nm of the sensor microtiterplate in response to pH. A favorable pH-dependence over a wide range of 6 pH units is found. The luminescence

response to changes of pH was read upon excitation with a wide-range excitation filter at 355 nm every 5 min. The best reproducibility was achieved after about 60 min but reliable values are found after 10 min, already. This can enable virtual online measurements, if the changes of pH do not occur on a too rapid timescale. This shows a good long-term capability of the sensor plate for high-throughput pH measurements in the acidic to the neutral pH range. The pH response of the sensor microtiterplate from 2-8 can be fitted with $y=3760 \cdot \text{pH} + 34920$ ($r^2=0.98$).

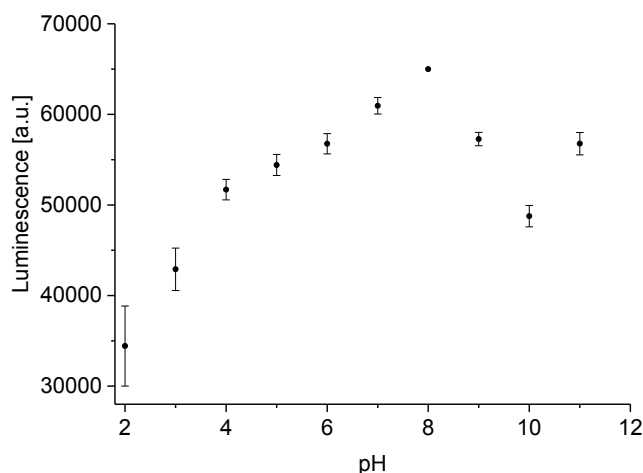


Figure 50 Response of sensor microtiterplate with Eu^{3+} -TTA-PDA-Gall (Ac-MOPS-CAPS buffer (10 mmol L^{-1}) to variation pH ($\lambda_{\text{em}} = 615 \text{ nm}$, $\lambda_{\text{exc}} = 355 \text{ nm}$, $n=8$).

In Fig. 51 we show that pH sensing is still possible after 24 h with a pH-dependence over a wide range of 5 pH units, and good reproducibility

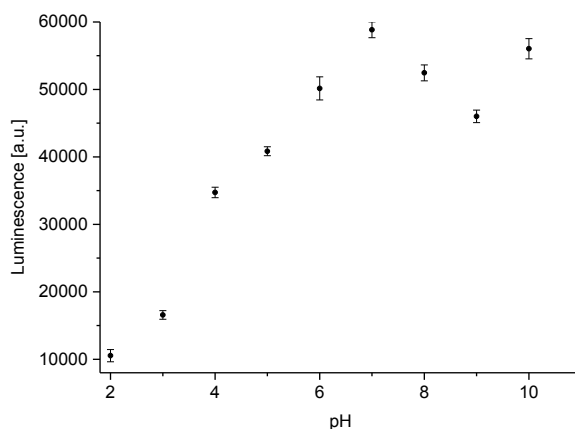


Figure 51 Response of sensor microtiterplate with Eu^{3+} -TTA-PDA-Gall (Ac-MOPS-CAPS buffer (10 mmol L^{-1}) to variation pH ($\lambda_{\text{em}} = 615 \text{ nm}$, $\lambda_{\text{exc}} = 355 \text{ nm}$, $n=8$) after 24 h.

2.3 Conclusion

Our new concept shows that it is possible to design pH indicators that are composed of only one type of molecule that carries various ligands with multiple protonation sites. The various pK_a values of the ligands enable a pH-dependent luminescence response of the lanthanide complexes over a range of 8 pH units which is unique for a single indicator molecule. The complex shares the typical advantages of lanthanide complexes such as a large Stokes' shift of >260 nm and a longwave 615 nm emission which both are a benefit for the use in sensors or measurements in strongly scattering media. New low-cost optical sensor membranes for continuous wide-range measurement of pH over 5 pH units could be fabricated. They are fully reversible, have a long operational lifetime and response times that are common for luminescent pH sensor membranes. Finally, a sensor microtiterplate with long operational lifetime and a response range of 6 pH units demonstrates that our new sensor concept can also be used for high-throughput sensing of pH.

2.4 Experimental section

Materials

2-Thenoyltrifluoroacetone and pyridine-2,6-dicarboxylic acid (PDA) were obtained in 99% purity from Sigma–Aldrich and gallic acid (Gall) was obtained in 99% purity from Fluka. EuCl_3 in 99.99% purity was obtained from Sigma–Aldrich. Ac-MOPS-CAPS buffer solution was prepared by dissolving 10 mmol/L (99% purity, from ROTH) of each, 3-(*N*-Morpholino)-propanesulfonic acid (MOPS) and *N*-cyclohexyl-3-aminopropanesulfonic acid (CAPS) and acetic acid (glacial, 100% purity, from Merck) (Ac) in bidistilled water. Stock solutions of europium chloride were prepared by dissolving 100 $\mu\text{mol/L}$ of EuCl_3 in Ac-MOPS-CAPS buffer (10 mmol/L) of various pH 2–11. Ligand stock solutions of the same concentration (100 $\mu\text{mol/L}$) in the same buffer were prepared over the whole pH range. Diluted solutions of Eu^{3+} -TTA-Gall-PDA were obtained by mixing 200 μL of Eu^{3+} stock solution, 600 μL of TTA stock solution, 200 μL of Gall stock solution, and 200 μL

of PDA stock solution with 800 μL of Ac-MOPS-CAPS buffer to 2 mL at the respective pH (2-11). These solutions were also mixed in variable molar ratio (i.e. volume of Eu^{3+} : Ligand 1: Ligand 2: Ligand 3) for every pH and the complexes were allowed to form in solution. Ionic strength was kept constant at 10 mM with NaCl during all measurements. The cellulose acetate (Mw 30,000 Da, 39.8 wt% acetyl content) was from Sigmaaldrich and a biaxial polyethylene terephthalate foil (MylarTM) of 125 μm thickness from Goodfellow (Bad Nauheim, Germany) served as solid support for the sensor membranes. Membrane thicknesses are given as adjusted during the knife coating process.

Apparatus

pH was adjusted with a pH meter CG 842 from Schott. All absorption spectra were recorded at room temperature on a Varian Cary 50 Bio UV-Visible Spectrophotometer by using quartz cells with a 1 cm path length. Luminescence measurements of complexes in aqueous solution were carried out on an Aminco Bowman AB2 luminescence spectrometer. Slit widths for excitation and emission were 4 nm and 4 nm, respectively. Sensor membranes were characterized on a Jasco 6300 spectrofluorimeter equipped with a flow cell oriented with 30° incident angle. A 150 W Xenon lamp served as excitation source and the slit widths of excitation and emission wavelength were 5 nm and 5 nm, respectively. Microtiterplate measurements were performed with a BMG Fluostar OPTIMA with filters for excitation of 355 nm (40 nm FWHM) and emission of 615 nm (10 nm FWHM). All spectroscopic measurements were conducted at 22°C.

Fabrication of sensor membranes and sensor microtiterplates

A 10 % wt. polymer solution of CA is made in dimethyl formamide (DMF), as well as a solution of 10 mmol/L of Eu^{3+} -TTA-Gall-PDA (1:3:1:1) in DMF. 250 μL of indicator solution and 750 μL of CA in DMF are added into a preheated (60 °C) glass vial and mixed violently for about 48 h. This is the sensor cocktail. 200 μL of warm cocktail are knife coated on a Mylar foil strip to spread the cocktail on the carrier foil. The thickness of the wet sensor membrane can be adjusted to 60 or 30

μm, respectively. The sensor membrane is dried in an oven for 24 h at 60 °C to evaporate the DMF, this yield final membrane thickness about 6 and 3 μm, respectively. Membranes of 2.0 cm diameter are cut with a hole puncher and mounted in the flow cell where buffers of various pH are pumped by a Gilson minipulse 3 pump with a speed of 1.5 mL/min.

Transparent flat bottom micro plates (product number 655101) from Greiner BIO-ONE GmbH were filled with 25 μL of cocktail. The microtiterplate was dried in an oven for 3 h at 40 °C to evaporate the DMF solvent, washed 6 times with bidistilled water, and the respective buffer (100 μmol/L, pH 2-11) was added.

2.5 References

- [1] J. Peng, Y. Song, P. Yuan, X. Cui, and G. Qiu, "The remediation of heavy metals contaminated sediment," *J. Hazard. Mater.*, vol. 161, pp. 633–640, 2009.
- [2] M. O. Rivett, S. R. Buss, P. Morgan, J. W. N. Smith, and C. D. Bemment, "Nitrate attenuation in groundwater: a review of biogeochemical controlling processes," *Water Res.*, vol. 42, pp. 4215–4232, 2008.
- [3] P.-Y. Stergiou, A. Foukis, M. Filippou, M. Koukouritaki, M. Parapouli, L. G. Theodorou, E. Hatziloukas, A. Afendra, A. Pandey, and E. M. Papamichael, "Advances in lipase-catalyzed esterification reactions," *Biotechnol. Adv.*, vol. 31, pp. 1846–1859, 2013.
- [4] M. Galbe and G. Zacchi, "Pretreatment: the key to efficient utilization of lignocellulosic materials," *Biomass and bioenergy*, vol. 46, pp. 70–78, 2012.
- [5] P. Paroutis, N. Touret, and S. Grinstein, "The pH of the secretory pathway: measurement, determinants, and regulation," *Physiology*, vol. 19, pp. 207–215, 2004.
- [6] X. Zhang, Y. Lin, and R. J. Gillies, "Tumor pH and its measurement," *J. Nucl. Med. Off. Publ. Soc. Nucl. Med.*, vol. 51, p. 1167, 2010.
- [7] M. Koch, G. Bowes, C. Ross, and X. Zhang, "Climate change and ocean acidification effects on seagrasses and marine macroalgae," *Glob. Chang. Biol.*, vol. 19, pp. 103–132, 2013.
- [8] R. Gotor, P. Ashokkumar, M. Hecht, K. Keil, and K. Rurack, "Optical pH sensor covering the range from pH 0–14 compatible with mobile-device readout and based on a set of rationally designed indicator dyes," *Anal. Chem.*, vol. 89, pp. 8437–8444, 2017.
- [9] C. R. Schröder, B. M. Weidgans, and I. Klimant, "pH fluorosensors for use in marine systems," *Analyst*, vol. 130, pp. 907–916, 2005.
- [10] M. S. Juarez Tomas, B. Wiese, and M. E. Nader-Macías, "Effects of culture conditions on the growth and auto-aggregation ability of vaginal *Lactobacillus johnsonii* CRL 1294," *J. Appl. Microbiol.*, vol. 99, pp. 1383–1391, 2005.

- [11] E. H. Drosinos, M. Mataragas, P. Nasis, M. Galiotou, and J. Metaxopoulos, "Growth and bacteriocin production kinetics of *Leuconostoc mesenteroides* E131," *J. Appl. Microbiol.*, vol. 99, pp. 1314–1323, 2005.
- [12] E. Simova, Z. Simov, D. Beshkova, G. Frengova, Z. Dimitrov, and Z. Spasov, "Amino acid profiles of lactic acid bacteria, isolated from kefir grains and kefir starter made from them," *Int. J. Food Microbiol.*, vol. 107, pp. 112–123, 2006.
- [13] M. Hara-Chikuma, Y. Wang, S. E. Guggino, W. B. Guggino, and A. S. Verkman, "Impaired acidification in early endosomes of CIC-5 deficient proximal tubule," *Biochem. Biophys. Res. Commun.*, vol. 329, pp. 941–946, 2005.
- [14] S. Muhrizal, J. Shamshuddin, I. Fauziah, and M. A. H. Husni, "Changes in iron-poor acid sulfate soil upon submergence," *Geoderma*, vol. 131, pp. 110–122, 2006.
- [15] P. Wiczling, M. J. Markuszewski, M. Kaliszan, K. Galer, and R. Kaliszan, "Combined pH/organic solvent gradient HPLC in analysis of forensic material," *J. Pharm. Biomed. Anal.*, vol. 37, pp. 871–875, 2005.
- [16] A. S. Vasylevska, A. A. Karasyov, S. M. Borisov, and C. Krause, "Novel coumarin-based fluorescent pH indicators, probes and membranes covering a broad pH range," *Anal. Bioanal. Chem.*, vol. 387, pp. 2131–2141, 2007.
- [17] M. Schindler, S. Grabski, E. Hoff, and S. M. Simon, "Defective pH regulation of acidic compartments in human breast cancer cells (MCF-7) is normalized in adriamycin-resistant cells (MCF-7adr)," *Biochemistry*, vol. 35, pp. 2811–2817, 1996.
- [18] H. Izumi, T. Torigoe, H. Ishiguchi, H. Uramoto, Y. Yoshida, M. Tanabe, T. Ise, T. Murakami, T. Yoshida, and M. Nomoto, "Cellular pH regulators: potentially promising molecular targets for cancer chemotherapy," *Cancer Treat. Rev.*, vol. 29, pp. 541–549, 2003.
- [19] Z. Liu, J. Liu, and T. Chen, "Phenol red immobilized PVA membrane for an optical pH sensor with two determination ranges and long-term stability," *Sens. Actuat. B*, vol. 107, pp. 311–316, 2005.
- [20] A. A. Belyustin, "The centenary of glass electrode: from Max Cremer to FGK Baucke," *J. Solid State Electrochem.*, vol. 15, pp. 47–65, 2011.
- [21] O. S. Wolfbeis, "Fiber-optic chemical sensors and biosensors," *Anal. Chem.*, vol. 78, pp. 3859–3873, 2006.
- [22] D. Wencel, T. Abel, and C. McDonagh, "Optical chemical pH sensors," *Anal. Chem.*, vol. 86, pp. 15–29, 2013.
- [23] B. M. Weidgans, C. Krause, I. Klimant, and O. S. Wolfbeis, "Fluorescent pH sensors with negligible sensitivity to ionic strength," *Analyst*, vol. 129, pp. 645–650, 2004.
- [24] S. Schreml, R. J. Meier, M. Kirschbaum, S. C. Kong, S. Gehmert, O. Felthaus, S. Kuchler, J. R. Sharpe, K. Wöltje, and K. T. Weiß, "Luminescent dual sensors reveal extracellular pH-gradients and hypoxia on chronic wounds that disrupt epidermal repair," *Theranostics*, vol. 4, p. 721, 2014.
- [25] A. Kriltz, C. Löser, G. J. Mohr, and S. Trupp, "Covalent immobilization of a fluorescent pH-sensitive naphthalimide dye in sol–gel films," *J. Sol-gel Sci. Technol.*, vol. 63, pp. 23–29, 2012.
- [26] C.-G. Niu, X.-Q. Gui, G.-M. Zeng, A.-L. Guan, P.-F. Gao, and P.-Z. Qin, "Fluorescence ratiometric

- pH sensor prepared from covalently immobilized porphyrin and benzothioxanthene," *Anal. Bioanal. Chem.*, vol. 383, pp. 349–357, 2005.
- [27] F. B. M. Suah, M. Ahmad, and M. N. Taib, "Optimisation of the range of an optical fibre pH sensor using feed-forward artificial neural network," *Sens. Actuat. B*, vol. 90, pp. 175–181, 2003.
 - [28] C.-G. Niu, X.-Q. Gui, G.-M. Zeng, and X.-Z. Yuan, "A ratiometric fluorescence sensor with broad dynamic range based on two pH-sensitive fluorophores," *Analyst*, vol. 130, pp. 1551–1556, 2005.
 - [29] J. Lin and D. Liu, "An optical pH sensor with a linear response over a broad range," *Anal. Chim. Acta*, vol. 408, pp. 49–55, 2000.
 - [30] G. Nishimura, Y. Shiraishi, and T. Hirai, "A fluorescent chemosensor for wide-range pH detection," *Chem. Commun.*, vol. 42, pp. 5313–5315, 2005.
 - [31] C. Florea, Larisa Fay, T. Lahiff, Emer Phelan, and O'Connor, "Dynamic pH mapping in microfluidic devices by integrating adaptive coatings based on polyaniline with colorimetric imaging techniques," *Lab Chip*, vol. 13, pp. 1079–1085, 2013.
 - [32] L. Ferrari, L. Rovati, P. Fabbri, and F. Pilati, "Disposable fluorescence optical pH sensor for near neutral solutions," *Sensors (Switzerland)*, vol. 13, pp. 484–499, 2013.
 - [33] D. Aigner, B. Ungerböck, T. Mayr, R. Saf, I. Klimant, and S. M. Borisov, "Fluorescent materials for pH sensing and imaging based on novel 1,4-diketopyrrolo-[3,4-c]pyrrole dyes," *J. Mater. Chem. C*, vol. 1, pp. 5685–5693, 2013.
 - [34] T. Gunnlaugsson, J. P. Leonard, K. Sénéchal, and A. J. Harte, "pH responsive Eu(III)-phenanthroline supramolecular conjugate: Novel off-on-off luminescent signaling in the physiological pH range," *J. Am. Chem. Soc.*, vol. 125, pp. 12062–12063, 2003.
 - [35] A. Picot, A. D'Aléo, and P. L. Baldeck, "Long-lived two-photon excited luminescence of water-soluble europium complex: Applications in biological imaging using two-photon scanning microscopy," *J. Am. Chem. Soc.*, vol. 130, pp. 1532–1533, 2008.
 - [36] M. Turel, M. Čajlaković, E. Austin, J. P. Dakin, G. Uray, and A. Lobnik, "Direct UV-LED lifetime pH sensor based on a semi-permeable sol-gel membrane immobilized luminescent Eu³⁺ chelate complex," *Sens. Actuat. B*, vol. 131, pp. 247–253, 2008.
 - [37] G. liang Gu, R. ren Tang, Y. hu Zheng, and X. ming Shi, "Synthesis, characterization and fluorescence properties of novel pyridine dicarboxylic acid derivatives and corresponding Tb(III) complexes," *Spectrochim. Acta - A*, vol. 71, pp. 209–214, 2008.
 - [38] D. K. Singha, P. Majee, S. K. Mondal, and P. Mahata, "pH-Controlled Luminescence Turn-On Behaviour of a Water-Soluble Europium-Based Molecular Complex," *Eur. J. Inorg. Chem.*, vol. 2016, pp. 4631–4636, 2016.
 - [39] M. V. Kirillova, M. F. C. Guedes da Silva, A. M. Kirillov, J. J. R. Fraústo da Silva, and A. J. L. Pombeiro, "3D hydrogen bonded heteronuclear Coll, NiII, CuII and ZnII aqua complexes derived from dipicolinic acid," *Inorganica Chim. Acta*, vol. 360, pp. 506–512, 2007.
 - [40] L. N. Puntus, V. F. Zolin, T. A. Babushkina, and I. B. Kutuza, "Luminescence properties of isomeric and tautomeric lanthanide pyridinedicarboxylates," *J. Alloys Compd.*, vol. 380, pp. 310–314, 2004.

- [41] A. F. S. Abbasi, A. Daneshfar, S. Hamdghadareh, "quantification of sub-nano molar levels of Gallic acid by adsorptive stripping voltammetry," *Int. J. Electrochem. Sci.*, vol. 6, pp. 4843–4852, 2011.
- [42] P. Dwibedy, G. R. Dey, D. B. Naik, K. Kishore, and P. N. Moorthy, "Pulse radiolysis studies on redox reactions of gallic acid: One electron oxidation of gallic acid by gallic acid-OH adduct," *Phys. Chem. Chem. Phys.*, vol. 1, pp. 1915–1918, 1999.
- [43] A. I. S. Silva, N. B. D. Lima, A. M. Simas, and S. M. C. Gonçalves, "Europium complexes: Luminescence boost by a single efficient antenna ligand," *ACS Omega*, vol. 2, pp. 6786–6794, 2017.
- [44] F. Cao, Z. Yuan, J. Liu, and J. Ling, "Europium(III)-diketone complex as portable luminescent chemosensor for naked eye Cu^{2+} detection and recyclable on-off-on vapor response," *RSC Adv.*, vol. 5, pp. 102535–102541, 2015.
- [45] Z. Zhao, F. Kubota, N. Kamiya, and M. Goto, "Selective extraction of scandium from transition metals by synergistic extraction with 2-thenoyltrifluoroacetone and tri-n-octylphosphine oxide," *Solvent Extr. Res. Dev.*, vol. 23, pp. 137–143, 2016.
- [46] M. Ransom and H. G. Brittain, "Circularly polarized luminescence studies of the Eu (III) bis (pyridine-2, 6-dicarboxylate) complexes with chiral α -hydroxycarboxylic acids," *Inorganica Chim. Acta*, vol. 65, pp. L147–L149, 1982.
- [47] M. Taha, I. Khan, and J. A. P. Coutinho, "Complexation and molecular modeling studies of europium(III)-gallic acid-amino acid complexes," *J. Inorg. Biochem.*, vol. 157, pp. 25–33, 2016.
- [48] J. L. Rosenstreich and D. E. Goldberg, "Formation Constants of Complexes of 2-Thenoyltrifluoroacetone and 3-Thenoylacetone," *Inorg. Chem.*, vol. 4, pp. 909–910, 1965.
- [49] R. J. Meier, J. M. B. Simbürger, T. Soukka, and M. Schäferling, "A FRET based pH probe with a broad working range applicable to referenced ratiometric dual wavelength and luminescence lifetime read out," *Chem. Commun.*, vol. 51, pp. 6145–6148, 2015.
- [50] J. Qi, D. Liu, X. Liu, S. Guan, F. Shi, H. Chang, H. He, and G. Yang, "Fluorescent pH sensors for broad-range pH measurement based on a single fluorophore," *Anal. Chem.*, vol. 87, pp. 5897–5904, 2015.

Parts of this chapter have been published

Wafaa Waleed Al-Qaysi and Axel Duerkop, *Analyst*, 2018, 143, 3176-3183

Author contributions

WW performed all experimental work and wrote the manuscript. AD revised the manuscript.

3. Sensor and sensor microtiterplate with expanded pH detection range and their use in real samples

3.1 Introduction

Over the past two decades one has witnessed high research activities in the field of optical sensors which serve as cost effective, durable, compact and comparatively sensitive devices to quantify a large variety of analytes. Among the optical chemical sensors, a large number of optical pH sensors (so called pH opt(r)odes) have been developed [1],[2]. pH optodes are used for measurement and control of pH in many fields such as chemistry, biology, biochemistry, molecular biotechnology, clinical chemistry, medical and environmental, and marine sciences, industrial production monitoring, the automotive industry, telecommunication industries and in engineering research [3],[4]. One of the main reasons for the development of pH optodes are the lack of necessity of a reference electrode and their electrical safety [5]. pH optodes are based on pH-induced reversible changes of optical properties of immobilized indicator(s) like absorbance [6], reflectance [7] or luminescence [8]. Further, chemiluminescence, energy transfer [9] or light scattering, luminescence lifetime, refractive index, diffraction and polarization may vary upon changes of pH [10]. pH optodes have advantages with respect to low production costs, small size, light weight, ease of handling and immunity to electromagnetic interferences. This allows pH optodes to be used in presence of flammable or explosive compounds or for continuous in-vivo measurements (e.g. in the blood stream) [11],[12]. Typically, pH optodes consist of a pH-sensitive dye (i.e. the pH-indicator) immobilized in a polymer matrix which has to provide suitable mechanical stability, a strong noncovalent or covalent interaction with the indicator (to prevent leaching) and a sufficient water uptake [13]. The response of luminescent pH optodes is a function of the concentration of the acidic and basic forms of the indicator [14], which follows the Henderson-Hasselbalch equation (mass action law) but not the activity of the hydrogen ion. Although most optical pH-indicators are essentially (de)protonatable chromophores [15], most sensors containing one indicator cover not more than 3-4 pH units [16].

Various concepts for widening the response of luminescent sensors to pH were suggested over the past years. Double layer spin-coating of two kinds of quantum dots (QDs) with 525 nm and 605 nm emission in one layer and a mixture of neutral red and methyl yellow in the other layer resulted in sensor membranes in which the QD emission is transmitted depending on the pH-dependent absorption of the indicator couple. This concept requires one excitation and two detection wavelengths for the ratiometric readout of pH [17]. The embedding of a mixture of microbeads of two indicators (having different pK_a s) into a hydrogel matrix yielded sensor membranes with LED-compatibility also requires two emission wavelengths and another reference dye to be used, if referenced lifetime-based sensing is done [18].

The concept of using multiple indicators from the same class of dyes, yet with various substitution patterns was shown by several authors [19],[20]. A series of naphthalimide pH indicators yielded a series of novel optical sensors with a wide working range. A necessary feature is that the emission intensity of all indicators shows the same change (decrease) at higher pH to facilitate the combination of many dyes in one sensor membrane [8]. Similarly, 8 new aza-BODIPY indicators with pK_a values from the acidic to the basic range were used to fabricate sensors that respond from pH 2-9 by combining four BODIPYs in the same sensor foil [21]. An array of 12 BODIPY derivatives as pH indicators with four reference dyes was joined on a dipstick for determination of pH via luminescence. pH can be determined with LED excitation on a dipstick in a home-made inexpensive device that is attached to a smartphone [22]. A useful feature of all these multi-indicator sensors is that all dyes inside the sensor membrane have the same excitation and emission maxima. This enables the use of simpler equipment with only one excitation source and one emission wavelength. However, prior fabrication these sensors require considerable effort for the synthesis of the many derivatives of the indicators.

We therefore recently introduced a new concept for wide-range pH indicators and sensors that employs lanthanide complexes with ligands that have various pK_a s [23]. Hence, a wider pH range becomes accessible. Potential candidates for such luminescent probes are complexes of Eu^{3+} , Tb^{3+} ,

Dy³⁺ and Sm³⁺ that provide 8-9 coordination sites [24] and strong luminescence in the visible range. The advantage of this concept is that only one excitation and detection wavelength are required for detection of pH, unlike in ratiometric schemes which use dye mixtures that require several excitation and emission readouts. This lower instrumental demand facilitates the pH readout and sensor integration into miniaturized devices. A further advantage is that the synthetic effort to obtain various ligands is much less (many ligands can be purchased) compared to the many steps required to prepare several derivatives of the same class of a luminescent dye. Therefore, this multi-pK_a-ligands scheme can open a gate for new wide-range optical pH probes and sensors. A similar concept based on an organic dye uses a 10-(4-aminophenyl)-5,15-dimesitylcorrole with three deprotonation steps [25]. Until now, only one group used one single ligand on a lanthanide complex for a broad range sensor of pH [26].

In this paper we show that a simple lanthanide complex with only two different ligands attached to the Eu³⁺ ion yields a pH indicator with the widest detection range obtained from a single molecule, so far. The new indicator has a wider the detection range in a sensor membrane and a sensor microplate than in earlier work. We attached 2-thenoyl trifluoroacetone as deprotonable antenna ligand and pyridine-2,6-dicarboxylic acid as bidentate aromatic ligand. PDA can strongly coordinate to Eu³⁺ ions via the carboxylic acid groups and retains a deprotonable group after complexation. A Eu- TTA- PDA complex feed ratio of 1:3:2 shows a wide-range luminescence response from pH 2-10. Embedding the indicator into a cellulose acetate polymeric membrane on a Mylar foil as a support yields a sensor membrane with a working range from pH 2-8. For high-throughput applications sensor microtiterplates showed the same wide pH 2-8 working range and operational stability over one day. The sensor microplate proved its applicability to various real samples with no pre-treatment by delivering pHs close to those acquired with a pH electrode as reference.

3.2 Results and discussion

3.2.1 Choice of ligands and conceptual remarks

In lanthanide complexes, the excitation light absorbed by the ligands is transferred to the ligand triplet state by intersystem crossing and then intramolecularly transferred to the Ln^{3+} ion. This sensitized luminescence of lanthanides is widely used in probes and labels in analytical, chemical, medical and biological sciences [27]. Lanthanide complexes exhibit favourable luminescence properties including sharp emission peaks, excellent photostability, large Stokes' shifts, a high quantum yield for optical sensing and a long excited-state lifetime ranging from μs to ms (Eu^{3+} , Tb^{3+}) [28]. However, lanthanide ions show low absorbance and weak emission in aqueous solution due to low absorption coefficients, low quantum yields or low yields of the transitions following absorption. This drawback can be overcome through coordinating highly absorbent chelating ligands like β -diketonates or aromatic carboxylic acids that efficiently sensitize lanthanide luminescence [29]. The ligands should be bidentate (or have more than two coordination sites) to strongly coordinate to the lanthanide ion and contain deprotonable groups in coordinated state. We therefore used bidentate water-soluble 2-thenoyltrifluoroacetone that is a well-known antenna ligand for Eu^{3+} . TTA has a pK_a of 6.38 and its antenna effect is dependent on the protonation in complexed state [30],[31]. Pyridine-2,6-dicarboxylic acid (PDA) also is a water-soluble, strongly coordinating ligand for lanthanide ions. It retains one carboxylic acid group after complexation to Eu^{3+} . PDA has $\text{pK}_{a1} = 2.16$ and a $\text{pK}_{a2} = 2.8$ [32],[33],[34]. Unlike in our previous work, we omitted gallic acid as a ligand to be coordinated because its first pK_a is between the one of PDA and of TTA. This does not further expand the detection range of the indicator complex. The pK_{a2} of gallic acid at about 10 did not yield an expansion of the working range at $\text{pH} > 10$ of both, the indicator in solution and the sensors [23]. Therefore, gallic acid was no more considered. Moreover, we hoped to obtain more linear calibration plots due to the higher spread of the pK_a s of TTA and PDA and an improved stoichiometric ratio of the ligands.

The feed ratio of the Eu-TTA-PDA complex of 1:3:2 was experimentally optimized and is based on similar formation constants of Eu-PDA in 1:2 molar ratio [35], and of TTA in 1:3 molar ratio [36]. Although TTA and PDA could occupy more than the 8-9 coordination sites on a Eu^{3+} ion with this feed ratio, our sensors showed a better response to pH and a brighter emission compared to a Eu-TTA-PDA ratio of 1:3:1 or 1:2:2. Presumably, the response to pH is due to the presence of not only one complex species, as in our previous work [23]. As a stoichiometry of the Eu-TTA-PDA complex of 1:3:2 gives the best response to pH we refer to Eu-TTA-PDA in a feed ratio of 1:3:2 as the indicator in the following. The same Ac-MOPS-CAPS buffer (10 mmol/L) was chosen as in previous work. Britton-Robinson buffer cannot be used because precipitation of insoluble EuPO_4 may occur.

3.2.2 Absorption spectra of the indicator

The pH- dependent absorption spectra of the ligands alone as well as the absorption spectra of the Eu^{3+} -TTA-PDA complex (in molar ratio 1:3:2) were acquired in buffer at various pH. Figure 52 shows the pH-dependent absorption of PDA with a maximum at 273 nm with certain pH-dependence. TTA shows a strongly pH-dependent absorption band with a maximum at 355 nm (figure 53). These absorption maxima shift hypsochromically upon complexation compared to those of the pure ligands. As shown in Fig. 54, the Eu^{3+} -TTA-PDA complex shows two absorption maxima. The shortwave absorption maximum is located at 270 nm and shows higher absorbance ($\epsilon = 3.95 \times 10^4 \text{ L (mol cm)}^{-1}$ at pH 8) and is little dependent of pH. The more longwave absorption band shows a maximum at 340 nm ($\epsilon = 3.50 \times 10^4 \text{ L (mol cm)}^{-1}$ at pH 8) which increases from pH 2-8. The absorption maximum of Eu^{3+} -TTA-PDA (1:3:2) at 340 nm is strongly shifted (15 nm hypsochromically) with respect to the absorption spectra of the pure TTA ligand. These shifts of the maxima indicate the formation of the complex. The titration plot of the absorbance at 340 nm shows that the pK_a of TTA has slightly shifted to 6.8 upon complexation compared to 6.38 [31] in solution.

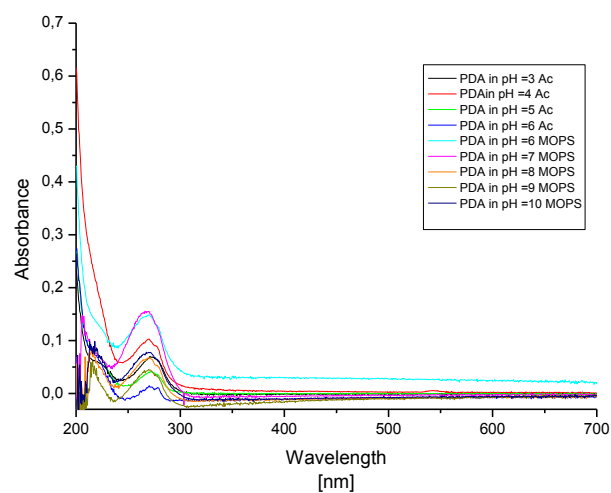


Figure 52 Absorption spectra of PDA, $c = 20 \mu\text{mol/L}$ (Ac or MOPS- buffer 10 mmol L^{-1}).

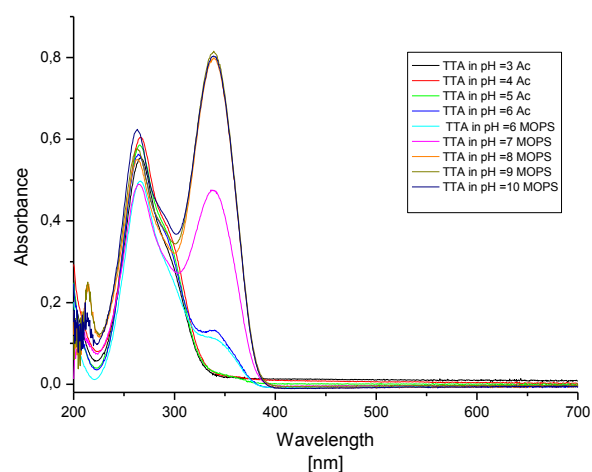


Figure 53 Absorption spectra of TTA, $c = 30 \mu\text{mol/L}$ (Ac or MOPS- buffer 10 mmol L^{-1}).

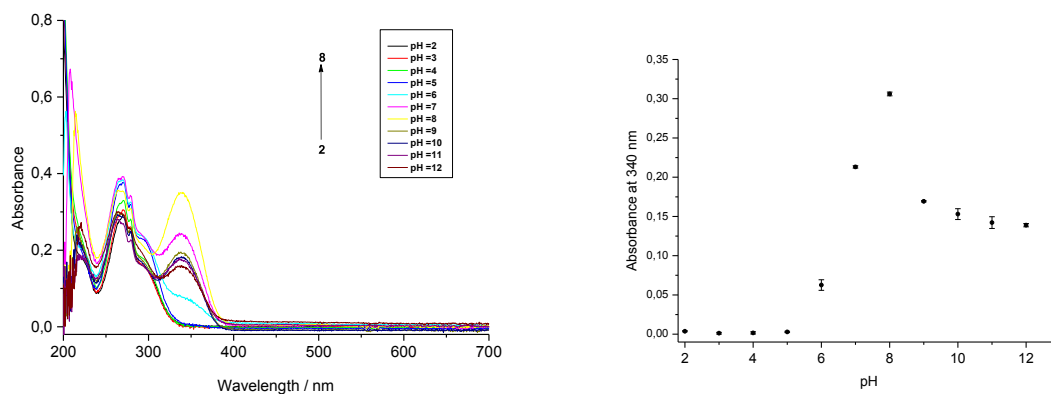


Figure 54 Absorption spectra of Eu^{3+} -TTA-PDA ($c=10 \mu\text{mol L}^{-1}$ related to $c(\text{Eu}^{3+})$, 10 mmol L^{-1} , Ac-MOPS-CAPS buffer, $n=3$) and related titration plot.

3.2.3 Excitation spectra of the indicator

The excitation spectra ($\lambda_{\text{em}} = 615 \text{ nm}$; $^5\text{D}_0 \rightarrow ^7\text{F}_2$ luminescence transition of Eu^{3+}) of the Eu^{3+} -TTA-PDA complex in a molar ratio 1:3:2 in buffer are shown in figure 55. There are two bands visible. The shortwave excitation band (located at 280 nm) is strongly pH-dependent from pH 2-10 which is in contrast to the absorption spectra where the longwave band shows stronger pH dependence (figure 54). However, the excitation spectra in figure 55 are in accordance with the excitation spectra of Eu-TTA and Eu-PDA complexes (see figures 56 and 57) under the same conditions. Here, only PDA shows pH-dependent excitation at 280 nm and only second order stray light is visible for Eu-TTA. Hence, only PDA complexed with Eu^{3+} seems to contribute to the pH-dependence of the excited state. The second band in figure 55 at 308 nm is second order diffraction. The third excitation band at 460 nm increases only minute until pH 8. Additionally, the titration plot has an almost linear shape pH from 4-10. The shape of the plot is affected by complex stoichiometry and a Eu-TTA-PDA ratio of 1:3:2 yielded a most linear plot.

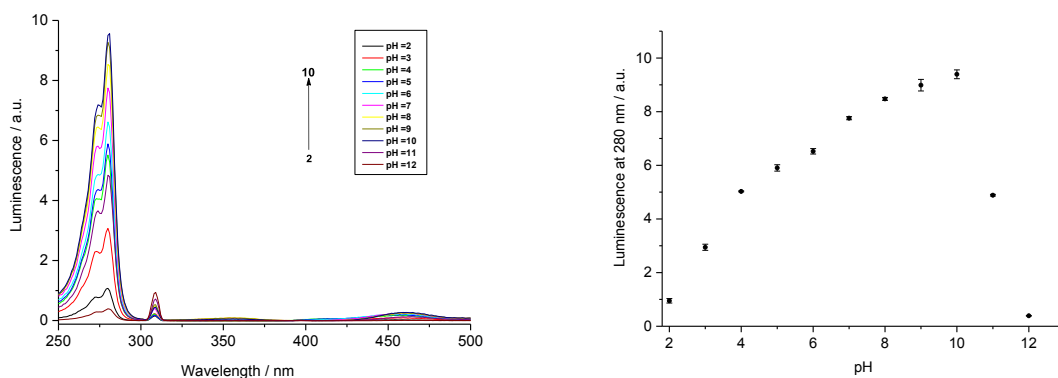


Figure 55 Excitation spectra of Eu^{3+} -TTA-PDA ($c=10 \mu\text{mol L}^{-1}$ related to $c(\text{Eu}^{3+})$, 10 mmol L^{-1} , Ac-MOPS-CAPS buffer, $\lambda_{\text{em}} = 615 \text{ nm}$, $n=3$) and related titration plot.

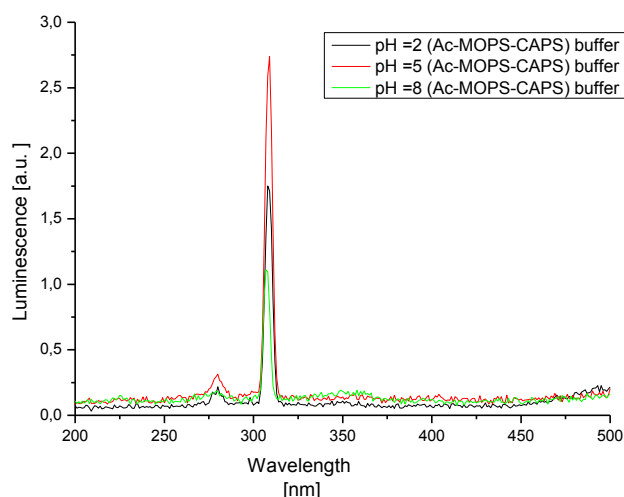


Figure 56 Excitation spectra of Eu^{3+} -TTA in molar ratio 1: 3, $c = 10 \mu\text{mol L}^{-1}$ (10 mmol L^{-1} , Ac-MOPS-CAPS buffer, $\lambda_{\text{em}} = 615 \text{ nm}$).

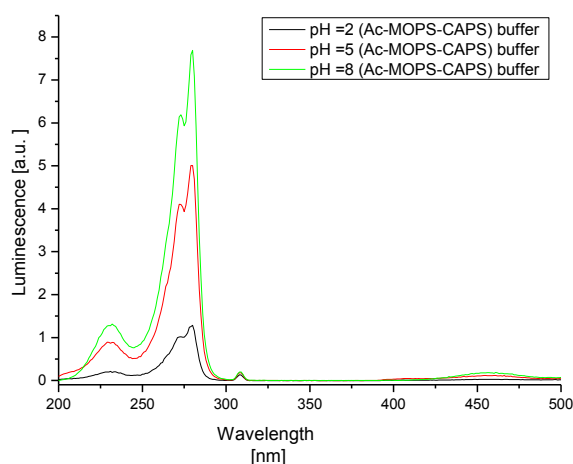


Figure 57 Excitation spectra of Eu^{3+} -PDA in molar ratio 1: 2, $c = 10 \mu\text{mol L}^{-1}$ (10 mmol L^{-1} , Ac-MOPS-CAPS buffer, $\lambda_{\text{em}} = 615 \text{ nm}$).

3.2.4 Emission spectra of the indicator

The luminescence spectra of Eu^{3+} -TTA-PDA (molar ratio 1:3:2) upon using 280 nm excitation show three typical Eu^{3+} emission bands at 580 nm, 594 nm and at 615 nm, respectively, at all pH values (figure 58). These correspond to the $^5\text{D}_0 \rightarrow ^7\text{F}_2$, $^5\text{D}_0 \rightarrow ^7\text{F}_1$, and $^5\text{D}_0 \rightarrow ^7\text{F}_0$ transitions of Eu^{3+} . An enhancement of the fluorescence intensity at 615 nm with pH over a wide range from pH 2 to 10 is clearly visible. The working range of the indicator over 8 orders of magnitude was expected with regard to the excitation spectra. Tb complexes with PDA derivatives showed similar behaviour, yet less pH dependence [29]. This is the broadest range covered by an optical pH-

indicator based on a single type of molecule, so far. Importantly, the shape of the titration plot was significantly improved with the new indicator with respect to our previous work. Formerly, we noticed a low increase of the luminescence emission of the indicator from pH 2-6 and a pronounced increase at pH 7-10. The current titration plot has a much more uniform slope over a wider range from pH 4-10 and only has a slightly steeper slope from pH 2-4. The pH-dependence from pH 4–10 can be fitted linearly very well with $y = 1.72 + \text{pH} \cdot 0.830$ ($r^2 = 0.992$). The emission drops at $\text{pH} \geq 11$. This can be attributed to the formation of traces of insoluble $\text{Eu}(\text{OH})_3$ at high pH. A related FRET indicator system with a europium chelate donor and a pH indicator based on a fluorescein only shows a response over 6 pH units in solution [37]. However, no sensor application was reported with this indicator couple. Hence, the concept of combining various ligands with various pK_a s in one molecule to spread the detection range of the luminescent indicator works very well. Similarly to earlier multi-indicator concepts [8], [21], only one excitation and emission wavelength are required which can simplify the equipment for the measurements down to e.g. an LED and a photodiode. Unlike in previous multi-indicator concepts, no complicated organic multistep syntheses are required to obtain a collection of indicators with various pK_a s because the various pK_a s are intrinsically contained inside every single indicator molecule via the complexed ligands. The emission spectra show that reducing the number of deprotonable ligands around Eu^{3+} from 3 to 2 does not compromise the performance of the resulting indicator complex.

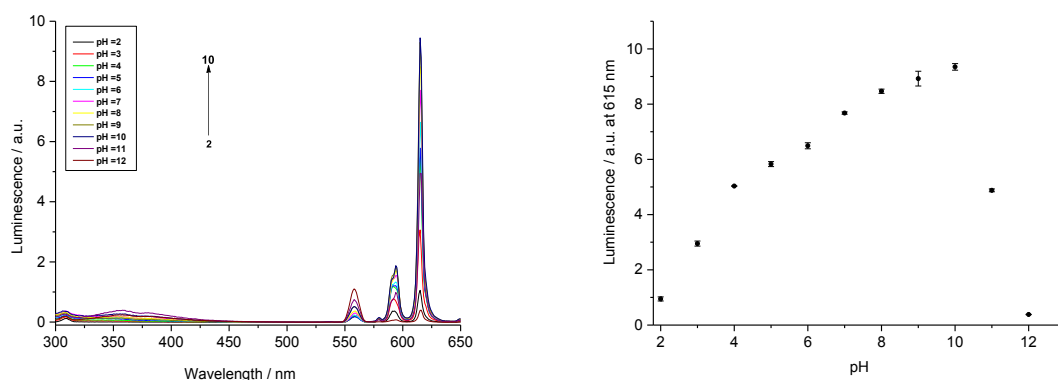


Figure 58 Emission spectra of Eu^{3+} -TTA-PDA ($c=10 \mu\text{mol/L}$ related to $c(\text{Eu}^{3+})$, 10 mmol L^{-1} , Ac-MOPS-CAPS buffer, $\lambda_{\text{exc}}=280 \text{ nm}$, $n=3$) and related titration plot.

3.2.5 Excitation spectra of pH-sensor membrane

The Eu-TTA-PDA indicator was embedded into a suitable polymeric cocktail with cellulose acetate (CA). We found that CA allows easy permeation of protons due to its hydrophilicity from the OH-groups and ester groups that are attached on the carbohydrate backbone. CA is stable over a wide range of pH and retains lanthanide indicators inside the sensor foils. After three days of stirring at elevated temperature in DMF the cocktail is homogeneous and can be knife-coated onto a layer of mylar foil (125 μm thick) as a support. Visual inspection reveals a strong luminescence of the complex inside the membrane upon irradiation with a UV-lamp at 254 nm (figure 59).

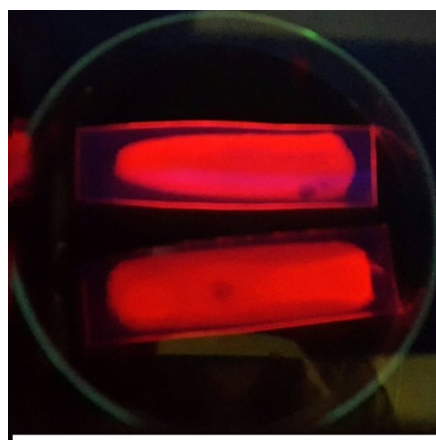


Figure 59 pH sensor foil containing Eu^{3+} -TTA- PDA (1:3:2) upon illumination with a UV lamp (254 nm).

The pH-dependent excitation spectra of a sensor membrane containing Eu^{3+} -TTA- PDA by using $\lambda_{\text{em}} = 615 \text{ nm}$ of Eu^{3+} are shown in figure 60. The shortwave band is second order diffraction at 308 nm. The excitation at 350 nm shows pH-dependence from pH 2 to 8 over a wide range of 6 pH units. As shown for the complex in the previous chapter the pH-dependent excitation maximum is bathochromically shifted 70 nm compared to the aqueous solution. We therefore acquired excitation spectra of Eu^{3+} -TTA (1:3) and Eu^{3+} -PDA (1:2) in aqueous buffer in order to determine whether this shift of the pH dependent excitation band is due to the ligands or due to the CA polymer. A comparison of the excitation spectra of the complexes Eu^{3+} -PDA (figure 57) and of Eu^{3+} -TTA-PDA (figure 55) shows that pH dependent excitation in buffer is always at 280 nm. Eu^{3+} -TTA (figure 56)

just shows second order stray light, here. Figures 56 and 57 also show that there is no pH-dependent excitation from Eu^{3+} -TTA and Eu^{3+} -TTA-PDA at $\lambda_{\text{exc}} > 300$ nm in buffer. This means that the shift of the pH dependent excitation is a result of the embedding of the indicator into the CA. The change of the polarity of the microenvironment around the Eu^{3+} indicator inside the polymer membrane is probably the reason for this shift. Nevertheless, this longwave excitation is very beneficial with respect to sensing because potentially less of luminescence background will occur in real samples. The pH response of the sensor membrane from 2-8 can be fitted with a sigmoidal Boltzmann fit with $y = 576.2 + ((130.1-576.2)/(1+\exp((\text{pH} - 5.966)/0.6205)))$ ($r^2 = 0.987$) which gives the sensor membrane a good resolution.

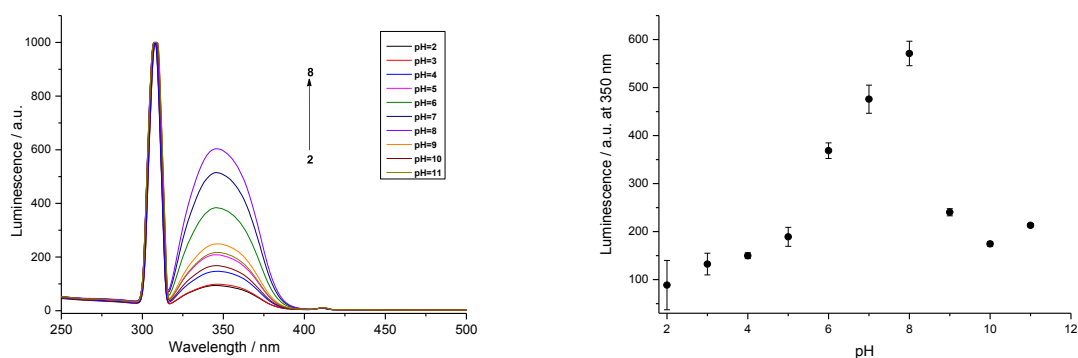


Figure 60 Excitation spectra of pH sensor membrane containing Eu^{3+} -TTA-PDA (10 mmol L^{-1} , Ac-MOPS-CAPS buffer, $\lambda_{\text{em}} = 615 \text{ nm}$, $n=4$) and related titration plot.

3.2.6 Emission spectra of pH-sensor membrane

In figure 61, we show the luminescence spectra of a sensor membrane containing Eu^{3+} -TTA-PDA by using $\lambda_{\text{exc}} = 350 \text{ nm}$ at various pH. Similar to the luminescence spectra in aqueous buffer (fig. 58) appear the typical bands of the Eu^{3+} emission at 580 nm, 594 nm, and at 615 nm, respectively. This means that the hydrophilic environment around the indicator is retained inside the membrane. The longwave pink coloured emission at 615 nm nicely meets the range where less luminescence background in real samples can be expected. Moreover, the Stokes' shift of $>260 \text{ nm}$ is large which enables easy separation of emitted light from scattered excitation or co-excited shortwave emitting biomatter, even with less expensive optical equipment.

The sensor membrane has a working range from pH 2-8 over 6 pH units. This is even one pH unit wider than in our earlier work [23] although only two different ligands are attached (compared to three different ones, formerly). We attribute this to the fact that obviously gallic acid (in the former complex [23]) did not contribute too significantly to the excitation energy transfer to the Eu^{3+} -ion which is why we did not see its contribution at pHs > 9. Hence, the dynamic range of the sensor membrane is only slightly smaller than that of the indicator in solution. The pH response of the sensor membrane from pH 2-8 can be fitted with a sigmoidal Boltzmann fit with $y = 606.4 + ((60.21 - 606.4) / (1 + \exp((\text{pH} - 6.137) / 1.132)))$ ($r^2 = 0.985$) which also gives the sensor a better resolution than in previous work.

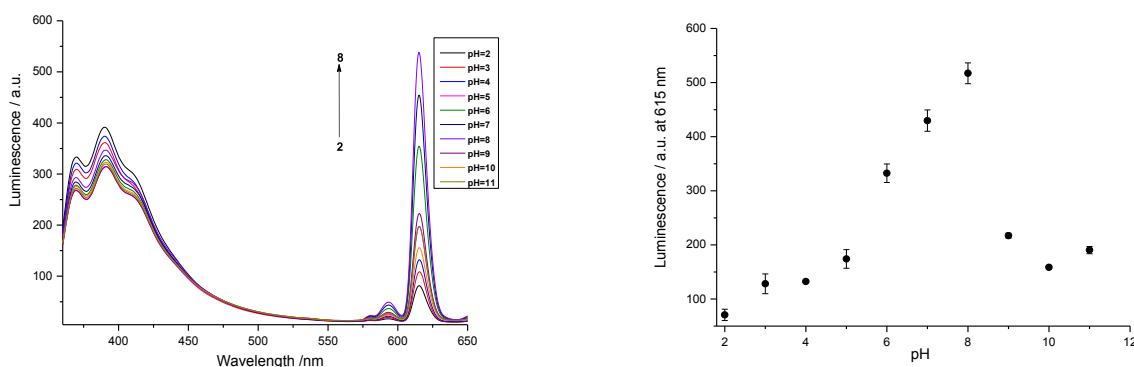


Figure 61 Emission spectra of pH sensor membrane containing Eu^{3+} -TTA-PDA (10 mmol L^{-1} , Ac -MOPS-CAPS buffer, $\lambda_{\text{exc}} = 350 \text{ nm}$, $n=4$) and related titration plot.

3.2.7 Response time and reversibility of pH-sensor membrane

The forward response time t_{90} per pH unit is on average at 13.5 min and the back response time is 12.6 min. However, 4.5 min are required for the exchange of the sample medium in the flow cell which is why response times of as low as 540 s (forward) and 486 s are more plausible. These response times closely resemble those of earlier sensors [23] and are similar or more rapid to what was found earlier [38], [39], [40]. More rapid t_{95} values of about 60 s when going from pH 2 to pH 12 were also found, but in this scheme two dyes had to be employed, already [18]. Furthermore, the dyes had to be covalently conjugated to particles that then were enclosed inside a sensor membrane, making membrane fabrication more complicated compared to

our sensors were only the indicator had to be mixed with the polymer. Furthermore, the response time of our sensor membrane can be reduced, as well by using thinner (30 μm) membranes (see next paragraph). Similar response times of sensor membranes were published but again the membranes contained various immobilized dyes which requires more effort for the synthesis of indicators and membrane fabrication to cover a wide pH range [8], [41]. Importantly, the present sensor has a huge Stokes' shift > 260 nm and more longwave 615 nm emission. This is beneficial when measurements in strongly scattering real samples are performed and co-excited luminescence background of such sample should not interfere with detection of pH.

Figure 62 and 63 show only minute leaching (1 % loss of luminescence intensity at $t = 2800$ s compared to the luminescence intensity at $t = 500$ s) of the complex off the sensor membrane. One can also conclude that long-term and on-line pH sensing over hours is possible with these membranes. Again, the measurement range spans over 6 pH units and is well reversible. The response of the membrane with 60 μm (figure 63) is a bit slower. The back response time of the membranes is considerably shorter than when switching from acidic to neutral pH. This behavior was also seen in earlier experiments [23, 40] and can be an additional advantage, if samples are monitored that show high and distinct changes towards acidic pH.

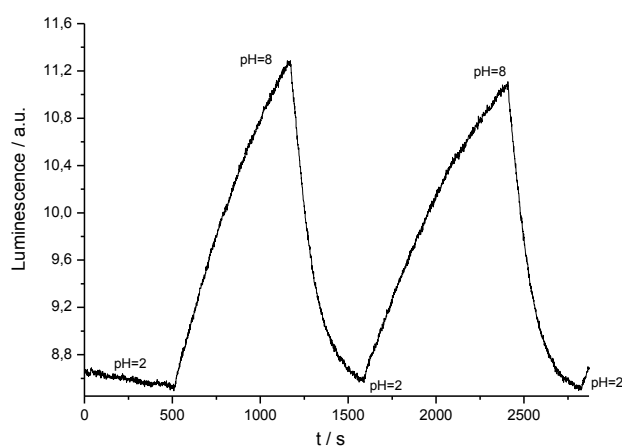


Figure 62 Reversibility of pH sensor membrane (30 μm) when switching from pH 2-8.

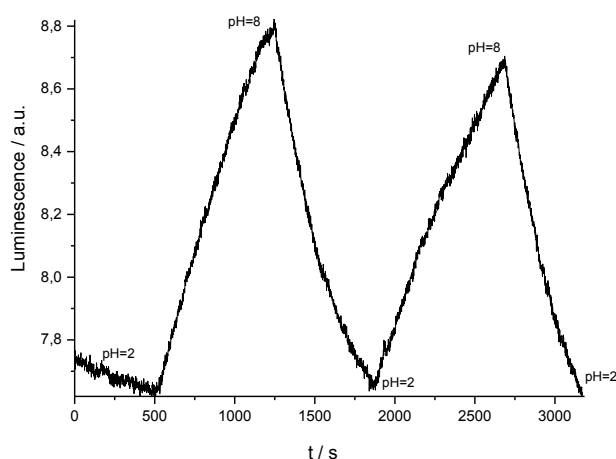


Figure 63 Reversibility of pH sensor membrane (thickness 60 μm) when switching from pH 2-8

3.2.8 pH sensor microtiterplate

The sensor cocktail containing Eu^{3+} -TTA-PDA is strongly luminescent in a microtiterplate (figure 64) under excitation with a 366 nm UV-lamp. The sensor microtiterplate is dried at lower temperature and for a shorter time than sensor membranes to avoid cracks of the layer inside the microtiterplate wells. Possible reasons are less solvent (DMF) resistance of the polystyrene microtiterplate compared to the mylar (used as supporting material for the sensor membranes) and larger differences of the thermal expansion coefficients of the sensor cocktail and the polystyrene (of the microplate) than the difference is between the cocktail and the mylar.

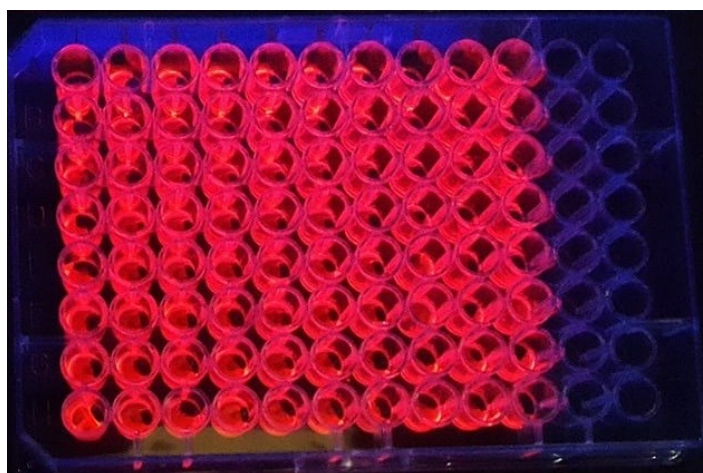


Figure 64 pH sensor microtiterplate with Eu^{3+} -TTA-PDA (1:3:2) upon illumination with UV lamp (366 nm).

In figure 65, we show the luminescence titration plot of the of the sensor microtiterplate at 615 nm. A favorable pH-increase over a wide range of 6 pH units is found. The luminescence response to changes of pH was read upon excitation with a wide-range excitation filter at 355 nm each 5 min. The best reproducibility was achieved after 15 min but reliable values are found after 10 min, already (see next section). This can enable virtual online measurements, if the pH change of a sample does not occur too fast. Moreover, this response is in the same range, as found for the sensor membranes (see previous section). The pH response of the sensor microtiterplate at 15 min from 2-8 can be fitted with $y = -8643 + 7911 \cdot \text{pH}$ ($r^2=0.983$). Moreover, it is obvious that pH sensing over 6 pH units is possible for several hours with good reproducibility. Even after one day, the decrease of the slope of the calibration plot between pH 2-8 is only 6,6%. This is much more stable than with our previous indicator which showed a higher change of the slope and a reduced dynamic range after one day [24]. Hence the sensor microtiterplate with Eu^{3+} -TTA-PDA shows a considerably improved long-term stability for high-throughput measurements of pH in the acidic to the slightly alkaline pH range.

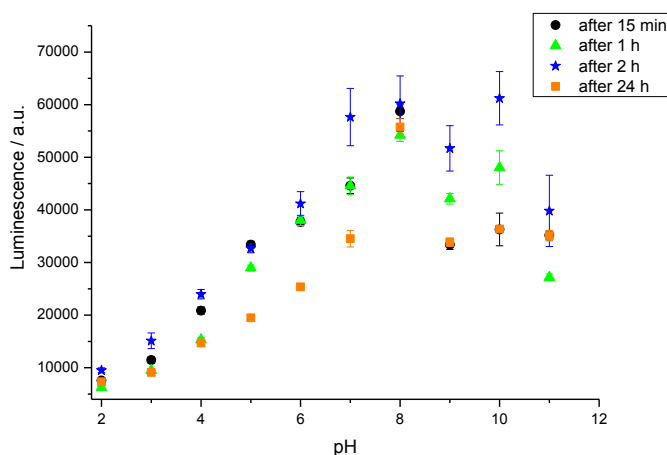


Figure 65 Response of sensor microtiterplate with Eu^{3+} -TTA-PDA (Ac-MOPS-CAPS buffer (10 mmol L^{-1}) to variation pH ($\lambda_{\text{em}} = 615 \text{ nm}$, $\lambda_{\text{exc}} = 355 \text{ nm}$, $n=8$) after 15 min, 1 h, 2h and 24 h.

3.2.9 Application of the pH sensor microtiterplate to real samples

The pH sensor microtiterplate was tested with real samples of various origins. We took water from three rivers in the Regensburg area, the university lake and urine from a healthy

volunteer. The real samples and buffer solutions from pH 2-8 (for calibration) were pipetted into the wells of a sensor microtiterplate and the luminescence intensity was measured over 1 h in 5 min intervals. Then, the pH of the real samples was derived from the calibration plot. After that, the pH obtained with the sensor microtiterplate was compared with the pH value taken with a glass electrode. It is obvious from table 1 that after 10 or 15 min the difference is just ± 0.2 pH unit. Importantly, there is only little change of the pH from the sensor microtiterplate over 15 min. After 1 h, higher deviations occur with respect to the measurements of the pH-electrode. This demonstrates the stability of the sensor spots inside the wells of the microtiterplate, even in the presence of real samples. The overall well agreement of the pH values obtained with the electroanalytical and the optical method shows that the sensor microtiterplate is a viable tool for screening of pH in real samples.

Table 5 Comparison of pH found with the sensor microtiterplate ($\lambda_{\text{exc}} = 355$ nm, $\lambda_{\text{em}} = 615$ nm, $n=4$) over time with the pH measured with a glass electrode.

Samples	glass electrode	microtiterplate after 10 min	microtiterplate after 15 min	microtiterplate after 1 h
river Danube	7.08	7.11	6.94	6.73
river Regen	6.56	6.15	6.06	6.56
river Naab	6.03	5.95	5.83	5.48
university lake	6.90	6.94	6.85	6.91
tap water	7.50	8.05	7.82	7.43
urine	6.50	6.47	6.44	6.69

3.3 Conclusion

A simple lanthanide complex consisting of an Eu^{3+} ion with only two selected ligands carrying deprotonable groups with different pK_{a} can serve as a wide-range pH indicator with a working range of 8 pH units. This is unique for an indicator consisting of a single molecule. The pH sensor membranes containing this indicator in cellulose acetate permit stable measurements over hours and have a dynamic range of 6 pH units. This is one pH unit wider than that of a former sensor using a lanthanide complex as the indicator. The embedding of the sensor cocktails in the

wells of a microtiterplate yields a high-throughput sensing tool for pH that can be used for up to 24 h. This makes the sensor microtiterplate environmentally friendly because the waste of multiple disposable sensors could be avoided by its use. The plate responds within 10-15 minutes and the pHs read from various real samples against those obtained from a glass electrode showed a very good agreement. In future, such new lanthanide indicators could be designed with additional ligands for covering an ever wider pH range.

3.4 Materials and methods

Materials

Pyridine-2,6-dicarboxylic acid (PDA) and 2-Thenoyltrifluoroacetone were obtained in 99% purity from Sigma–Aldrich. EuCl_3 was obtained in 99.99% purity from Sigma–Aldrich. Ac-MOPS-CAPS buffer solution was prepared by dissolving 10 mmol L^{-1} of 3-(*N*-Morpholino)-propanesulfonic acid (MOPS) and *N*-cyclohexyl-3-aminopropanesulfonic acid (CAPS) (each from ROTH in 99% purity) and acetic acid (glacial, 100% purity, from Merck) (Ac) in bidistilled water. Stock solutions of europium chloride were prepared by dissolving 100 $\mu\text{mol L}^{-1}$ of EuCl_3 in Ac-MOPS-CAPS buffer (10 mmol L^{-1}) of pH 2-11. Ligand stock solutions of the same concentration (100 $\mu\text{mol L}^{-1}$) in the same buffer were prepared over the whole pH range. Diluted solutions of Eu^{3+} -TTA- PDA were obtained by mixing 200 μL of Eu^{3+} stock solution, 600 μL of TTA stock solution, and 400 μL of PDA stock solution with 800 μL of Ac-MOPS-CAPS buffer to 2 mL at the respective pH (2-11). These solutions were also mixed in variable molar ratio (i.e. volume of Eu^{3+} : Ligand 1: Ligand 2) for every pH and the complexes were allowed to form in solution. Ionic strength was kept constant at 10 mM with NaCl during all measurements. The cellulose acetate (M_w 30,000 Da, 39.8 wt% acetyl content) was from Sigma-Aldrich and a biaxial polyethylene terephthalate foil (MylarTM) of 125 mm thickness from Goodfellow (Bad Nauheim, Germany) served as solid support for the sensor membranes. Membrane thicknesses are given as adjusted during the knife coating process.

Apparatus

pH was adjusted with a pH meter CG 842 from Schott. All absorption spectra were recorded at room temperature on a Varian Cary 50 Bio UV-Visible Spectrophotometer in quartz cells with a path length of 1 cm. Luminescence measurements in aqueous solution were carried out on an Aminco Bowman AB2 luminescence spectrometer. Slit widths for excitation and emission were 4 nm and 4 nm, respectively. Sensor membranes were characterized on a Jasco FP-6300 spectrofluorimeter equipped with a flow cell oriented with a 30° incident angle. A 150 W Xenon lamp served as excitation source and the slit widths for excitation and emission were 5 nm and 5 nm, respectively. Microtiterplate measurements were performed with a BMG Fluostar OPTIMA with filters for excitation of 355 nm (40 nm FWHM) and emission of 615 nm (10 nm FWHM). All spectroscopic measurements were conducted at 22°C.

Fabrication of sensor membranes and sensor microtiterplates

A 10 % wt. polymer solution of CA is made in dimethyl formamide (DMF), as well as a solution of 10 mmol L⁻¹ of Eu³⁺-TTA- PDA (1:3:2) in DMF. 250 µL of indicator solution and 750 µL of CA in DMF are added into a preheated (60 °C) glass vial and mixed violently for 72 h. This is the sensor cocktail. 200 µL of warm cocktail are knife-coated on a Mylar foil strip to spread the cocktail on the carrier foil. The thickness of the wet sensor membrane can be adjusted to 60 or 30 µm, respectively. The sensor membrane is dried in an oven for 24 h at 60 °C to evaporate the DMF, this yield final membrane thickness about 6 and 3 µm, respectively. Membranes of 2.0 cm diameter are cut with a hole puncher and mounted into the flow cell. Buffers of various pH are pumped by a Gilson minipulse 3 pump with a speed of 1 mL min⁻¹ through the flow cell.

Transparent flat bottom micro plates (number 655101) from Greiner BIO-ONE were filled with 25 µL of cocktail. The microtiterplate was dried in an oven for 6 h at 45 °C to evaporate the DMF solvent, washed 3 times with bidistilled water, and the respective buffer (100 µmol L⁻¹, pH 2-11) or real sample was added.

3.5 References

- [1] Y. Ying, G. yuan Si, F. jun Luan, K. Xu, Y. wei Qi, and H. nan Li, "Recent research progress of optical fiber sensors based on D-shaped structure," *Opt. Laser Technol.*, vol. 90, pp. 149–157, 2017.
- [2] J. Lin, "Recent development and applications of optical and fiber-optic pH sensors," *Trends Anal. Chem.*, vol. 19, pp. 541–552, 2000.
- [3] X. D. Wang and O. S. Wolfbeis, "Fiber-optic chemical sensors and biosensors (2008-2012)," *Anal. Chem.*, vol. 85, pp. 487–508, 2013.
- [4] O. Korostynska, K. Arshak, E. Gill, and A. Arshak, "Review on State-of-the-art in Polymer Based pH Sensors," *Sensors*, vol. 7, pp. 3027–3042, 2007.
- [5] L. Florea, C. Fay, E. Lahiff, T. Phelan, N. E. O'Connor, B. Corcoran, D. Diamond, and F. Benito-Lopez, "Dynamic pH mapping in microfluidic devices by integrating adaptive coatings based on polyaniline with colorimetric imaging techniques," *Lab Chip*, vol. 13, pp. 1079–1085, 2013.
- [6] Á. P. Timbó, P. V. F. Pinto, H. A. Pinho, L. P. De Moura, J. B. Chretien, F. W. Viana, R. G. D. Filho, E. B. Da Silva, M. E. R. Da Silva, J. W. M. Menezes, G. D. F. Guimarães, and W. B. Fraga, "pH optical sensor based on thin films of sol-gel with bromocresol purple," *Sens. Actuat. B*, vol. 223, pp. 406–410, 2016.
- [7] X. Yang, Y. Gao, Z. Huang, X. Chen, Z. Ke, P. Zhao, Y. Yan, R. Liu, and J. Qu, "Fluorescent probe based on heteroatom containing styrylcyanine: pH-sensitive properties and bioimaging in vivo," *Mater. Sci. Eng. C*, vol. 52, pp. 97–102, 2015.
- [8] J. Qi, D. Liu, X. Liu, S. Guan, F. Shi, H. Chang, H. He, and G. Yang, "Fluorescent pH sensors for broad-range pH measurement based on a single fluorophore," *Anal. Chem.*, vol. 87, pp. 5897–5904, 2015.
- [9] A. Cusano, F. J. Arregui, M. Giordano, and A. Cutolo, "Optochemical nanosensors in chapter Fundamentals of Optical Sensors," *CRC Press. Taylor Fr. Gr. Boca Raton, USA*, pp. 30–50, 2012.
- [10] D. Wencel, T. Abel, and C. McDonagh, "Optical chemical pH sensors," *Anal. Chem.*, vol. 86, pp. 15–29, 2014.
- [11] O. S. Wolfbeis, "Fiber Optic Chemical Sensors and Biosensors, Ch. 19," *CRC Press. Boca Raton*, vol. 2, p. 267–300., 1991.
- [12] E. Bakker, P. Bühlmann, and E. Pretsch, "Carrier-based ion-selective electrodes and bulk optodes. 1. General characteristics," *Chem. Rev.*, vol. 97, pp. 3083–3132, 1997.
- [13] B. M. Weidgans, C. Krause, I. Klimant, and O. S. Wolfbeis, "Fluorescent pH sensors with negligible sensitivity to ionic strength," *Analyst*, vol. 129, pp. 645–650, 2004.
- [14] J. Janata, "Do optical sensors really measure pH?," *Anal. Chem.*, vol. 59, pp. 1351–1356, 1987.
- [15] N. Strömberg, E. Mattsson, and A. Hakonen, "An imaging pH optode for cell studies based on covalent attachment of 8-hydroxypyrene-1,3,6-trisulfonate to amino cellulose acetate films," *Anal. Chim. Acta*, vol. 636, pp. 89–94, 2009.
- [16] F. B. M. Suah, M. Ahmad, and M. N. Taib, "Optimisation of the range of an optical fibre pH sensor using feed-forward artificial neural network," *Sens. Actuat. B*, vol. 90, pp. 175–181,

2003.

- [17] Y. Hiruta, N. Yoshizawa, D. Citterio, and K. Suzuki, "Highly durable double sol–gel layer ratiometric fluorescent pH optode based on the combination of two types of quantum dots and absorbing pH indicators," *Anal. Chem.*, vol. 84, pp. 10650–10656, 2012.
- [18] A. S. Vasylevska, A. A. Karasyov, S. M. Borisov, and C. Krause, "Novel coumarin-based fluorescent pH indicators, probes and membranes covering a broad pH range," *Anal. Bioanal. Chem.*, vol. 387, pp. 2131–2141, 2007.
- [19] S. Capel-Cuevas, M. P. Cuéllar, I. de Orbe-Payá, M. C. Pegalajar, and L. F. Capitán-Vallvey, "Full-range optical pH sensor based on imaging techniques," *Anal. Chim. Acta*, vol. 681, pp. 71–81, 2010.
- [20] M. Zhang, R. V. Søndergaard, E. K. P. Kumar, J. R. Henriksen, D. Cui, P. Hammershøj, M. H. Clausen, and T. L. Andresen, "A hydrogel based nanosensor with an unprecedented broad sensitivity range for pH measurements in cellular compartments," *Analyst*, vol. 140, pp. 7246–7253, 2015.
- [21] M. Strobl, T. Rappitsch, S. M. Borisov, T. Mayr, and I. Klimant, "NIR-emitting aza-BODIPY dyes—new building blocks for broad-range optical pH sensors," *Analyst*, vol. 140, pp. 7150–7153, 2015.
- [22] R. Gotor, P. Ashokkumar, M. Hecht, K. Keil, and K. Rurack, "Optical pH sensor covering the range from pH 0–14 compatible with mobile-device readout and based on a set of rationally designed indicator dyes," *Anal. Chem.*, vol. 89, pp. 8437–8444, 2017.
- [23] W. W. Al-Qaysi and A. Duerkop, "Luminescent europium complex for wide-range pH sensor and sensor microtiterplate," *Analyst*, vol. 143, pp. 3176–3184, 2018.
- [24] E. G. Moore, A. P. S. Samuel, and K. N. Raymond, "From antenna to assay: lessons learned in lanthanide luminescence," *Acc. Chem. Res.*, vol. 42, pp. 542–552, 2009.
- [25] C.-Y. Li, X.-B. Zhang, Z.-X. Han, B. Åkermarck, L. Sun, G.-L. Shen, and R.-Q. Yu, "A wide pH range optical sensing system based on a sol–gel encapsulated amino-functionalised corrole," *Analyst*, vol. 131, pp. 388–393, 2006.
- [26] M. Turel, M. Čajlaković, E. Austin, J. P. Dakin, G. Uray, and A. Lobnik, "Direct UV-LED lifetime pH sensor based on a semi-permeable sol-gel membrane immobilized luminescent Eu³⁺+chelate complex," *Sens. Actuat. B*, vol. 131, pp. 247–253, 2008.
- [27] A. Picot, A. D'Aléo, P. L. Baldeck, A. Grichine, A. Duperray, C. Andraud, and O. Maury, "Long-lived two-photon excited luminescence of water-soluble europium complex: Applications in biological imaging using two-photon scanning microscopy," *J. Am. Chem. Soc.*, vol. 130, pp. 1532–1533, 2008.
- [28] T. Gunnlaugsson, J. P. Leonard, K. Sénéchal, and A. J. Harte, "pH responsive Eu(III)-phenanthroline supramolecular conjugate: Novel off-on-off luminescent signaling in the physiological pH range," *J. Am. Chem. Soc.*, vol. 125, pp. 12062–12063, 2003.
- [29] G. liang Gu, R. ren Tang, Y. hu Zheng, and X. ming Shi, "Synthesis, characterization and fluorescence properties of novel pyridine dicarboxylic acid derivatives and corresponding Tb(III) complexes," *Spectrochim. Acta - Part A Mol. Biomol. Spectrosc.*, vol. 71, pp. 209–214, 2008.
- [30] F. Cao, Z. Yuan, J. Liu, and J. Ling, "Europium(III) -diketone complex as portable luminescent

- chemosensor for naked eye Cu^{2+} detection and recyclable on-off-on vapor response," *RSC Adv.*, vol. 5, pp. 102535–102541, 2015.
- [31] Z. Zhao, F. Kubota, N. Kamiya, and M. Goto, "Selective extraction of scandium from transition metals by synergistic extraction with 2-thenoyltrifluoroacetone and tri-n-octylphosphine oxide," *Solvent Extr. Res. Dev.*, vol. 23, pp. 137–143, 2016.
- [32] D. K. Singha, P. Majee, S. K. Mondal, and P. Mahata, "pH-Controlled Luminescence Turn-On Behaviour of a Water-Soluble Europium-Based Molecular Complex," *Eur. J. Inorg. Chem.*, vol. 2016, pp. 4631–4636, 2016.
- [33] M. V. Kirillova, M. F. C. Guedes da Silva, A. M. Kirillov, J. J. R. Fraústo da Silva, and A. J. L. Pombeiro, "3D hydrogen bonded heteronuclear CoII , NiII , CuII and ZnII aqua complexes derived from dipicolinic acid," *Inorg. Chim. Acta*, vol. 360, pp. 506–512, 2007.
- [34] L. N. Puntus, V. F. Zolin, T. A. Babushkina, and I. B. Kutuza, "Luminescence properties of isomeric and tautomeric lanthanide pyridinedicarboxylates," *J. Alloys Compd.*, vol. 380, pp. 310–314, 2004.
- [35] M. Ransom and H. G. Brittain, "Circularly polarized luminescence studies of the Eu (III) bis (pyridine-2, 6-dicarboxylate) complexes with chiral α -hydroxycarboxylic acids," *Inorganica Chim. Acta*, vol. 65, pp. L147–L149, 1982.
- [36] J. L. Rosenstreich and D. E. Goldberg, "Formation Constants of Complexes of 2-Thenoyltrifluoroacetone and 3-Thenoylacetone," *Inorg. Chem.*, vol. 4, pp. 909–910, 1965.
- [37] R. J. Meier, J. M. B. Simbürger, T. Soukka, and M. Schäferling, "A FRET based pH probe with a broad working range applicable to referenced ratiometric dual wavelength and luminescence lifetime read out," *Chem. Commun.*, vol. 51, no. 28, pp. 6145–6148, 2015.
- [38] A. Kriltz, C. Löser, G. J. Mohr, and S. Trupp, "Covalent immobilization of a fluorescent pH-sensitive naphthalimide dye in sol–gel films," *J. Sol-gel Sci. Technol.*, vol. 63, pp. 23–29, 2012.
- [39] L. Ferrari, L. Rovati, P. Fabbri, and F. Pilati, "Disposable fluorescence optical pH sensor for near neutral solutions," *Sensors (Switzerland)*, vol. 13, no. 1, pp. 484–499, 2013.
- [40] D. Aigner, B. Ungerböck, T. Mayr, R. Saf, I. Klimant, and S. M. Borisov, "Fluorescent materials for pH sensing and imaging based on novel 1,4-diketopyrrolo-[3,4-c]pyrrole dyes," *J. Mater. Chem. C*, vol. 1, pp. 5685–5693, 2013.
- [41] C. J. Tsou, C. Y. Chu, Y. Hung, and C. Y. Mou, "A broad range fluorescent pH sensor based on hollow mesoporous silica nanoparticles, utilising the surface curvature effect," *J. Mater. Chem. B*, vol. 1, pp. 5557–5563, 2013.

This chapter has been submitted to Sensors and Actuators B Chemical

Wafaa Waleed Al-Qaysi and Axel Duerkop

Author contributions

WW performed all experimental work and wrote the manuscript. AD revised the manuscript.

4. Abbreviations

ϵ	Absorption coefficient
AIE	Aggregation-induced emission
ANN	Artificial neural network
BY	Brilliant yellow
CIVs	Counterion-induced vesicles
ED	electric dipole
exc	Excitation spectrum
em	Emission spectrum
Gall	Gallic acid
HPTS	1-hydroxypyrene-3,6,8-tirsulphonate
IC	Internal conversion
ISC	Intersystem crossing
IS	Ionic strength
LBL	layer-by-layer
LED	Light emitting diode
LPFG	Long-period fiber grating
MD	Magnetic dipole
MOF	Metal–organic framework
NCF	No-core fiber
NCQDs	N-doped carbon quantum dots

NIR	Near infrared
NR	Neutral red
NMR	Nuclear magnetic resonance
PDA	Pyridine-2,6-dicarboxylic acid
Φ	Quantum yield
QD	Quantum dot
RSD	Relative standard deviation
S_0	Ground singlet state
S_1	Excited singlet state
TPE	Tetraphenylethene
TTA	2-thenoyl trifluoroacetone
T_1	Triplet state
UV	Ultraviolet
pK_a	Acid dissociation constant

5. Summary

5.1 In English

The aim of my work was to design new low-cost optical luminescent pH sensor membranes and a sensor microtiterplate containing lanthanide complexes for continuous quantitation of pH over a wide range. These sensors should overcome the typical drawbacks of classical optical indicator dyes with a dynamic range of up to 3 pH units only (due to the mass action law) and of electrochemical sensors which cannot be miniaturized to μm -size or enable imaging over larger areas (e.g. in cell culture). We therefore introduced a new design concept for wide-range pH indicators and sensors that employs lanthanide complexes with ligands that have various pK_{a} s. Hence, a wider pH range becomes accessible.

First, we complexed europium with three different ligands with various pK_{a} s to form an indicator. These ligands are Gallic acid (Gall) a trihydroxybenzoic type of phenolic acid that can strongly coordinate to Eu^{3+} ions via the carboxylic acid groups and has $\text{pK}_{\text{a}1} = 4.5$ and $\text{pK}_{\text{a}2} = 10$. Pyridine-2,6-dicarboxylic acid (PDA) is the second ligand that has $\text{pK}_{\text{a}1} = 2.16$ and $\text{pK}_{\text{a}2} = 2.8$. 2-Thenoyl trifluoroacetone (TTA) with a pK_{a} of 5.61 is the third ligand that is coordinated to Eu^{3+} ions. TTA is captures excitation light and efficiently transfers it to Eu^{3+} inducing a strong luminescence. We found that the Eu-TTA-PDA-Gall complex in a feed ratio (1:3:1:1) in aqueous buffer delivers a high luminescence emission that is dependent on pH over up to 8 orders of magnitude from pH 2–10 in aqueous solution. This is a unique pH response for a single indicator molecule. It was therefore embedded into a suitable polymeric membrane made from cellulose acetate (CA) in DMF in order to obtain pH sensor membranes. We found a reversible response of the emission intensity of the sensor membranes over a wide range of pH 2–pH 7 over 5 orders of magnitude within several minutes. Moreover, the first high-throughput pH sensor microtiterplate based on this indicator showed a dynamic range from pH 2–8 over 6 orders of magnitude and is suitable for up to 24 h of continuous use. The emission drop of the sensor membranes and of the microplate at high pH and

the response time were improved by using thinner sensor foils of 30 μm instead of 60 μm . A response time down to 300 s was achieved.

Further, we show a simpler lanthanide complex with only two different ligands having various pK_{a} s attached to the Eu^{3+} ion. This yields a pH indicator with the widest detection range obtained from with single molecule, so far. We attached 2-thenoyl trifluoroacetone as deprotonable antenna ligand and pyridine-2,6-dicarboxylic acid as bidentate aromatic ligand. A Eu-TTA-PDA complex feed ratio of 1:3:2 shows a wide-range luminescence response from pH 2-10. Embedding the indicator into a cellulose acetate polymeric membrane on a Mylar support yields a sensor membrane with a working range from pH 2-8. This detection range in a sensor membrane is one pH unit wider than described for the earlier complex. For high-throughput applications the sensor microtiterplate showed the same wide working range of pH 2-8 and operational stability over one day. The sensor microplate proved its applicability to various real samples (river waters, urine and others) with no pre-treatment by delivering pH values close to those acquired with a pH electrode as reference.

The advantage of the use of lanthanide complex indicators with ligands that have various pK_{a} s is that only one excitation and detection wavelength are required for detection of pH, unlike in other work where dye mixtures often require several excitation and emission readouts. This lower instrumental demand facilitates the pH readout and sensor integration into miniaturized devices. A further advantage is that the synthetic effort to obtain various ligands is much less compared to the many synthesis steps required to prepare several derivatives of the same class of dyes (to retain excitation and emission wavelengths) for multi-indicator sensors. Therefore, this multi- pK_{a} -ligands-design scheme for pH indicators can open a gate for new luminescent wide-range optical pH indicators and sensors to widen the sensing range of pH ever further towards pHs of either 0 or 14. However, this entails the challenge to find ligands with appropriate pK_{a} s that complex strongly enough to prevent dissociation at extreme pH.

Fabrication and use of new sensors and sensor microplates for ions in high throughput screening to monitor cell growth, cell status and cell toxicity could not be performed any more due to time constraints.

5.2 Zusammenfassung auf Deutsch

Ziel der Arbeit war es, neue kostengünstige optische lumineszente-pH-Sensormembranen und eine Sensor-Mikrotiterplatte mit Lanthanoidkomplexen zur kontinuierlichen Quantifizierung des pH-Wertes über einen weiten Bereich zu entwickeln. Diese Sensoren sollen die typischen Nachteile klassischer optischer Indikatorfarbstoffe mit einem dynamischen Bereich von bis zu 3 pH-Einheiten (aufgrund des Massenwirkungsgesetzes) und elektrochemischen Sensoren überwinden, die nicht auf μm -Größe miniaturisiert werden können oder die Lumineszenzauslesung über größere Flächen ermöglichen (z.B. in der Zellkultur). Wir haben daher ein neues Designkonzept für Indikatoren und Sensoren mit weitem pH-Bereich eingeführt, welches Lanthanoidkomplexe mit Liganden mit verschiedenen pK_s -Werten verwendet. Dadurch wird ein breiterer pH-Bereich zugänglich.

Zunächst haben wir Europiumionen mit drei verschiedenen Liganden mit verschiedenen pK_s -Werten zu einem Indikator komplexiert. Diese Liganden sind Gallussäure (Gall), eine Trihydroxybenzoesäure, die über die Carbonsäuregruppen stark an Eu^{3+} -Ionen koordinieren kann und $\text{pK}_{s1} = 4,5$ und $\text{pK}_{s2} = 10$ aufweist. Pyridin-2,6-dicarbonsäure (PDA) ist der zweite Ligand und verfügt über $\text{pK}_{s1} = 2,16$ und $\text{pK}_{s2} = 2,8$. 2-Thenoyltrifluoraceton (TTA) mit einem pK_s -Wert von 5,61 ist der dritte Ligand, der an Eu^{3+} -Ionen koordiniert ist. TTA ist ein Antennenligand, der Anregungslicht einfängt und es effizient zu Eu^{3+} überträgt, wodurch eine starke Lumineszenz induziert wird. Wir haben herausgefunden, dass der Eu-TTA-PDA-Gall-Komplex in einem ligendenerhältnis (1:3:1:1) in wässrigem Puffer eine hohe Lumineszenzemission liefert, die in wässriger Lösung für bis zu 8 Größenordnungen eine pH-Abhängigkeit zwischen pH 2-10 besitzt. Dies ist ein einzigartiger pH-Bereich für ein einzelnes Indikatormolekül. Es wurde daher in eine geeignete polymere Membran aus Celluloseacetat (CA) in DMF eingebettet, um pH-Sensormembranen zu generieren. Wir erhielten ein reversibles Signal der Emissionsintensität der Sensormembranen über einen weiten Bereich von pH 2-pH 7 über 5 Größenordnungen innerhalb

von einigen Minuten. Darüber hinaus zeigte die erste Hochdurchsatz-pH-Sensor-Mikrotiterplatte auf Basis dieses Indikators einen dynamischen Bereich von pH 2-8 über 6 Größenordnungen und ist für bis zu 24 h Dauereinsatz geeignet. Der Emissionsabfall der Sensormembranen und der Mikroplatte bei hohem pH-Wert und die Ansprechzeit wurden durch Verwendung dünnerer Sensorfolien von 30 μm anstelle von 60 μm verbessert. Eine Ansprechzeit von bis zu 300 s wurde erreicht. Ferner zeigen wir einen einfacheren Lanthanoidkomplex mit nur zwei verschiedenen Liganden, die verschiedene pK_s -werte besitzen und an das Eu^{3+} -Ion gebunden wurden. Dies ergibt einen pH-Indikator mit dem größten Detektionsbereich, der bisher mit einem einzelnen Molekül erzielt wurde. Wir haben 2-Thenoyltrifluoraceton als deprotonierbaren Antennenliganden und Pyridin-2,6-dicarbonsäure als zweizähligen aromatischen Liganden gebunden. Ein Eu-TTA-PDA-Komplex-ligandenverhältnis von 1:3:2 wies eine Lumineszenzreaktion mit einem breiten Bereich von pH 2-10 auf. Die Einbettung des Indikators in eine Celluloseacetat-Polymermembran auf einem Mylar-Träger ergibt eine Sensormembran mit einem Arbeitsbereich von pH 2-8. Dieser Detektionsbereich in einer Sensormembran ist um eine pH-breite weiter als für den früheren Komplex beschrieben. Für Hochdurchsatzanwendungen zeigte die Sensor-Mikrotiterplatte den gleichen breiten Arbeitsbereich von pH 2-8 und eine Betriebsstabilität über einen Tag. Die Sensor-Mikrotiterplatte hat ihre Anwendbarkeit für verschiedene reale Proben (Flusswasser, Urin und andere) ohne Vorbehandlung bewiesen, indem pH-Werte geliefert wurden, die denen nahekamen, die mit einer pH-Elektrode als Referenz gemessen wurden. Der Vorteil der Verwendung von Lanthanoidkomplexindikatoren mit Liganden, die verschiedene pK_s -werte aufweisen, besteht darin, dass nur eine Anregungs- und Detektionswellenlänge für die Detektion des pH-Wertes erforderlich ist (im Gegensatz zu anderen Veröffentlichungen, bei denen Farbstoffmischungen oft mehrere Anregungs- und Emissionsausgaben erfordern). Diese geringeren instrumentellen Anforderungen erleichtert die pH-Auslesung und Sensorintegration in miniaturisierte Geräte. Ein weiterer Vorteil besteht darin, dass der synthetische Aufwand, um verschiedene Liganden zu erhalten, im Vergleich zu den vielen Syntheseschritten, die zur

Herstellung mehrerer Derivate der gleichen Farbstoffklasse (um die Anregungs- und Emissionswellenlängen beizubehalten) für Mehrfachindikator-Sensoren nötig sind, viel geringer ist. Daher kann dieses Multi-pK_s-Liganden-Design-Schema für pH-Indikatoren einen Zugang zu neuen lumineszierenden optische Weitbereichs-pH-Indikatoren und -Sensoren öffnen, um den Erfassungsbereich des pH immer weiter in Richtung pH-Werten von entweder 0 oder 14 zu erweitern. Dies bringt jedoch die Herausforderung mit sich, Liganden mit geeigneten pK_s-werten zu finden, die stark genug komplexieren, um eine Dissoziation bei extremem pH zu verhindern.

Die Herstellung und Verwendung neuer Sensoren und Sensor-Mikroplatten für Ionen im Hochdurchsatz-Screening zur Überwachung des Zellwachstums, des Zellstatus und der Zelltoxizität konnte aufgrund von Zeitbeschränkungen nicht mehr durchgeführt werden.

بالإضافة الى ذلك فالرسالة تعرض معقد بسيط للانتشاد مع اثنين فقط من الروابط المختلفه ذات ثوابت تفكك حوامض مختلفه تستطيع ان تلامس أيون الايروبيوم وهذا يعطي مستشعر للرقم الهيدروجيني ذو مدى اوسع من مدى خلال جزئيه واحده حتى الان. لقد تم ربط ثايونيل ثلاثي الفلور اسيتون كرابط انتينه غير بروتين مع بريدن -2-6-ثنائي حامض الكربوكسيل ذات النسبة الموليه كرابط أروماني ثنائي الترابط. وعاليه من الرقم 1:3:2(Eu: TTA:PDA:Ga) أظهر أستجابته استشعارية واسعة المدى الهيدروجيني يتراوح من 2-10.

تم تضمين المؤشر الى غشاء بوليميري من خلات السيليلوز على داعمة مايكل لينتج غشاء الاستشعار الواسع المدى للرقم الهيدروجيني من 2-8 مدى الكشف. مدى الكشف هذا في غشاء الاستشعار هو أوسع وحده واحده من الرقم الهيدروجيني مما وصف في المعقد الاول. أما بالنسبه الى التطبيقات ذات الانتاجيه العاليه أظهر المايكرو تيتربلت نفس نطاق العمل الواسع من 2-8 من الرقم الهيدروجينية والاستقراره ليوم واحد. وقد أثبت أستشعار المايكرو تيتربليت بانها قابله للتطبيق على عينات حقيقيه مختلفه (ماء النهر, الادرار وغيره) بدون اية معالجات مسبقه لها من خلال توفير الرقم الهيدروجيني قريبا جدا من تلك المسجله والمأخوذه من قطب الرقم الهيدروجيني كمرجع. أن الفائده من أستخدام معقدات اللانثنايد كمؤشرات مع الروابط التي تحتوي على ثوابت هو ان اثاره واحده و كشف الطول الموجي كافي للكشف عن الرقم الهيدروجيني على عكس الطرق الاخرى التي يتطلب مزج الصبغات الى اثارات وقراءات عده. لذا يعتبر هذا ابسط واقل جهاز تكلفه لقراءه الرقم الهيدروجيني ودمج اجهزه الاستشعار في اجهزه مصغره. وهنالك ميزه اخرى اذ ان تحضير روابط مختلفه يتطلب جهد قليل قياسا بالعديد من الخطوات التحضيريه التي تتطلب لتحضير العديد من المشتقات لنفس النوع من الصبغات (لنفس الانبعاث, الاشعاع والطول الموجي) لاجهزه الاستشعار المتعدده, لذا التخطيط لتصميم روابط مختلفه ثابت تفكك الحامضي لمؤشرات الرقم الهيدروجيني يمكن ان تفتح بوابه لمؤشرات جديده واسعه المدى لمؤشر الرقم الهيدروجيني والاستشعار لتوسيع مدى استشعار الرقم الهيدروجيني المستمر أوسع ليشمل من 0-14. على كل حال, يتبع هذا التحدي للعثور على روابط لها ثوابت تفكك حوامض مناسبه لتكوين معقدات قويه لمنع التفكك عند توسيع الرقم الهيدروجيني.

أن تصنيع وأستخدام أستشعار جديد وأستشعار مايكرو تايتر بليت للايونات عاليه الانتاجيه لتنظيم نمو الخليه وحالة الخلية وتسمم الخليه لم تجرى وذلك بسبب القيود الزمنيه

5.3 الخلاصة بال عربي

ان الهدف من هذه الدراسة هو تصميم أغشية استشعار ضوئي للاوس الهيدروجيني جديد وحساسه وذات تكلفه منخفضه لتكوين مايكروتايتز بليت يحتوي على معقدات اللانثانيد لقياس كمي مستمر للتغيرات في الاوس الهيدروجيني ضمن مدى واسع. هذا التصميم يجب ان يتغلب على العيوب النمطيه التي تصاحب صبغات المؤشر الضوئي الكلاسيكي بمدى تصحيح واسع يصل الى 3 ألاس الهيدروجيني (بسبب قانون الكتله) وأجهزة الاستشعار الكهروكيميائية التي لا يمكن تصغير حجمها الى مايكرومتر اولتصوير مسافه واسعه (مثلا النسيج الخلوي). لذا في هذه الدراسة ادخالنا مفهوم جديد لتصميم مؤشرات ذات مدى واسع للتغيرات في الاوس الهيدروجيني وأجهزة استشعار تحتوي على معقدات اللانثانيد وربطه مع ليكنيدات تحتوي على ثوابت مختلفه لتفكك الحامض وبالتالي يصبح الاس الهيدروجيني الواسع المدى متاح.

اولا, ربطنا اليوروبيم مع ثلاث ليكنيدات مختلفه ذات ثوابت مختلفه لتفكك الحامض لتوليد مستشعر. هذه اليكنيدات هي: حامض الجاليك (جال) وهو تراي هيدروكسي بنزوك وهو نوع من حامض الفينول الذي ممكن أن يتناسق بقوه مع أيون الايروبيوم عن طريق مجاميع حامض الكاربوكسيلك (ذو ثابت بي كي أي=4.5, بي كي أي=2=10). اليكند الثاني هو مجاميع بيردين-2-6-حامض ثنائي الكاربوكسيل الذي له ثابت (بي كي أي=2.16, بي كي أي=2=2.8). اليكند الثالث ثايونيل ثلاثي الفلور أسيون (ت ت أ) ذو ثابت تفكك حامض أولي (5.61) وهو يتناسق مع أيون الايروبيوم ويعمل كرابط انتينه ولاقط والذي يجذب الضوء المثار وينقله بكفاءه الى ايون الايروبيوم ليعطي استشعار عالي.

وقد وجد أن Eu-TTA-PDA-Gall المركب بنسبه 1:3:1:1 في محلول مائي قد أعطى أنبعاث أستشعار عالي يعتمد على الرقم الهيدروجيني يصل الى 8 وحدات من حجم الرقم الهيدروجيني من 2-10 في المحلول المائي. هذه استجابته فريده للاوس الهيدروجيني لجزيئه مؤشر واحد, لذلك تم تضمينه في غشاء بوليمري مناسب مصنع من خلاصات السليلوز في مذيب ثنائي مثيل فورمايد من أجل الحصول على أغشية استشعار للرقم الهيدروجيني. وقد وجد أستجابته عاكسه لشدة الانبعاث لاغشية الاستشعار لمدى واسع من الرقم الهيدروجيني من 2-7 ما يصل الى 5 وحدات بدقائق معدوده بلاضافه لذلك كان أول أستشعار للرقم الهيدروجيني لمايكروتايتز بليت أعطى سرعه انتاجيه عاليه عندهذا المؤشر واطهر مدى واسع من الرقم الهيدروجيني من 2-8 أعلى من 6 وحدات وهو مناسب لكي يستعمل لمدة 24 ساعه بصوره متواصله. تم تحسين انخفاض الانبعاث للاغشية المستشعر هو المايكروبلت لاستشعار الرقم الهيدروجيني العالي باستخدام رقائق أستشعار رقيقه واستعمال 30 مايكرومتر بدلا من 60 مايكرومتر مع زمن أستجابته أقل من 300 ثانيه.

List of Figures

Figure 1	A diagram depicting the approximate energy levels for aqueous lanthanide ions [21].	5
Figure 2	Diagram representing the interactions leading to the splitting of the electronic energy levels of a Eu^{3+} ion. In the diagram, energy increases when going up [2].	6
Figure 3	General architecture of luminescent lanthanide complexes.	8
Figure 4	Jablonski Energy Diagram of Absorbance Energy Transfer Emission (AETE) mechanism for a Ln^{3+} complex [33].	10
Figure 5	Calibration graphs of the proposed pH sensing membrane electrode plotted by the data obtained from pH ion meter and (b) potential graph [65].	16
Figure 6	Dynamic response of the proposed electrode for step changes in pH (1.9–12.22) [65].	16
Figure 7	Acid-to-base and base-to-acid pH measurements of the different 5-bilayer IJP electrodes from the same printed batch. Inset plots represent the average potential –pH dependence for a) acid to base and b) base to acid direction. (the error bars represent the standard deviation of five different electrodes; bars are smaller than the data symbols employed) [70].	17
Figure 8	Variation of the absorbance spectra of polyaniline film (PA-1) with pH at 600 and 840 nm [111].	26
Figure 9	Absorption spectra of (PAA/BY)5PAA multilayer sensor in different pH solutions [118].	27
Figure 10	Spectral response of the optical fiber sensor respect to the pH. The spectral reference (absorption=0) was taken at pH1 [120].	28
Figure 11	Schematic of a no-core optical fiber with pH coating [121].	29
Figure 12	Stability curve of no-core pH sensor for both acidic basic [122].	30
Figure 13	Excitation spectra of glass-immobilized HPTS at various pH values (phosphate buffers, 23 °C, emission taken at 520 nm.). The shoulder at 455 nm. Is assigned to a Raman band [129].	31
Figure 14	Excitation spectra of glass-immobilized HCC at various pH values (phosphate buffer, 23 °C, emission taken at 460 nm.). The shoulder at around 400 nm. Is assigned to a Raman band [129].	31
Figure 15	Response of the HPTS-based sensor towards changes in pH. The upper level corresponds to pH 8.15 Excitation at 465 nm. Emission taken at 520 nm. [129].	32
Figure 16	Fluorescence intensity versus pH values and the resulting linear relationship [141].	34
Figure 17	Optical response of the pH-sensitive agarose Petri dish [171].	42
Figure 18	Response curves of 2b in D4 (dye content 1%, layer thickness 5 μm) to dynamic changes of pH [61].	43
Figure 19	Response reproducibility of the membrane at 624.0 nm for the alternative change in pH from 5.90 to 3 different pH values of 4.04, 2.01, and 0.68, respectively. (Conditions for preparation of membrane, solution contains 0.0375m/v MGO, absorbance at 625 nm, respectively, preparation time, 2 min. and preparation temperature, 60 °C [106].	44
Figure 20	Fluorescence responses vs. time by alternately pumping different pH buffer solutions (a) 11.02; (b) 8.08, (c) 4.96, (d) 2.17. The fluorescence intensities are in arbitrary units given by the time scanning, Mode of the Hitachi F 4500 instrument [134].	45

Figure 21	pH titration plot of membrane M-3 in the presence of 0, 0.1 and 1.0 M sodium sulphate (absorption measured at 560 nm.), showing the effect of ionic strength [95]. ..	46
Figure 22	Absorption spectra of Eu^{3+} : Acid Blue 45, in various molar ratio, $n=100$ nmol, at pH=9, MOPS buffer (10 mmol L^{-1}).....	64
Figure 23	Absorption spectra of Eu^{3+} : Ali, in molar ratio 1:3, $n=100$ nmol, Ac or MOPS buffer (10 mmol L^{-1}), variation of color upon variation of pH.....	64
Figure 24	Absorption spectra of Tb^{3+} : Ali, in molar ratio 1:3, $n=100$ nmol, Ac or MOPS buffer (10 mmol L^{-1}), variation of color upon variation of pH.....	65
Figure 25	Absorption spectra of Tb^{3+} : PDA:Gall in molar ratio 1:3:2, $c=10 \mu \text{mol L}^{-1}$ related to $c(\text{Tb}^{3+})$, Ac-MOPS-CAPS buffer (10 mmol L^{-1}).	65
Figure 26	Excitation spectra of Tb:PDA:Gall in molar ratio 1:3:2, $c=10 \mu \text{mol L}^{-1}$ related to $c(\text{Tb}^{3+})$, Ac-MOPS-CAPS buffer (10 mmol L^{-1}), $\lambda_{\text{em}}=544 \text{ nm}$	66
Figure 27	Emission Spectra of Tb:PDA:Gall in molar ratio 1:3:2, $c=10 \mu \text{mol L}^{-1}$ related to $c(\text{Tb}^{3+})$, Ac-MOPS- CAPS buffer (10 mmol L^{-1}), $\lambda_{\text{exc}}=280 \text{ nm}$	66
Figure 28	Absorption Spectra of Eu-Gall in molar ratio 1:1, $c=10 \mu \text{mol L}^{-1}$ related to $c(\text{Eu}^{3+})$, Ac or MOPS buffer (10 mmol L^{-1}).....	69
Figure 29	Absorbance Spectra of Eu-PDA in molar ratio (1:1), $c=10 \mu \text{mol L}^{-1}$ related to $c(\text{Eu}^{3+})$, Ac or MOPS buffer (10 mmol L^{-1}).....	69
Figure 30	Absorbance Spectra of Eu-TTA-Gall in molar ratio (1:3:1), $C=10 \mu \text{mol L}^{-1}$, Ac or MOPS buffer (10 mmol L^{-1}), and titration plot derived from the absorption spectra of Eu-TTA-Gall in 1:3:1 molar ratio at 340 nm.	70
Figure 31	Absorption Spectra of Eu^{3+} -TTA-PDA-Gall ($c=10 \mu \text{mol L}^{-1}$ related to $c(\text{Eu}^{3+})$, Ac-MOPS- CAPS buffer (10 mmol L^{-1} $n=3$).	71
Figure 32	Excitation Spectra of Eu^{3+} -Gall in molar ratio 1:1, ($c=10 \mu \text{mol L}^{-1}$ related to $c(\text{Eu}^{3+})$, Ac or MOPS buffer (10 mmol L^{-1})), $\lambda_{\text{em}}=615 \text{ nm}$	71
Figure 33	Excitation Spectra of Eu^{3+} -TTA in molar ratio 1:3, ($c=10 \mu \text{mol L}^{-1}$ related to $c(\text{Eu}^{3+})$, Ac -MOPS -CAPS buffer (10 mmol L^{-1}), $\lambda_{\text{em}}=615 \text{ nm}$	72
Figure 34	Excitation Spectra of Eu^{3+} -TTA-Gall ($c=10 \mu \text{mol L}^{-1}$ related to $c(\text{Eu}^{3+})$, Ac or MOPS buffer (10 mmol L^{-1}), $\lambda_{\text{em}}=615 \text{ nm}$	72
Figure 35	Excitation Spectra of Eu^{3+} -TTA-PDA-Gall ($c=10 \mu \text{mol L}^{-1}$ related to $c(\text{Eu}^{3+})$, Ac-MOPS-CAPS buffer..(10 mmol L^{-1}), $\lambda_{\text{em}}=615 \text{ nm}$, $n=3$).	73
Figure 36	Emission spectra of Eu-Gall in 1:1 molar ratio ($c=10 \mu \text{mol L}^{-1}$ related to $c(\text{Eu}^{3+})$, Ac or MOPS buffer 10 mmol L^{-1}), $\lambda_{\text{exc}}=300 \text{ nm}$	73
Figure 37	Emission spectra of Eu-TTA in 1:3 molar ratio ($c=10 \mu \text{mol L}^{-1}$ related to $c(\text{Eu}^{3+})$, Ac -MOPS- CAPS buffer 10 mmol L^{-1}), $\lambda_{\text{exc}}=280 \text{ nm}$	74
Figure 38	Emission spectra of Eu-TTA-Gall in 1:3:1 molar ratio ($c=10 \mu \text{mol L}^{-1}$ related to $c(\text{Eu}^{3+})$, Ac or MOPS buffer 10 mmol L^{-1}), $\lambda_{\text{exc}}=345 \text{ nm}$ and titration plot derived from the emission spectra of Eu-TTA- Gall in 1:3:1 molar ratio at 615 nm.	75
Figure 39	Emission spectra of Eu-PDA in 1:1 molar ratio; ($c=10 \mu \text{mol L}^{-1}$ related to $c(\text{Eu}^{3+})$, Ac or MOPS buffer 10 mmol L^{-1}), $\lambda_{\text{exc}}=345 \text{ nm}$ and titration plot derived from the emission spectra of Eu-PDA in 1:3:1 molar ratio at 615 nm.	75
Figure 40	Emission Spectra of Eu^{3+} -TTA-PDA-Gall ; $c(\text{Eu}^{3+})$, Ac or MOPS buffer 10 mmol L^{-1} , $\lambda_{\text{exc}}=345 \text{ nm}$	76
Figure 41	Emission Spectra of Eu^{3+} -TTA-PDA-Gall ($c=10 \mu \text{mol L}^{-1}$ related to $c(\text{Eu}^{3+})$, Ac or MOPS buffer 10 mmol L^{-1}), $\lambda_{\text{exc}}=280 \text{ nm}$	77

Figure 42	Emission Spectra of Eu^{3+} -TTA-PDA-Gall, ($c = 10 \mu\text{mol L}^{-1}$ related to $c(\text{Eu}^{3+})$, Ac-MOPS-CAPS buffer (10 mmol L^{-1}), $\lambda_{\text{exc}} = 280 \text{ nm}$, $n=3$).....	78
Figure 43	pH sensor foil containing Eu^{3+} -TTA- PDA-Gall (1:3:1:1) upon illumination with a UV lamp.(366 nm.).	79
Figure 44	Excitation spectra of sensor membrane containing Eu^{3+} -TTA-PDA-Gall in molar ratio 1:3:1:1, ($c=10 \text{ mmol L}^{-1}$ related to Eu^{3+} , Ac-MOPS-CAPS buffer (10 mmol L^{-1}), $\lambda_{\text{em}} = 615 \text{ nm}$, $n=4$). The sudden drops of the emission at 352 nm in the spectra are an instrumental artifact.....	79
Figure 45	Emission spectra of pH sensor membrane containing Eu^{3+} -TTA-PDA-Gall (Ac – MOPS-CAPS buffer (10 mmol L^{-1}), $\lambda_{\text{exc}} = 350 \text{ nm}$, $n=4$).....	81
Figure 46	Reversibility of a $60 \mu\text{m}$ pH sensor membrane in Ac-MOPS-CAPS buffer (10 mmol L^{-1}) over time at variation pH.	82
Figure 47	Reversibility of pH sensor membrane ($60 \mu\text{m}$) when switching from pH 2-7.	82
Figure 48	Reversibility of pH sensor membrane (thickness $30 \mu\text{m}$) when switching from pH 2-7.	83
Figure 49	pH sensor microtiterplate with Eu^{3+} -TTA-PDA-Gall (1:3:1:1) upon illumination with UV lamp (366 nm.).	83
Figure 50	Response of sensor microtiterplate with Eu^{3+} -TTA-PDA-Gall (Ac-MOPS-CAPS buffer (10 mmol L^{-1}) to variation pH ($\lambda_{\text{em}} = 615 \text{ nm}$, $\lambda_{\text{exc}} = 355 \text{ nm}$, $n=8$).	84
Figure 51	Response of sensor microtiterplate with Eu^{3+} -TTA-PDA-Gall (Ac-MOPS-CAPS buffer (10 mmol L^{-1}) to variation pH($\lambda_{\text{em}} = 615 \text{ nm}$, $\lambda_{\text{exc}} = 355 \text{ nm}$, $n=8$) after 24 h.	84
Figure 52	Absorption spectra of PDA, $c = 20 \mu\text{mol/L}$ (Ac or MOPS- buffer 10 mmol L^{-1})	96
Figure 53	Absorption spectra of TTA, $c = 30 \mu\text{mol/L}$ (Ac or MOPS- buffer 10 mmol L^{-1})	96
Figure 54	Absorption spectra of Eu^{3+} -TTA-PDA ($c=10 \mu\text{mol L}^{-1}$ related to $c(\text{Eu}^{3+})$, 10 mmol L^{-1} , Ac-MOPS-CAPS buffer, $n=3$) and related titration plot.	96
Figure 55	Excitation spectra of Eu^{3+} -TTA-PDA ($c=10 \mu\text{mol L}^{-1}$ related to $c(\text{Eu}^{3+})$, 10 mmol L^{-1} , Ac-MOPS-CAPS buffer, $\lambda_{\text{em}} = 615 \text{ nm}$, $n=3$) and related titration plot.	97
Figure 56	Excitation spectra of Eu^{3+} -TTA in molar ratio 1: 3, $c = 10 \mu\text{mol L}^{-1}$ (10 mmol L^{-1} , Ac-MOPS-CAPS buffer, $\lambda_{\text{em}} = 615 \text{ nm}$).	98
Figure 57	Excitation spectra of Eu^{3+} -PDA in molar ratio 1: 2, $c = 10 \mu\text{mol L}^{-1}$ (10 mmol L^{-1} , Ac-MOPS-CAPS buffer, $\lambda_{\text{em}} = 615 \text{ nm}$).	98
Figure 58	Emission spectra of Eu^{3+} -TTA-PDA ($c=10 \mu\text{mol/L}$ related to $c(\text{Eu}^{3+})$, 10 mmol L^{-1} , Ac-MOPS-CAPS buffer, $\lambda_{\text{exc}} = 280 \text{ nm}$, $n=3$) and related titration plot.	99
Figure 59	pH sensor foil containing Eu^{3+} -TTA- PDA (1:3:2) upon illumination with a UV lamp (254 nm).	100
Figure 60	Excitation spectra of pH sensor membrane containing Eu^{3+} -TTA-PDA (10 mmol L^{-1} , Ac –MOPS-CAPS buffer, $\lambda_{\text{em}} = 615 \text{ nm}$, $n=4$) and related titration plot.....	101
Figure 61	Emission spectra of pH sensor membrane containing Eu^{3+} -TTA-PDA (10 mmol L^{-1} , Ac –MOPS-CAPS buffer, $\lambda_{\text{exc}} = 350 \text{ nm}$, $n=4$) and related titration plot.....	102
Figure 62	Reversibility of pH sensor membrane ($30 \mu\text{m}$) when switching from pH 2-8.	103
Figure 63	Reversibility of pH sensor membrane (thickness $60 \mu\text{m}$) when switching from pH 2-8	104

Figure 64	pH sensor microtiterplate with Eu^{3+} -TTA-PDA (1:3:2) upon illumination with UV lamp (366 nm).....	104
Figure 65	Response of sensor microtiterplate with Eu^{3+} -TTA-PDA (Ac-MOPS-CAPS buffer (10 mmol L ⁻¹) to variation pH (λ_{em} = 615 nm, λ_{exc} = 355 nm, n=8) after 15 min, 1 h, 2h and 24 h.	105

List of Tables

Table 1	The electronic configurations of rare earth elements [17]. The lanthanides (from La to Lu) have filled inner orbitals with 46 electrons. Scandium and yttrium have 18 electrons in the inner orbitals.....	4
Table 2	Comparison of the properties between optical sensors and electrochemical sensors (i.e. a glass electrode).	20
Table 3	Precision and accuracy of certified Tris buffer measurements [174].	44
Table 4	Spectroscopy properties of tested Eu/Tb- complexes.....	62
Table 5	Comparison of pH found with the sensor microtiterplate ($\lambda_{\text{exc}} = 355 \text{ nm}$, $\lambda_{\text{em}} = 615 \text{ nm}$, $n=4$) over	106

6. Curriculum Vitae

Name: Wafaa Waleed Nafea Al-Qaysi

Address: Iraq.Baghdad, AL-Karkh 2 / AL-Bayaa street/Q863/BlukNo.37/H.No.39

Telephone No.: 009647903342885 and 017629261692

Email: wafaaalkaissy@yahoo.com and Wafaa Al-qaysi@chemie.uni.regensburg.de

Nationality: Iraqi

Date of Birth: 27/ 12/ 1976

Place of Birth: Iraq-Baghdad

Gender: Female

Material status: Single, Religion: Muslim

1- Education

11/2014 - 11/2018 Promotionsstudium, Chemie – Universität Regensburg, Dissertation:
“New Luminescent Europium Complexes as Indicators and in Sensors for pH in Biosamples and Water Samples” Institut für Analytische Chemie, Chemo- und Biosensorik (PD Dr. Axel Duerkop).

10/2002 - 09/2004 Master of Science, Chemie – Universität Baghdad, Masterarbeit:
“Spectral Analysis and a study of Toxicity and Microbiological Activity of two Known Antibiotics and some of their new derivatives”

10/1996 - 07/1999 Bachelor of Science, Chemie – Universität AL-Mustansiriya

2- Work experience

Dates: (2000-2013)

Position held: Lecturer in Department of Chemistry / College Science / Baghdad University

Main activities and responsibilities: Teaching in scientific Laboratories in Department of Chemistry, Baghdad University

3- Education and training Dates

Date: 2010 Promoted to Lecturer in Organic Chemistry / Baghdad University

/ College of Science / Department of Chemistry

4- Scientific and Teaching Experiences

Holding the responsibility Identification of Organic and for Petro Chemisitry& Polymers labs for the 4th years Chemistry Students (2010- till 2014).

5- Career

1- Assistant Chemist	Science / Chemistry	1999-2005
2- Assistant Lecturer	Science / Chemistry	2006 -2010
3- Lecturer Science	Science / Chemistry	2010 –till now

6- Scientific conference participation

- 1- Proceeding of 3rd Scientific Conference of the College of Science, Research, Baghdad, Iraq, 2009
- 2- International Conference on Iraqi Oil Studies, Preseners (Sporting Team), Baghdad, Iraq, 2010
- 3- The Relationship Between Different Universities and Research, Preseners, Baghdad, Iraq, 2011
- 4- 2nd Scientific Conference for Students, Preseners, Baghdad, Iraq, 2011
- 5- Third Scientific Conference on Nanotechnology and its Applications, Preseners, Baghdad, Iraq, 2011
- 6- First Scientific Conference on Biological Department, Preseners, Baghdad, Iraq, 2012
- 7- First International Conference of Remote Sensing and Image Processing, Preseners, Baghdad, Iraq, 2012
- 8- First Conference on Dust Storms and Their Environmental Effectrs, Preseners, Baghdad, Iraq, 2012
- 9- The First National Conference of Chemistry, Preseners, Baghdad, Iraq, 2012
- 10- International Conference for Developing Higher Education in Iraq, Preseners, Baghdad, Iraq, 2012
- 11- Mathmatech Conference, Preseners, Baghdad , Iraq, 2013
- 12- I attended on 11th BBMEC (international biosensor conference) from 27 – 30 September, Regensburg, Germany, 2015

7- Committees

- I was a member in the Attendance and Absence of 3rd stage students at Baghdad University - Science College – Chemistry department for three years (2006-2007-2008).
- I was a member in the examination of 3rd stage students for 2013-2014.
- I'm a member of the social committee - "Decorating section for university day celebration and Moulded of Prophet Mohammed" till now.
- I'm a member of The Committee of the Library department from 2006 - 2013.
- The Committee of the International Conference on Iraqi Oil studies on 2010.

8- Publications

- 1- Suaad, M.H.Al-Majidi, Wafaa W.N.Al-Kaisy, "Synthesis and Some Biological Studies of New Diazine, Triazine, Diazole, Thiazole and 4 Δ - Oxazoline derivatives . Proceeding of 3rd Scientific Conference of the College of Science University of Baghdad , PP.1413-1423, 2009
- 2- Wafaa W.N.Al-Kaisy, " Synthesis of Some New Derivatives of 1,2,4-Triazoles and Thiazole From 1,2,3,4-tetrahydrocarbazol and Study Their Biological Activity , Journal of Al-Nahrain University , Vol.13(2), June, pp.54-62 ,2010
- 3- Wafaa W.N.Al-Kaisy, Safaa H.F.Tuama, Suaad, M.H.Al-Majidi, Synthesis, Characterization and Evaluation of Antimicrobial Activity of Some New Acetylenic Amine and 2- Oxoazetidine of Carbazole , Am. J. Sci. Ind. Res., Vol. 4(4) pp .389-398 , 2013
- 4- W. W. Al-Qaysi and A. Duerkop, "Luminescent europium complex for wide-range pH sensor and sensor microtiterplate," *Analyst*, vol. 143, pp. 3176–3184, 2018.
- 5- W. W. Al-Qaysi and A. Duerkop, "Sensor and sensor microtiterplate with expanded pH detection range and their use in real samples". Has been submitted to **Sensors and Actuators B Chemical**.
- 6- W. W. Al-Qaysi and A. Duerkop, "Optical Wide-Range pH Sensors". Has been submitted to **Analytical and Bioanalytical Chemistry**

7. **Eidesstattliche Erklärung**

- 1- Ich erkläre hiermit an Eides statt, dass ich die vorliegende Arbeit ohne unzulässige Hilfe Dritter und ohne Benutzung anderer als der angegebenen Hilfsmittel angefertigt habe; die aus anderen Quellen direkt oder indirekt übernommenen Daten und Konzepte sind unter Angabe des Literaturzitats gekennzeichnet.
- 2- Weitere Personen waren an der inhaltlich-materiellen Herstellung der vorliegenden Arbeit nicht beteiligt. Insbesondere habe ich hierfür nicht die entgeltliche Hilfe eines Promotionsberaters oder anderer Personen in Anspruch genommen. Niemand hat von mir weder unmittelbar noch mittelbar geldwerte Leistungen für Arbeiten erhalten, die im Zusammenhang mit dem Inhalt der vorgelegten Dissertation stehen.
- 3- Die Arbeit wurde bisher weder im In- noch im Ausland in gleicher oder ähnlicher Form einer anderen Prüfungsbehörde vorgelegt.

Regensburg, 03-10-2018

Ort, Datum

Unterschrift